PACIFIC EARTHQUAKE ENGINEERING RESEARCH CENTER

Bar Buckling in Reinforced Concrete Bridge Columns

Wayne A. Brown
Dawn E. Lehman
John F. Stanton

University of Washington

PEER 2007/11
FEBRUARY 2008

Bar Buckling in Reinforced Concrete Bridge Columns

Wayne A. Brown
Department of Civil and Environmental Engineering
University of Washington

Dawn E. Lehman
Department of Civil and Environmental Engineering
University of Washington

John F. Stanton
Department of Civil and Environmental Engineering
University of Washington

PEER Report 2007/11
Pacific Earthquake Engineering Research Center
College of Engineering
University of California, Berkeley

February 2008

ABSTRACT

The goal of the research described in this report was to generate experimental data with which to study bar buckling in reinforced concrete columns. Eight circular columns, reinforced with longitudinal bars and circumferential spirals, were constructed and tested under constant axial load and cyclic lateral displacements. In the first four specimens, different displacement histories were used, including two highly asymmetric histories. In the second four specimens, the strength and stiffness of the spiral were the study parameters, which were varied independently. The columns were heavily instrumented, and special measures were adopted to detect the onset of bar buckling. This proved necessary because buckling was detected by the instruments before it became visible to the human eye.

Bar buckling always occurred during a half cycle of drift in which the strain increment was compressive, following a half cycle of substantial tensile strain increment. However, the absolute strain at buckling was in many cases tensile. It was also found that within the range of values studied, the stiffness and strength of the spiral had a statistically insignificant effect on the drift, or drift increment, at the onset of buckling.

ACKNOWLEDGMENTS

This work was supported primarily by the Earthquake Engineering Research Centers Program of the National Science Foundation under award number EEC-9701568 through the Pacific Earthquake Engineering Research Center (PEER). Any opinions, findings, and conclusion or recommendations expressed in this material are those of the author(s) and do not necessarily reflect those of the National Science Foundation.

This research would not have been possible without the great assistance from Vince Chaijaroen, who spent many hours helping with this project and providing his expertise. Golnaz Jankhah, Maggie Ortiz, Jason Perkizas, Ben Shuman, Owen Sullivan, and John Werner all helped for many hours to construct and test the specimens. Amanda Jellin, Jon Padovorac, Jason Pang, and Kyle Steuck helped not only with construction and testing but also with valuable opinions. Michelle Edmunds also provided some much-needed emotional support while the research was being conducted.

CONTENTS

LIST OF FIGURES

LIST OF TABLES

1 Introduction

1.1 CONTEXT

The goal underlying current design codes is to achieve life safety and prevent collapse in the event of a strong earthquake. However, the introduction of performance-based earthquake engineering launched a new philosophy according to which the designer strives to achieve a particular performance in response to a given seismic event. The performance of a structure is measured in terms of the damage states that may occur and the repairability of the structure associated with them. For a reinforced concrete bridge column, the damage states include cracking, yielding, spalling, longitudinal bar buckling, loss of confinement and loss of load-carrying capacity. Bar buckling is a crucial damage state, as it usually leads to spiral fracture and loss of confinement. Once bars have buckled, repair is difficult and it is likely that a column will require replacement.

A model is needed to allow the practicing designer to find the drift level at which bar buckling will initiate, given various design parameters. Ideally, such a model should be both accurate and easy to use; however, because bar buckling is a complex nonlinear phenomenon, especially in circular columns, an accurate model for predicting it has yet to be developed.

While bar buckling has been observed in many column tests, few tests have been conducted in which bar buckling formed the focus of the study and was closely observed and measured. Such tests are needed to provide a better understanding and the opportunity to calibrate analytical models.

1.2 OBJECTIVES

The goal of this research is to generate data on bar-buckling mechanisms for use by others in developing a numerical model and to further the profession's understanding of the phenomenon by means of observations and measurements made during the tests.

1.3 METHODS

A literature review was conducted on bar buckling. The search revealed studies of finite element analyses, isolated bar tests, scaled column tests, and statistical studies using databases of test results. The findings and results were gathered to identify the important parameters that influence bar buckling.

To generate data on bar buckling, eight 1/3-scale reinforced bridge cantilever columns were constructed and tested. The parameters that were varied were: the presence of cover concrete, the applied drift histories, the strength and stiffness of the transverse reinforcement, and the method of anchoring the longitudinal bars into the footing. The specimens were subjected to a constant axial load and a cyclic drift history. Each column was heavily instrumented with strain gages and potentiometers to capture horizontal displacement, column curvature, bar displacement, and bar strain. A digital photogrammetric system was also used to gather data on the displaced shape of the longitudinal bars and to gather displacement data for the column.

Observed and measured data were collected during testing and then analyzed to develop further understanding about the mechanism of bar buckling in circular reinforced concrete columns.

2 Previous Work

Many studies have researched the buckling behavior of reinforcing bars. The topic is both complicated and extremely difficult. The primary complexities result from the inelastic-cyclic response of the reinforcing bars and the Poisson expansion of the column core, but added difficulties are caused by the influence of the concrete cover and the transverse reinforcement in restraining the buckling of the longitudinal bars. The buckling behavior is further complicated by the fact that it involves both geometric and material nonlinearity. Focusing on these aspects separately and as part of the overall behavior, researchers have used analytical, experimental, and empirical techniques to better understand and prevent premature buckling of bars. Despite all of this work a reasonable understanding of the buckling behavior is still missing and no definitive models have yet been implemented. The following is a review of select experimental and analytical studies conducted to date.

2.1 EXPERIMENTAL AND ANALYTICAL WORK

Papia et al. (1988) performed an analytical study about bar instability in reinforced concrete members under axial compression. It was stated that under axial compression, failure of the system was always caused by buckling of the longitudinal reinforcement regardless of whether the buckling occurred between tie spacings or over multiple tie spacings. A model was developed including springs representing transverse ties to calculate the buckled length of the bar. From this length the critical load that causes buckling was determined. This model compared well with experimental results

Mau (1990) conducted some finite element modeling of reinforcing bars under monotonic loading. Using the tangent modulus Mau established a critical tie spacing to a bar diameter (s_h/d_b) ratio of 5 to 7. Below this s_h/d_b value the compressive load deflection curve would follow the tensile curve; above this value the bar became unstable upon reaching the yield point and the tangent modulus approached zero. This study focused on S_h/D ratios of 5 to 15.

Monti and Nuti (1992) conducted monotonic axial compression tests in order to develop a model of reinforcing bar behavior including buckling. Bars were placed in a test machine and their ends were fixed to prevent rotation. The bars were tested in both tension and compression. Length to bar diameter (s_h/d_b) ratios of 5, 8, and 11 were selected to show the effect of tie spacing. It was found that for s_h/d_b = 5 the tensile and compressive stress-strain curves were almost identical, whereas for larger values of s_h/d_b the curves diverged after the onset of yielding, as shown in Figure 2.1. Monti and Nuti used four different hardening rules to derive a model that accounts for inelastic buckling that can be incorporated in column models. This was based on the assumption that the transverse reinforcement would fully restrain the bar ends.

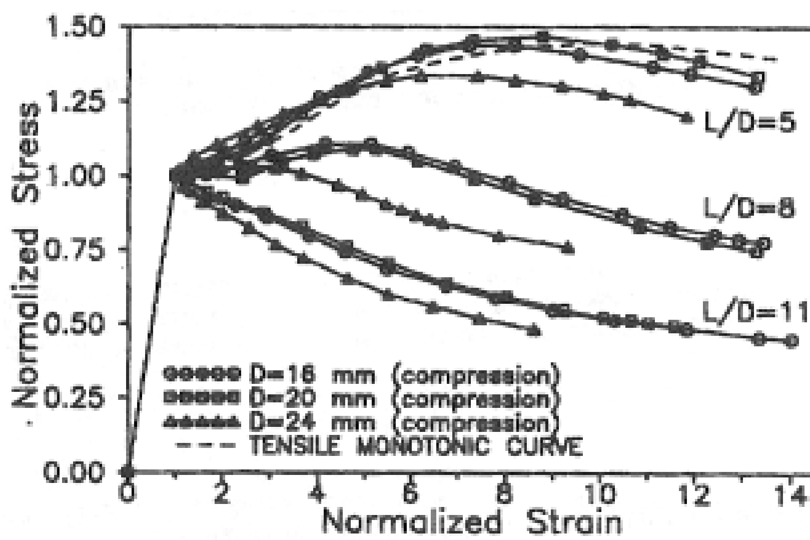

Fig. 2.1 Experimental monotonic compression curves taken from Monti and Nuti (1992).

Gomes and Appleton (1997) made modifications to the Menegotto-Pinto curve to take into account buckling of the reinforcing bars. This model included effects such as the Baushinger effect and isotropic strain hardening. The buckling stress-strain relationship is based on a simple plastic mechanism, as shown in Figure 2.2. It was assumed that the bars would be restrained at the ends and form plastic hinges (shown as black dots in Fig. 2.2) between tie spacings.

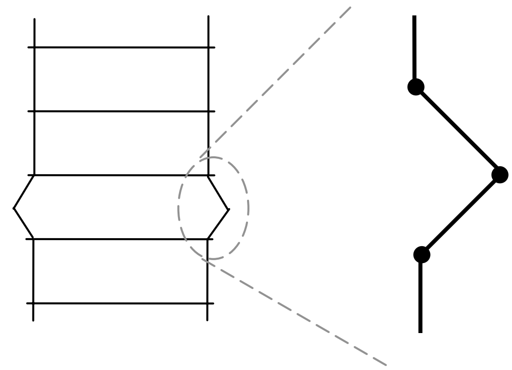

Fig. 2.2 Plastic buckling mechanism proposed by Gomes and Appleton.

Rodriguez et al. (1999) studied the cyclic behavior of reinforcing bars similar to Monti and Nuti (1992). The bars were tested with tie spacing to bar diameter (s_h/d_b) values of 2.5, 4, 6, and 8. The bars were placed in a cyclic test machine and held by grips. The grips did not provide a completely fixed connection and thus an effective length of 0.75 was found instead of the 0.5 value assumed by Monti and Nuti (1992) for a fully fixed bar. Buckling was defined empirically as the moment when the difference in strain on the two sides of the bar exceeded a given value:

$\varepsilon_2 - \varepsilon_1 \geq 0.2(\varepsilon_1)$ for monotonic and

$\varepsilon_1 - \varepsilon_2 \geq 0.2(\varepsilon_m^+ - \varepsilon_m^-)$ for cyclic

where ε_1 is the strain on the compressive side of the bar, ε_2 is the strain on the tensile side of the bar, and ε_m^+ and ε_m^- are the peak strains reached. It was found that the onset of buckling due to cyclic loading is largely affected by the reversal from tension and strongly depends on the maximum tensile strain reached before reversal. With these ideas in mind a model was produced that would predict the strain at which a bar would buckle. It was concluded that under cyclic loading buckling would occur after a return from a tensile strain at zero load (ε^+_0) to a new strain of ε_p as shown in Figure 2.3. The value of ε^*_p is considered constant if all other parameters are kept constant; thus if ε^+_0 were larger than ε^*_p, the bar would buckle under a net tensile strain (as discussed by Suda et al. 1996), and if $\varepsilon^+_0 = 0$, then $\varepsilon^*_p = \varepsilon_p$ and would be the monotonic case.

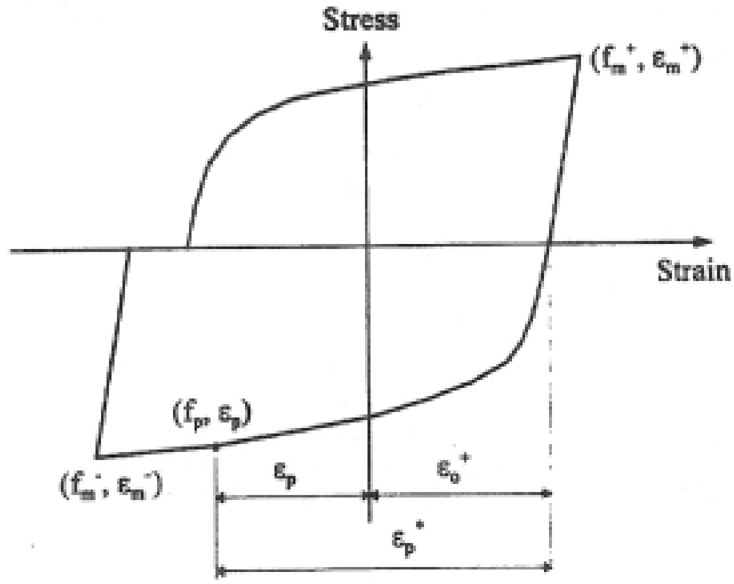

Fig. 2.3 Cyclic stress-strain curve shown in Rodriguez et al. (1999).

Dhakal and Maekawa (2002) studied rectangular columns and concluded that reinforcement stability depended on the longitudinal bars, the transverse reinforcement, and the interaction with the cover concrete. Using energy principles, they derived the buckling mode and shape for bars and thus how many ties spacings the bars would buckle over. They also developed a spalling criterion that included the lateral force from the bars buckling outwards in addition to the compressive strain on the concrete. These models were used in a finite element analysis of a cantilever column that was subjected to lateral and axial loads. The results of this model agreed fairly well with experimental results.

Moyer and Kowalsky (2003) tested four 18″ diameter cantilever columns. All columns were identically built; the only variable in the test was the drift histories of the specimens. From this study it was found that reinforcing bars tend to buckle from compressive stress after undergoing a large tensile strain, which is consistent with the hypothesis of Rodriguez et al. (1999). It was found that after the concrete core had cracked, the longitudinal bars are the sole carriers of the compression force until the cracks in the concrete close. It was stressed that the monitoring of the strain in the bars via strain gages was very important, as this was the most important factor in whether the bars would buckle or not.

Bae et al. (2005) conducted monotonic compression tests on No. 8 and No. 10 reinforcing bars in air. They varied both the length/diameter ratio of the test specimens and the load eccentricity to bar diameter (e/d_b) ratios. They assumed that the bars in a column would buckle between turns of the spiral, so they referred to the length/diameter ratio of their test specimens as the hoop spacing/bar diameter ratio, s_h/d_b. Every combination of $4 \leq s_h/d_b \leq 12$ and $0 < e/d_b \leq 0.5$ was tested with both bar sizes. The eccentricity was introduced by bending the bar before clamping it into the testing apparatus. Testing was conducted in a universal testing machine and the bar ends were assumed to be fixed against rotation. The yield strength was achieved for an s_h/d_b ratio of 6 for an initially straight bar ($e/d = 0$); this result was consistent with Monti and Nuti's work. For a given e/d ratio it was found that an increase in the s_h/d_b ratio resulted in a decrease in load-carrying capacity and ductility. For a s_h/d_b ratio of 4, load-carrying capacity could be held regardless of the e/d ratio used. It was also noted that all bars have a weak axis due to the ribs and would always buckle along their weak axis.

2.2 DATABASE STUDIES

Pantazopolou (1998) compiled a database of 300 column tests in order to identify the parameters that influenced bar buckling. The study showed the interaction between tie effectiveness, core deformation capacity, tie spacing, and bar diameter of the reinforcement on the instability in the columns. It was suggested that all of these parameters need to be included in a model; otherwise a large scatter would be found when plotting only one parameter at a time. These data were used to produce empirical guides to conservatively design columns to delay bar buckling.

Berry and Eberhard (2005) compiled a database of 450 column tests and developed an empirical model for bar buckling based on statistics. The model is used to predict the drift ratio (Δ_{bb_calc}/L) at which the reinforcing bars will buckle, and is given by

$$\frac{\Delta_{bb\_calc}}{L}(\%) = 3.25\left(1 + k_{e\_bb}\rho_{eff}\frac{d_b}{D}\right)\left(1 - \frac{P}{A_g f'_c}\right)\left(1 + \frac{L}{10D}\right) \tag{2.1}$$

where

k_{e_bb} = 40 for rectangular-reinforced columns;

k_{e_bb} = 150 for spiral-reinforced columns;

$\rho_{eff} = \rho_s\ _{ys}/\ '_c$, ρ_s = volumetric transverse reinforcement ratio;

$_{ys}$ = yield stress of the transverse reinforcement;

d_b = diameter of the longitudinal reinforcing bar;

P = applied axial load;

A_g = gross area of the cross section;

$'_c$ = concrete compressive strength;

L = distance from the column face to the point of inflection;

D = column depth.

2.3 DISCUSSION OF THE BEHAVIOR OF BAR BUCKLING

All previous research has focused on four parameters that seem to influence the instability of reinforcing bars in columns. These parameters are

The effect of cyclic loading. Cyclic load test have been carried out on rebars in air to determine the effects of cycling on inelastic buckling.

The lateral expansion of the concrete core while under compression, and its role in promoting bar buckling.

The presence of cover and its role in suppressing bar buckling.

The effects of the stiffness and strength of the transverse reinforcement in restraining the bars from buckling.

The bar itself experiences cyclic axial load (the white arrow in Fig. 2.4) that may be eccentric. The behavior of the bar alone (ignoring all other conditions) is in itself complicated because of the nonlinear behavior under cyclic yielding; thus most of the research has been done regarding cyclic response of reinforcing bars in air, with nominally fixed ends. In a reinforced concrete column, the problem is more complicated because the bar can have one of two separate behaviors. In the first, the bar buckles between two ties, or turns of spiral, and behaves like a bar of length *s* with fixed ends, where *s* is the spacing of the transverse reinforcement. In the second, the bar can buckle over several transverse reinforcement spacings, as suggested by Pantazopolou (1998) and Dhakal (2002). The buckling load is then a function of the stiffnesses of both the main bar and the ties.

The stiffness of the ties determines whether the bars buckle between the transverse ties or over several tie spacings. In theory, a critical tie stiffness exists above which the bar will buckle between two individual ties and behave as a fixed-ended member. At lower tie stiffnesses, the bar and several ties bow outwards together, and the ties act as restraining springs (shown as dark springs in Fig. 2.4). In a circular column, determining the stiffness of the spring that represents the circular tie when a longitudinal bar pushes radially outwards against it poses a problem. As radial force is applied to the tie, it moves outwards and loses contact with the concrete core over part of the circumference. The problem then becomes a contact problem, which is geometrically nonlinear even if the material remains elastic.

The expansion of the core concrete (gray arrows in Fig. 2.4) will also push on the bar, thus encouraging it to buckle outwards. This expansion could be due to the Poisson effect of pure axial compression, the compression due to bending, shear displacements along diagonal cracks, or any combination of these. The expansion of the concrete core could be thought of as a distributed load on in a "beam on elastic foundation" type model.

The cover concrete may also play a role in restraining the bars from buckling, but this is subject to considerable uncertainty. If the initial eccentricity of the bar was small and the cover was uncracked, the cover might partially restrain the bar from buckling. However, if the bar were initially not straight, perhaps due to core expansion, and if the cover were cracked (likely if the bar were not straight), then radial displacement of the bar might promote cover spalling. It is thus far from clear whether bar buckling causes cover spalling or the cover restrains bar buckling. The answer may even depend on the loading history; if it causes spalling at low displacements, the cover might spall before the bar even starts to buckle.

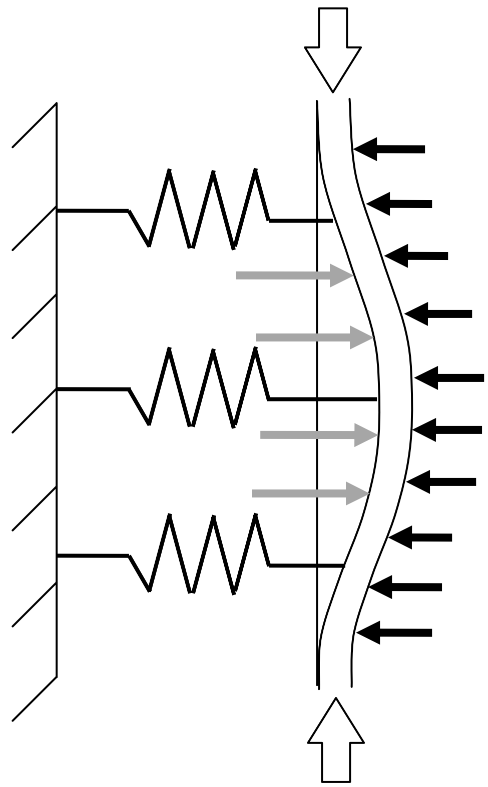

Fig. 2.4 Model of bar-buckling behavior.

2.4 GAPS IN CURRENT KNOWLEDGE

The above summary shows that some aspects of bar-buckling behavior are relatively well understood (e.g., the effect of buckling between bars when ties are rigid); however, most are not well understood at all (e.g., effects of tie flexibility, cover concrete, and core expansion). This is at least partly because most experimental research on columns was not focused on bar buckling and thus any data recorded were byproducts. To the authors' knowledge there have been no experimental programs that have any kind of measurement of bar buckling in columns, and all of the data that have been recorded were visual. Of the studies that have been conducted specifically to look at bar buckling, almost all have focused on a single component and have not looked at the entire picture. As Pantazopolou (1998) suggested, bar buckling can not be attributed to a single column parameter.

3 Experimental Setup

3.1 TEST MATRIX

A matrix of tests was developed to study the effects of the following parameters on the onset of bar buckling:

The absence or presence of cover concrete

The influence of drift history

The axial stiffness of the spiral reinforcement

The axial strength of the spiral reinforcement

The amount of end rigidity on the longitudinal bars (straight bars in grouted ducts or standard hooked bars cast into the footing)

Table 3.1 is an overview of the final test matrix. The configuration of the cover was varied between Specimens CT1 and CT2 in order to isolate its influence, while the influence of the displacement history was studied in Specimens CT2, CT3, and CT4. A comparison of the responses of Specimens CT4 and CT6 shows the influence of the bar embedment in the foundation. In Specimens CT4, CT5, CT7, and CT8 the strength and stiffness of the spiral reinforcement were varied to determine their effects on bar buckling.

In most specimens, cover concrete was not placed around the column in the plastic hinge zone of the column. This was done to eliminate the cover as a variable, after it was found in the first two specimens that the cover had largely spalled by the time bar buckling initiated. On Specimen CT1 cover was placed all around the column, and in Specimen CT2 cover was placed on one side of the specimen. CT3–CT8 had no cover. In Table 3.1 these parameters are stated as 1 for full cover, ½ for half cover, and 0 for no cover.

Three different drift histories were used. The first history was named the "benchmark" drift history (BDH), which was symmetric about the zero drift line and increased linearly in amplitude (see Fig. 3.1 and Table 3.2). The drift was incremented by multiples of the calculated yield displacement.

Table 3.1 Test matrix.

Name	Cover	Drift History	Spiral Stiffness	Spiral Strength	Bar End Condition
CT1	1	BDH	1	1	Grouted Ducts
CT2	1/2	BDH	1	1	Grouted Ducts
CT3	0	ODH	1	1	Grouted Ducts
CT4	0	RDH	1	1	Grouted Ducts
CT5	0	RDH	1/3	1	Grouted Ducts
CT6	0	RDH	1	1	Standard Hooks
CT7	0	RDH	1/6	1/2	Grouted Ducts
CT8	0	RDH	1	1/4	Grouted Ducts

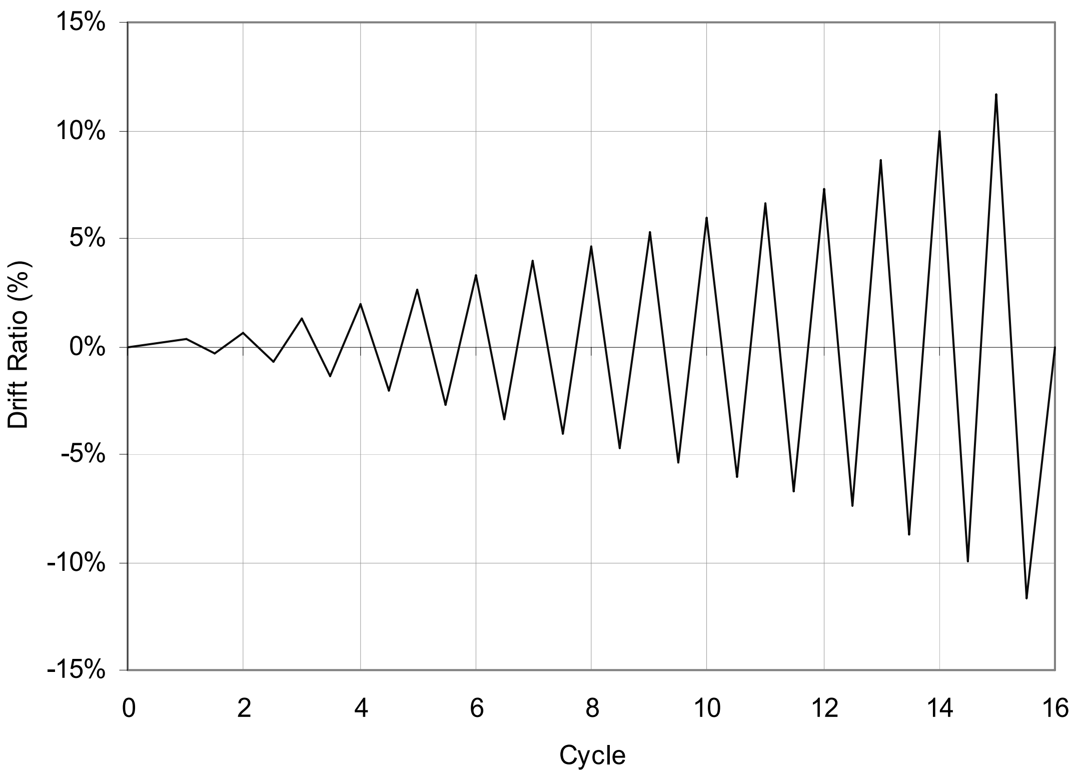

Fig. 3.1 Benchmark drift history (BDH).

The second and third drift histories were developed to investigate the concept of a critical return strain, as suggested by Rodriguez (1999) and Moyer (2003). As discussed in Section 2.1, those authors hypothesize that the bar must first undergo a critical tension strain, followed by a critical strain increment in the opposite, compressive direction before it buckles. In this research, drift was used as a substitute for strain because of the difficulty in obtaining reliable strain measurements from the gages at very high strains. Specimen CT3 was subjected to the "one-sided" drift history (ODH) which pulled the column to a drift of 8%, then cyclically returned the column to zero drift (see Fig. 3.2 and Table 3.3). This history was implemented to quantify the return drift increment required to cause bar buckling after a "tensile" drift that was judged to be larger than the threshold value needed to initiate buckling.

Specimens CT4–CT8 were subjected to the third, "ratcheting" drift history (RDH), in which the specimen was cycled with an increasing "tensile" drift but constant return drift. This history was designed to investigate the peak tensile drift ratio that the specimen must experience before bar buckling can occur (see Fig. 3.3 and Table 3.4). The target return drift increment for all cycles was 4%, the drift at which buckling was observed in Specimen CT3. Theoretical moment-drift curves for the ODH and RDH are shown in Figure 3.4. The ODH history holds the maximum drift constant while varying the return drift increment, and the RDH holds the return drift increment constant while varying the maximum drift.

Table 3.2 Peak values for drift history BDH.

Cycle	Drift Ratio	Displacement (in)
1	0.33% -0.33%	0.2 -0.2
2	0.67% -0.67%	0.4 -0.4
3	1.33% -1.33%	0.8 -0.8
4	2.00% -2.00%	1.2 -1.2
5	2.67% -2.67%	1.6 -1.6
6	3.33% -3.33%	2 -2
7	4.00% -4.00%	2.4 -2.4
8	4.67% -4.67%	2.8 -2.8
9	5.33% -5.33%	3.2 -3.2
10	6.00% -6.00%	3.6 -3.6
11	6.67% -6.67%	4 -4
12	7.33% -7.33%	4.4 -4.4
13	8.67% -8.67%	5.2 -5.2
14	10.00% -10.00%	6 -6
15	11.67% -11.67%	7 -7

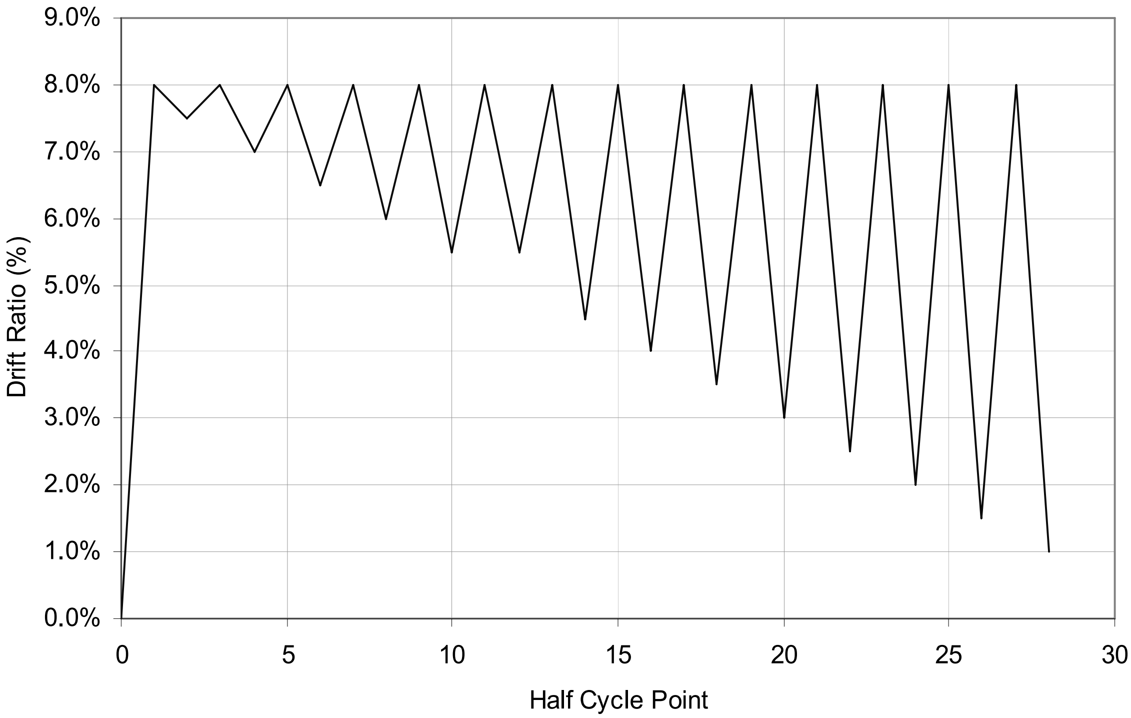

Fig. 3.2 One-sided drift history (ODH).

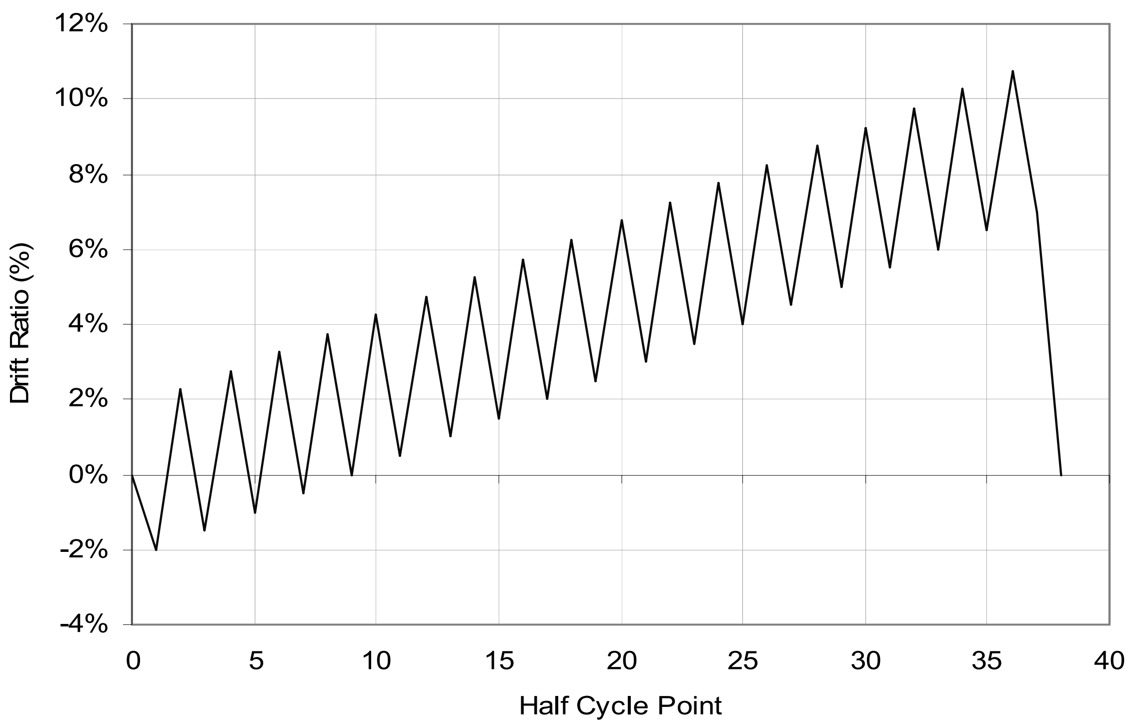

Fig. 3.3 Ratcheting drift history (RDH).

Table 3.3 Peak values for drift history ODH.

Half Cycle #	Drift Ratio	Displacement (in)
0	0.0%	0
1	8.0%	4.8
2	7.5%	4.5
3	8.0%	4.8
4	7.0%	4.2
5	8.0%	4.8
6	6.5%	3.9
7	8.0%	4.8
8	6.0%	3.6
9	8.0%	4.8
10	5.5%	3.3
11	8.0%	4.8
12	5.5%	3.3
13	8.0%	4.8
14	4.5%	2.7
15	8.0%	4.8
16	4.0%	2.4
17	8.0%	4.8
18	3.5%	2.1
19	8.0%	4.8
20	3.0%	1.8
21	8.0%	4.8
22	2.5%	1.5
23	8.0%	4.8
24	2.0%	1.2
25	8.0%	4.8
26	1.5%	0.9
27	8.0%	4.8
28	1.0%	0.6

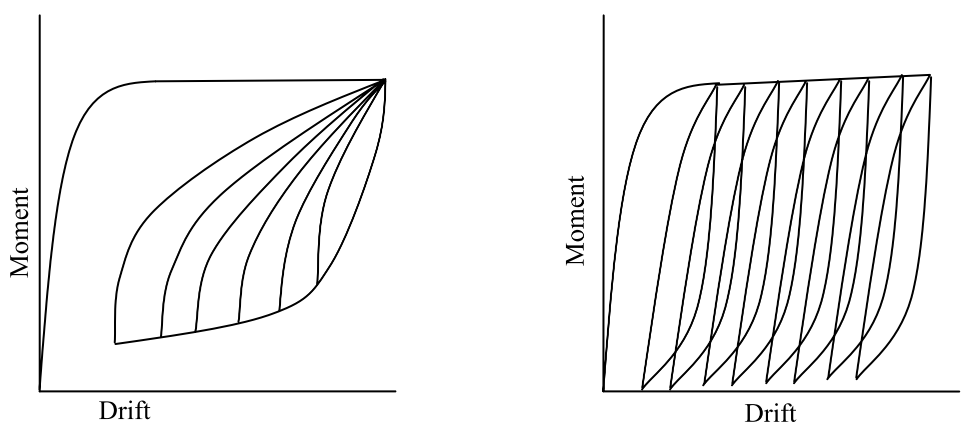

Fig. 3.4 Theoretical moment-drift curves for ODH (left) and RDH (right).

Table 3.4 Peak target values for drift history RDH.

Half Cycle #	Drift Ratio	Displacement (in)
0	0	0
1	-2.00%	-1.2
2	2.25%	1.35
3	-1.50%	-0.9
4	2.75%	1.65
5	-1.00%	-0.6
6	3.25%	1.95
7	-0.50%	-0.3
8	3.75%	2.25
9	0.00%	0
10	4.25%	2.55
11	0.50%	0.3
12	4.75%	2.85
13	1.00%	0.6
14	5.25%	3.15
15	1.50%	0.9
16	5.75%	3.45
17	2.00%	1.2
18	6.25%	3.75
19	2.50%	1.5
20	6.75%	4.05
21	3.00%	1.8
22	7.25%	4.35
23	3.50%	2.1
24	7.75%	4.65
25	4.00%	2.4
26	8.25%	4.95
27	4.50%	2.7
28	8.75%	5.25
29	5.00%	3
30	9.25%	5.55
31	5.50%	3.3
32	9.75%	5.85
33	6.00%	3.6
34	10.25%	6.15
35	6.50%	3.9
36	10.75%	6.45
37	7.00%	4.2
38	0.00%	0

Specimens CT5, CT7, and CT8, which had no cover, were each subjected to the RDH to investigate the influence of the spiral yield strength and spiral axial stiffness on the onset of bar buckling. CT5 used a smaller area of steel (A_s) and a higher yield strength (f_y) while keeping the total axial strength (A_s*f_y) constant. This allowed the axial stiffness (A_sE) to change while the axial strength remained constant. For CT8 the opposite was done and A_s remained the same while lowering the f_y, thus changing A_sE but keeping A_sf_y constant. For CT7 both stiffness and strength of the spirals was lowered. The stiffness and strength could have been varied by altering the spiral spacing, but that would have introduced an additional variable and the likelihood of buckling between the spiral turns, so was therefore rejected. In Table 3.1 the strength and stiffness values are shown as approximate fractions of the reference wire values.

The last parameter was the method of anchoring the longitudinal bars into the footing. In seven of the specimens the longitudinal bars were embedded into the footing using corrugated steel ducts filled with grout to minimize the uncertainty of the bond condition. This was done because (Raynor et al. 2002) found that bars embedded in a grouted duct have bond that is not only much better but is also more reliable than that associated with bars embedded directly in concrete. In Specimen CT7 a more traditional approach was taken by anchoring the bars straight into the concrete using standard hooks. This was done to investigate the effect of the column-footing connection.

3.2 TEST SPECIMENS

The specimens that were built and tested were 1/3 scale cantilever bridge columns with a 3:1 aspect ratio. The design was tailored to fit the existing reaction frame and test setup at the University of Washington Structural Research Lab. A general picture of column geometry is shown in Figure 3.5 and detailed construction drawings can be found in Appendix B.

A total of eight column specimens were made for the entire research study; however CT1–CT4 were built and tested by Freytag (2006). CT1–CT4 will collectively be referred to as Group 1 and CT5–CT8 will collectively be referred to as Group 2. Figure 3.5 shows the design specifically for Group 2. Group 1 footings were twice the depth (36″ in total) and contained no shear reinforcement. This proved to have no effect on the bar-buckling phenomenon, as the footings were designed to have all of the damage occur in the columns. This was seen in the tests to be the case.

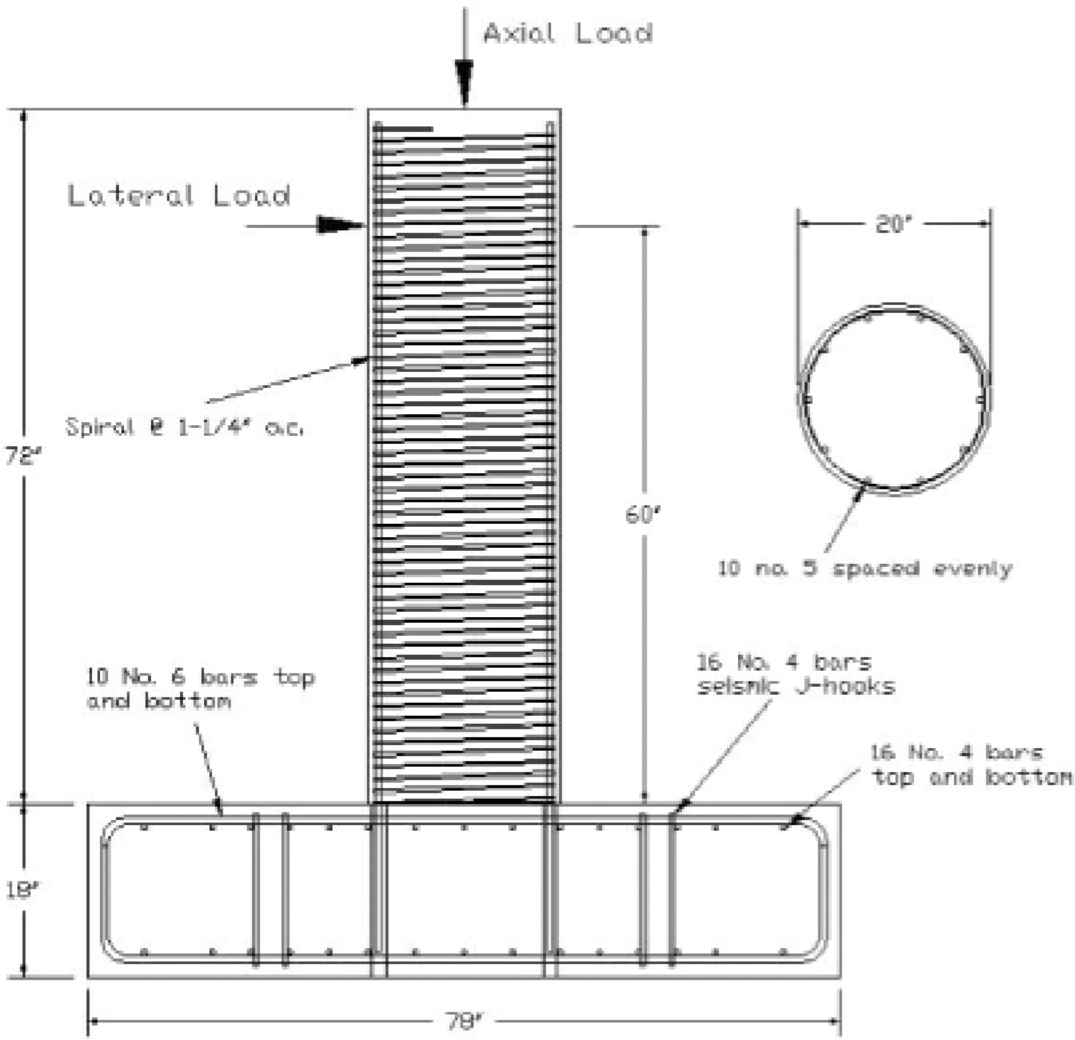

Fig. 3.5 Generic column geometry for all specimens.

All design parameters that were not specifically being tested were in accordance with ACI-318 and AASHTO LRFD Code provisions. Specimens were designed using capacity design to ensure that unwanted mechanisms, such as a footing failure, were suppressed and that a plastic hinge would form at the base of the column. Design values for the reinforcement ratios and material properties are shown in Table 3.5, where $'_c$ is the concrete 28-day strength, $'_g$ is the grout 28-day strength, $_y$ is the yield strength of the longitudinal bars, ρ_l is the longitudinal steel area and ρ_s is the volumetric spiral steel area.

The axial load for all columns was determined by 0.1 $'_c$ A_g, where A_g is the gross cross sectional area of the column and $'_c$ is the concrete strength. For Group 1, $'_c$ was taken as the

28-day design strength, while for Group 2 it was taken as the actual test-day strength. This was changed for Group 2 specimens due to the variable concrete strengths, and thus variable elastic moduli, for every specimen tested.

Table 3.5 Design values for material properties and reinforcement ratios.

	′c (psi)	′g (psi)	y (ksi)	ρ_l (%)	ρ_s (%)
Design Values	5000	6000	60	1.00	0.87

3.3 SPECIMEN CONSTRUCTION

3.3.1 Formwork

The formwork for the footings was the first item to be built. Two sets of formwork were built for Group 1 columns, and were used again for Group 2 specimens. The form walls were made of ¾″ 7-ply wood supported by 2x4 studs. Various supports were built to hold the corrugated ducts and PVC pipes in place during casting. One of these supports is shown in Figure 3.6, which used plywood discs to hold the corrugated ducts in place during casting. This system was used for both the tops and bottoms of the corrugated ducts and PVC pipes. PVC pipes were greased and wrapped backwards in duct tape to allow easy removal of the pipes after casting. These holes would serve as hold-down points on the reaction frame during testing. The placement of PVC pipes can be seen in Figure 3.8. The plywood was greased and caulked to allow easy removal of the forms and to prevent leaks.

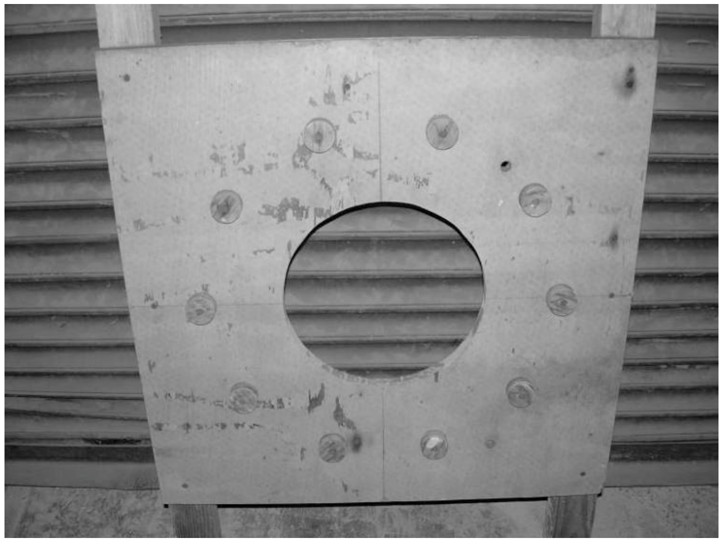

Fig. 3.6 Apparatus to hold corrugated ducts in place with plywood discs.

3.3.2 Footing Cage Construction

Footing cages were built with 10 No. 6 bars top and bottom longitudinally and 15 No. 4 bars top and bottom transversely (see Fig. 3.7). Flexural reinforcement was the same for Groups 1 and 2; however Group 2 footings required shear reinforcement, whereas Group 1 footings did not because they were much deeper. Shear reinforcement was provided by 16 J hooks that were inserted into the cage after completion. Footing cages were dropped into the formwork and then PVC and corrugated ducts were added as shown in Figure 3.8. Foam blocks were used to make depressions in the top surface of the concrete for the instruments that are described in Section 3.5.3.

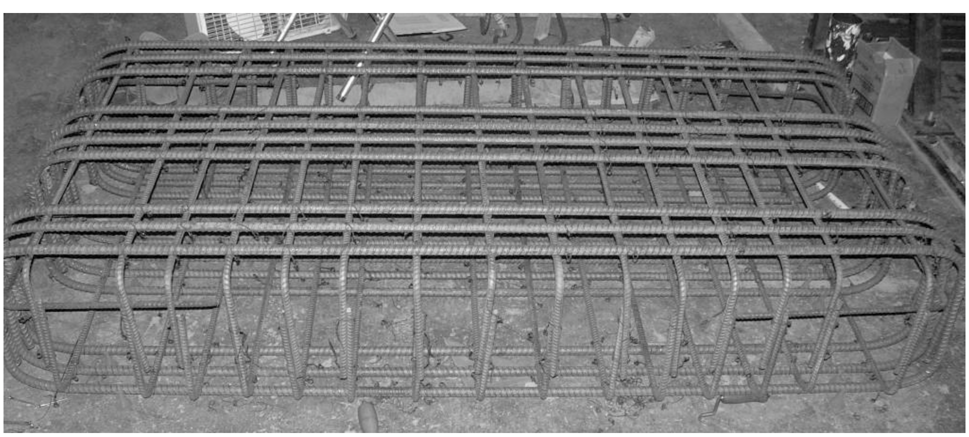

Fig. 3.7 Longitudinal and transverse bars in footing cage.

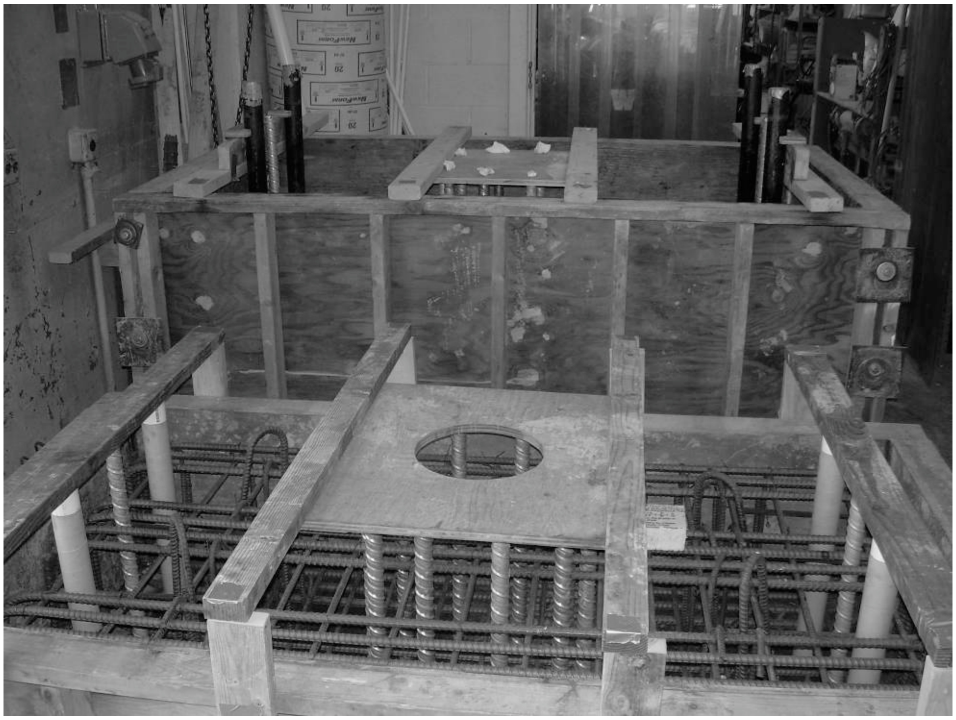

Fig. 3.8 Footings and formwork of CT7 and CT8 ready to be cast.

3.3.3 Column Cage Construction

To tie up the column cages a wooden jig (Fig. 3.9) was made. Each longitudinal bar was placed in the jig and oriented so that its weak axis was oriented parallel to the axis of rotation of the column. This was done as a conservative precaution because Bae et al. (2005) noted that bars would always buckle about their weak axis. Spirals were then placed around the longitudinal bars and tied at 1.25″ on center up the length of the column. Great care was taken to maintain accurate spacing in the bottom third of the column, as this is the critical hinge region where the bars will buckle. Figure 3.10 shows a completed version of one column cage.

Four different spiral types were used throughout the testing. The "regular" spiral was 0.244″ diameter smooth wire of 90 ksi yield strength. The regular wire was used in all tests except CT5, CT7, and CT8. In test CT8 the regular wire was annealed in house to lower its yield strength significantly. To anneal the wire, the wire was placed in a brick oven and heated to 750 C and left there for 2 hours. After 2 hours, the temperature was decreased by 50 C to 100 C

Fig. 3.9 Column cage close-up.

every few hours for 2 days, after which the spiral was left to cool in the oven for another day. The annealing process brought the yield strength of the wire down to approximately 30 ksi. This successfully reduced the axial strength of the wire while keeping Young's modulus the same. In Specimens CT5 and CT7 a 0.102″ diameter 1080-1090 alloy music wire was used instead of the regular wire. This "high-strength" wire has a yield strength of about 280 ksi. The high-strength wire was selected on the basis that it would as closely as possible satisfy

$$n\ A_{s\text{-}hs}\ f_{y\text{-}hs} \approx A_{s\text{-}r}\ f_{y\text{-}r} \qquad \text{and} \qquad f_{y\text{-}hs} \geq 2\ f_{y\text{-}r} \tag{3.1}$$

where n is a positive integer number of wires used, $A_{s\text{-}hs}$ is the area of one high-strength wire, $f_{y\text{-}hs}$ is the yield strength of the high-strength wire, $A_{s\text{-}r}$ is the area of one regular wire, and $f_{y\text{-}r}$ is the yield strength of the regular wire. It was found that two pieces of the high-strength wire above satisfied these requirements. This successfully reduced the axial stiffness of the wire while keeping the yield strength approximately the same. On column CT7 only a single piece of high-strength wire was used, thus reducing both the stiffness and strength of the spiral reinforcement.

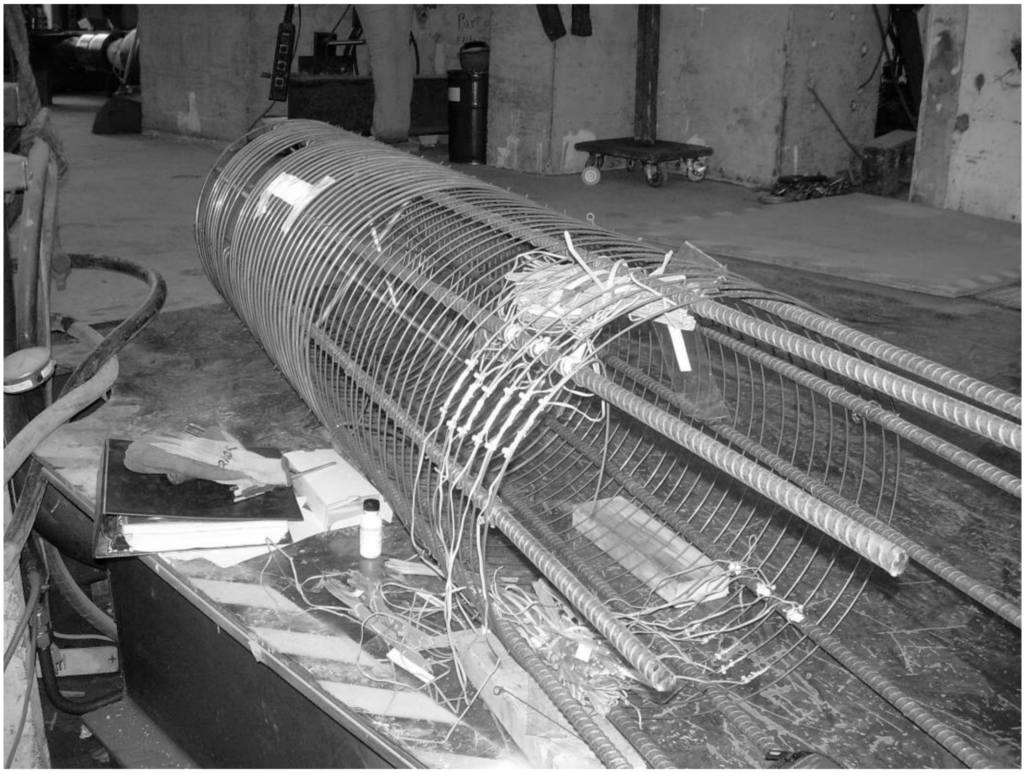

Fig. 3.10 Completed column cage.

3.3.4 Strain Gage Installation

Before assembly of the column cages the longitudinal bars were sanded and cleaned in the locations where strain gages would later be mounted. After assembly of the column cage, strain gages were affixed to these same locations on the front and back of the bars. Strain gages were also affixed on the front and back of the spirals. A drawing of the placement of strain gages can be found in Figures 3.30 and 3.32. Installing strain gages on the spirals on both sides proved difficult especially on the 0.102″ diameter wire and, not surprisingly, they generally gave poor results. All of the gage wires were routed along the spirals until they reached bar #3 and then were routed up to about 1/3 of the column height at which point they exited the column cage. All of the strain gages were protected from moisture and impact with coatings and electrical tape.

3.3.5 Footing Concrete Casting

The concrete for both the footing and the columns used the same mix. The concrete was provided by a ready-mix concrete supplier, and the mix design that was used is shown in Table 3.6. The design strength at 28 days was 5000 psi and was easily met in each pour.

Table 3.6 Mix design of concrete used according to supplier.

Material	Amount in Mix Design
Type I-II Portland cement	660 lb / yd^3
3/8 max coarse aggregate	1774 lb / yd^3
Fine aggregate	1378 lb / yd^3
Water	260 lb / yd^3
Water Reducer	43 oz / yd^4
Accelerator	86 oz / yd^5
Slump	6 in

3/8″ maximum aggregate was specified because cover and clear spacings in the columns were often quite small and good compaction would be difficult with larger aggregate.

Before placing concrete into the forms, a slump test was conducted to ensure that a desirable amount of workability was present in the concrete. Cylinders were made to test the concrete strength at 7 and 28 days as well as every test day. Concrete was placed into the forms (Fig. 3.11) and finished as well as possible. After casting the footings were covered with wet burlap for a few days to keep a moist curing environment. After a few days the PVC pipes were removed and the corrugated ducts were cut off flush with the concrete surface. The area where the column would later be cast was then roughened with a pneumatic hammer to increase the bond between the column and footing.

In the case of Specimen CT6 the column cage was placed into the footing forms so that it could be cast with the hooks directly into the concrete.

Fig. 3.11 Casting footing for Specimen CT5.

3.3.6 Cover Treatment

In the columns that had no cover, foam was used to block out the concrete that would normally form cover around the bars. A ½″ thick closed cell foam sheet was cut into 1″ strips and pushed in between the spirals (Fig. 3.12). This method was an improvement over the original method used in CT2. Instead of cutting strips of foam, CT2 was simply wrapped in on a layer of foam, but this caused a great amount of concrete to still cover the bars and spirals. For this reason Specimen CT2 is considered to have partial cover on one side, even though the plan had been to have no cover on that side. In Specimen CT7 the strip method took slightly too much cover away over a few turns of the spiral reinforcement, and in some places left the spiral not in contact with the concrete core. Relatively dry grout with fibers was placed between the spiral and the concrete to improve the contact between them. Figures 3.13–3.14 illustrate placement of the foam strips and one column with finished foam cover. After casting, the foam strips could easily be removed without damaging the strain gages.

Fig. 3.12 Placing foam in between spirals.

Fig. 3.13 Placing foam for elimination of cover concrete.

Fig. 3.14 After all foam is in place in Specimen CT5.

3.3.7 Grouting of Longitudinal Bars

This procedure was used for all specimens except CT6, in which the bars had standard hooks cast into the footing. Grouting the longitudinal bars into the corrugated ducts was completed last because this made many of the previous steps much easier.

The column cage was hung from an overhead crane and aligned with the corrugated ducts in the footing. The column was shimmed until the cage would sit level when lowered into the ducts. The grout that was used was Dayton Superior ® Sure-Grip bag mix. The grout was mixed according to the manufacturer's instructions for a "fluid" mix. Grout and water were measured out in a bucket then mixed for 2–3 minutes with an electric mixing paddle. The fluid grout was then poured into a funnel and into the corrugated ducts. The ducts were filled enough so that when the bars were lowered into the ducts, the grout would overflow slightly. The column bars were then lowered into the ducts and placed on the shims.

3.3.8 Column Concrete Casting

The same concrete mix that was used in the footings was also used in the columns. A 20″ diameter forming tube was cut to a 6-ft length and placed around the cage. Holes for various instruments (discussed in Section 3.5) were cut into the wall of the tube; the instruments were

Fig. 3.15 Instrument rods protruding out of forming tube.

inserted and then the tube was caulked to prevent leaks (see Fig. 3.15). Holes were cut to allow for 2″ PVC pipes to be inserted into the top of the tube to accommodate the actuator connection bolts (see Fig. 3.16). After casting, these PVC pipes were cut off flush with the column concrete. The column cage was aligned to the center of the forming tube and fixed with support chairs. The forming tube was leveled and then braced with wood to prevent movement and floating during casting (Fig. 3.17). The bottom of the tube was reinforced with duct tape, because cutting holes in the tube significantly weakened it, and caulked to prevent leaks. Concrete was poured into a clam shell bucket and raised over the top of the forming tube. An 8″ diameter rubber tremie tube was inserted into the forming tube and attached to the clam shell as shown in Figure 3.18. This method prevented the concrete from dropping through a long fall, possibly damaging the instrumentation and segregating.

During casting of CT8, the bottom of the forming tube began to bulge from insufficient reinforcement around the tube. Extra duct tape was quickly added to reinforce the tube. This halted but did not reverse the propagation, and led to the presence of a small amount of cover around the column base.

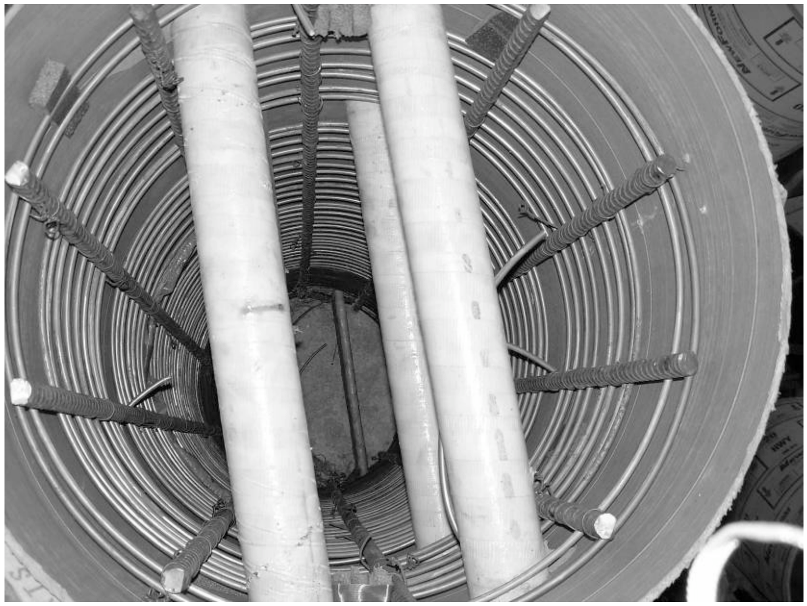

Fig. 3.16 Inside forming tube showing column cage and PVC pipes.

Fig. 3.17 Bracing for forming tube during casting.

Fig. 3.18 Placing concrete via clam shell and rubber pipe.

3.4 TEST SETUP

All specimens were built and tested in the University of Washington Structural Engineering Research Lab. Each specimen was tested in a self-reacting frame as shown in Figure 3.19. The reaction frame consisted of two parallel L-shaped frames made of W20x94 sections with moment connections. An HSS6x6x3/8 was used as a bracing element to provide additional stiffness. A concrete anchor block was pre-stressed between the two L frames on the bottom, to which test specimens could be anchored. Specimens were stressed into the concrete reaction block with high-strength post-tensioning rods to prevent overturning during testing. A W14x90 section was fixed between the two L frames and then was fixed to a 220kip, ±10″ capacity MTS actuator. This actuator provided the lateral force and had swivels on both ends to eliminate any moment in the actuator.

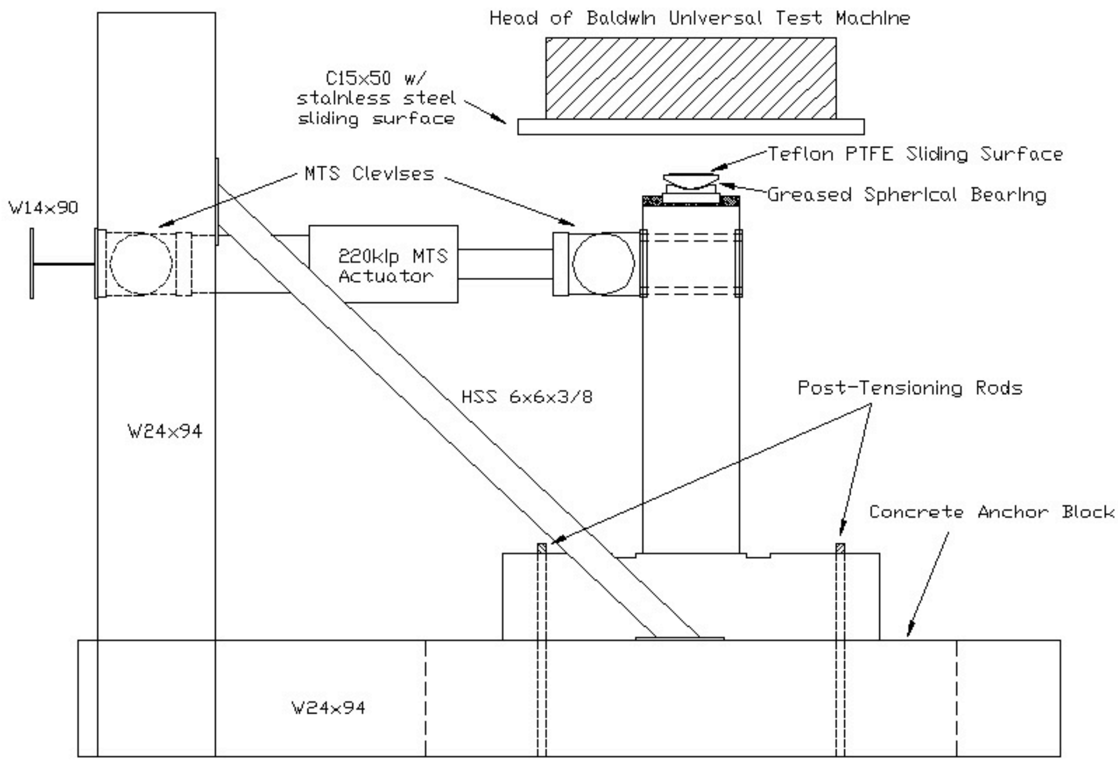

Fig. 3.19 Schematic side view of test setup.

The axial load was applied by the Baldwin Universal Testing Machine and was approximately constant throughout the test. The axial load was controlled manually and thus did vary slightly during column movement, but this variation was minimal (±7%). A C15x50 channel was fixed to the underside of the Baldwin head and coated with a mirror finish stainless steel sheet. A greased spherical bearing was centered and attached to the top of the column, and a sheet of greased Teflon PTFE was fixed to a steel plate and placed on top of this bearing (see Fig. 3.20). This system allowed both free rotation of the column top and provided minimal friction against the applied lateral load.

Figure 3.21 shows a picture of the final test setup.

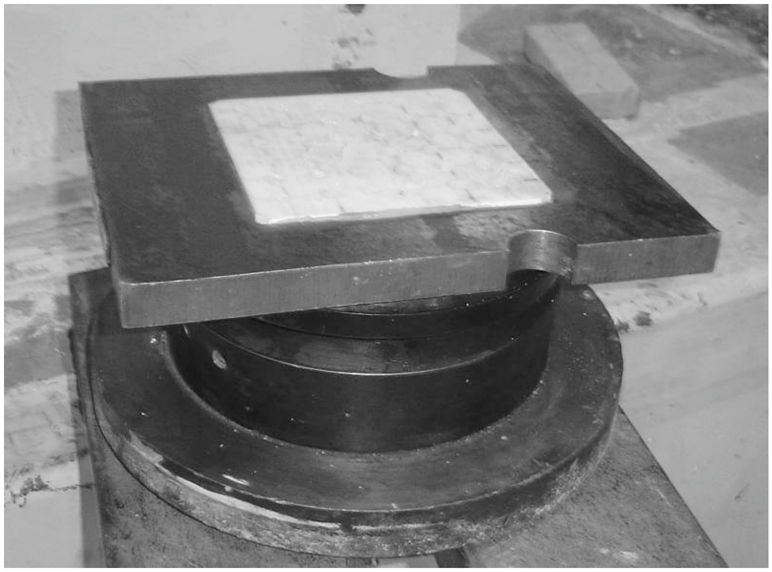

Fig. 3.20 Spherical bearing with greased Teflon PTFE.

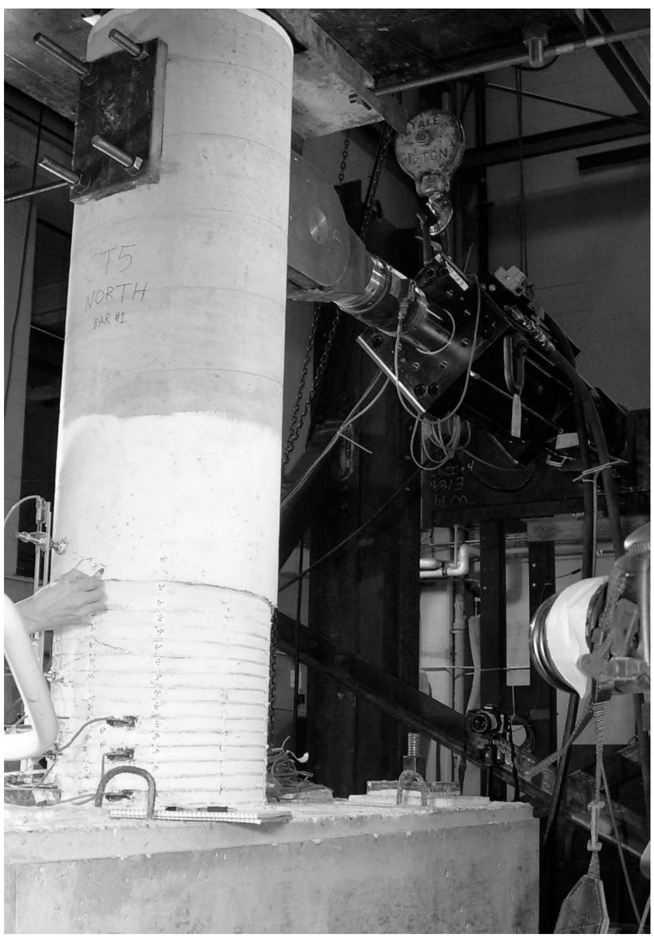

Fig. 3.21 Photo of test apparatus and specimen.

3.5 INSTRUMENTATION

3.5.1 Nomenclature

Each longitudinal bar was assigned a number as shown in Figure 3.22. Only Bars 1 and 6 were instrumented, but the other bars are still referenced by number in Chapter 4. Bar 1 was the north most bar and Bar 6 was the south most bar. Spiral turns were named A–F. A was the turn closest to the footing surface and F was the sixth turn of the spiral on the same side, see Figure 3.23. On one side of the column the two bottom spirals are touching, and in this case the very first spiral is not labeled (and also not instrumented). However, on the other side of the column the bottom two spirals are spaced out, and in this case the very bottom spiral turn is labeled A.

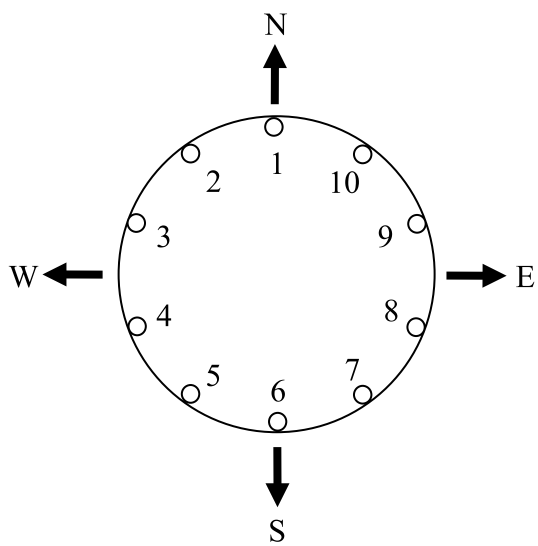

Fig. 3.22 Top view of bar numbering designations.

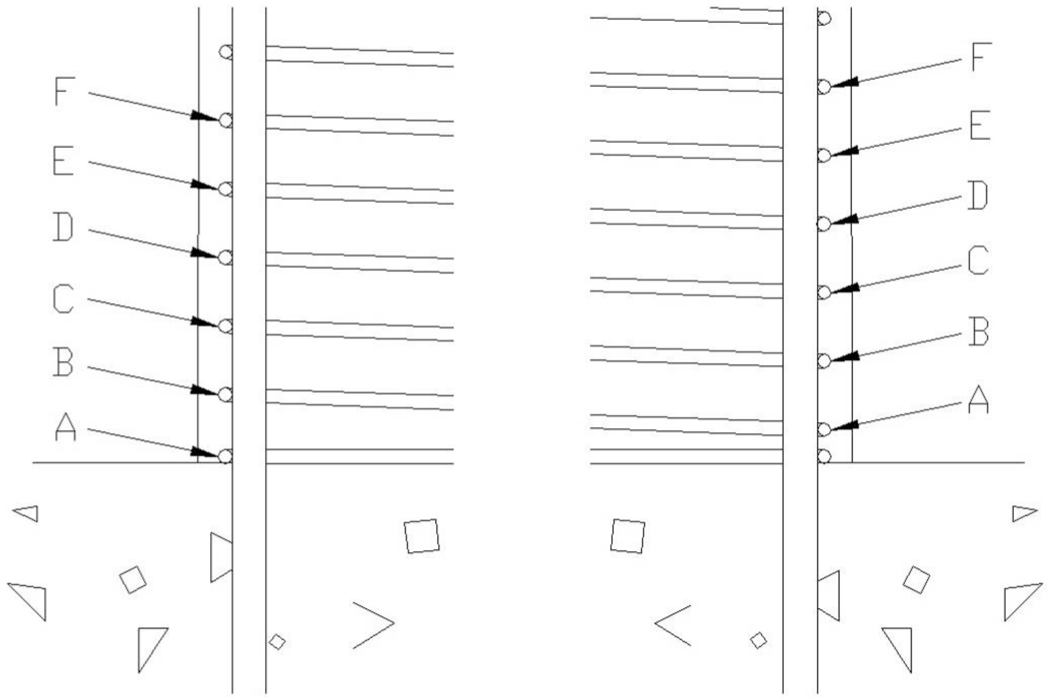

Fig. 3.23 Spiral numbering designation.

3.5.2 Global Behavior

The global behavior of the column was captured by a variety of instruments. The MTS actuator was equipped with both a load cell and a linear variable differential transformer (LVDT). The MTS load cell read the applied horizontal load and the LVTD measured the actuator elongation. The Baldwin Universal Testing Machine was also equipped with a load cell that recorded the applied axial load. The column drift at the height of lateral load application was also measured with a string potentiometer (string pot) which was attached to a fixed reference away from the reaction rig. The displacement of the W14x90 beam was measured as well to record the flexibility in the frame. Various stick potentiometers (pots) were used to measure any slip or rotation of the reaction rig relative to the floor and the specimen relative to the reaction rig. The MTS LVDT plus the displacement of the W14x90 plus any rig/specimen movement should equal the actual specimen displacement as measured by the string pot.

The displacement history was controlled via the LVDT on the MTS. This resulted in a displacement at every point that was smaller than intended due to rig flexibility. Running the test off of the displacement of the string pot was considered, in order to get the displacement history much closer to the intended one. However, the string pot was subject to greater errors than the LVDT, thus this approach was not used.

3.5.3 Column Curvatures

The curvature of the column was measured by inserting "curvature rods" through the concrete core. These rods were made of ½″ diameter threaded rod and were unbonded throughout most of the column diameter to prevent confinement of the core concrete. The rods were de-bonded by placing PVC pipe around them and then greasing and wrapping the PVC pipe with duct tape "sticky side out". The center 3″ to 4″ of each rod was not set in PVC pipe and thus was bonded to the core.

The four rods were arranged as shown in Figure 3.25 and offset approximately 3″ from the center line of the column (Fig. 3.26). The end of each rod one side of the column was attached to a string pot that measured its displacement laterally. In addition pots were attached between each curvature rod, and between the bottom rod and the ground, on each side of the column. From this the rotation angle between each rod can be found and from the rotation the average curvature over that length can also be calculated. Aluminum brackets were made so that the pots could be easily attached between rods and could also slide easily between brackets (Fig. 3.24).

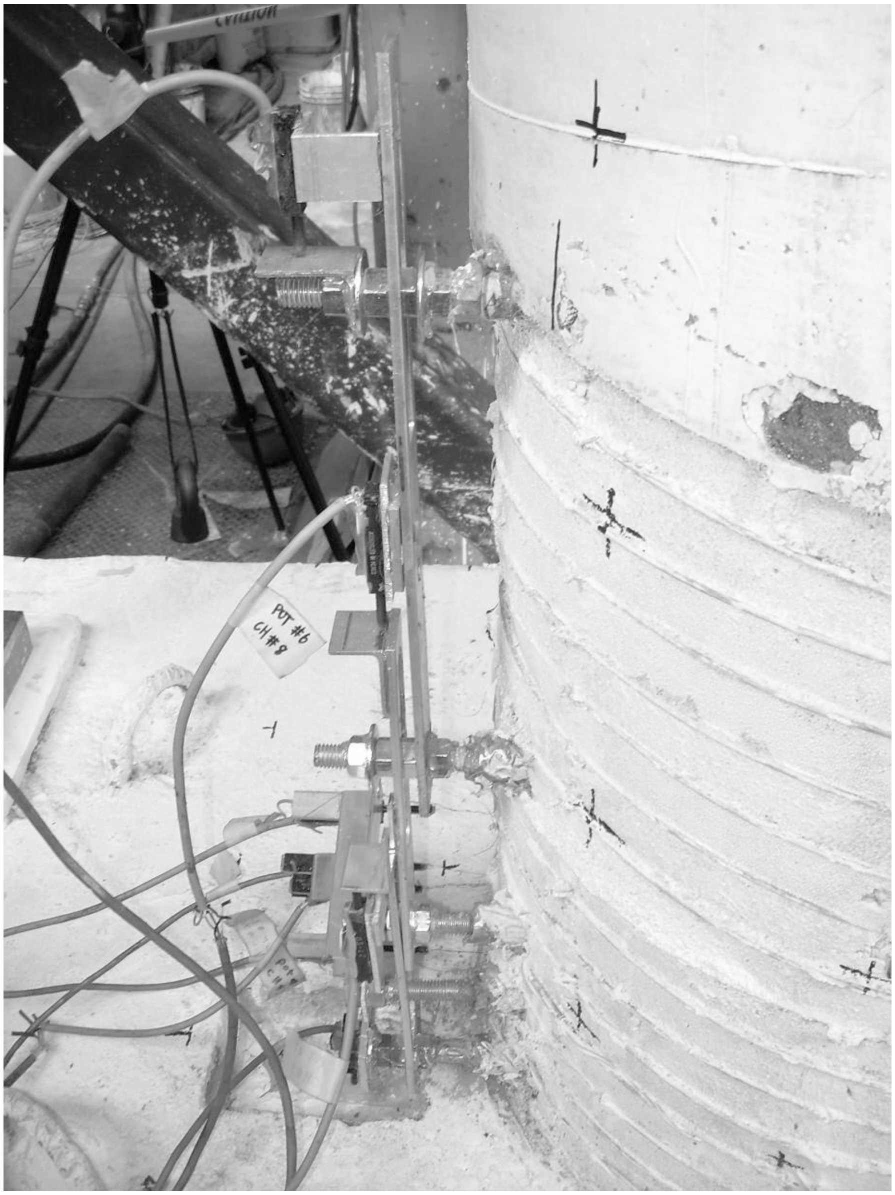

Fig. 3.24 Photo of curvature rod instrumentation setup.

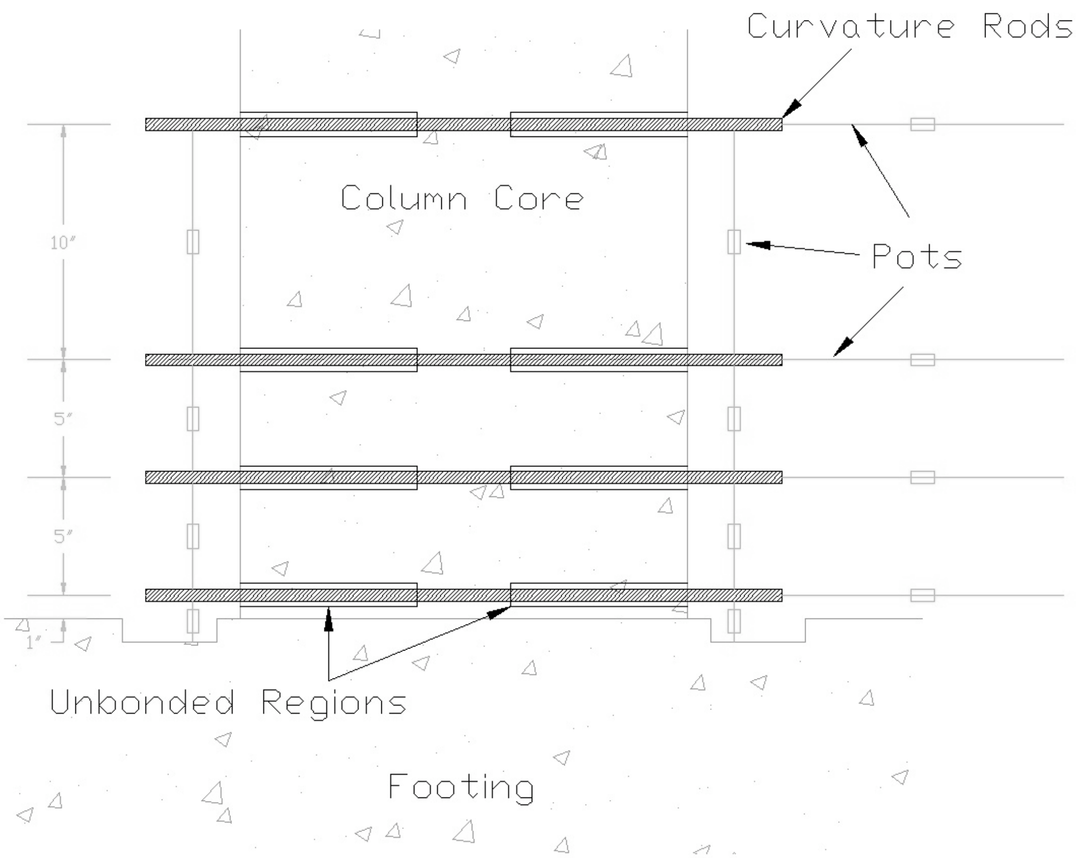

Fig. 3.25 Column section showing placement of rods for measuring curvature.

3.5.4 Bar-Buckling Displacements

Two different methods were devised to measure the lateral displacement of the bar relative to the column (bar-buckling displacement). Figure 3.26 shows both methods of measurement. Both methods used a wire that protruded from the bar and attached to a pot. This was achieved by tightly tying a very thin wire (0.010″ diameter) around the longitudinal bar prior to casting the column concrete. The wire was then glued to the bar with a small amount of epoxy to prevent it from moving. The remainder of the wire was coiled and taped to the outside of the foam that was used to eliminate cover concrete. The free parts of the wire were wrapped in masking tape to prevent any concrete from getting on the wire. Wires were placed at approximately 1″, 4″, and 7″ above the footing.

Method 1 used a string pot that was tied to the wire and fixed with the other string pots on the stationary instrument tower about 6 ft from the column. The lateral displacement of the bar was found by taking the difference between the readings of this string pot and the string pot attached to the curvature rod at the same elevation. This required the addition of another rod in the column; however, it was only used for this purpose and not for curvature measurements.

Method 2 used only one pot. This pot was attached directly to the curvature rod at the same height via an aluminum bracket that extended out to be in front of the wire. This pot was fixed directly to the wire from the bar and thus measured the bar displacement directly. This method was developed to eliminate the need to subtract two relatively large but nearly equal measurements of displacements and to rely on the accuracy of the difference.

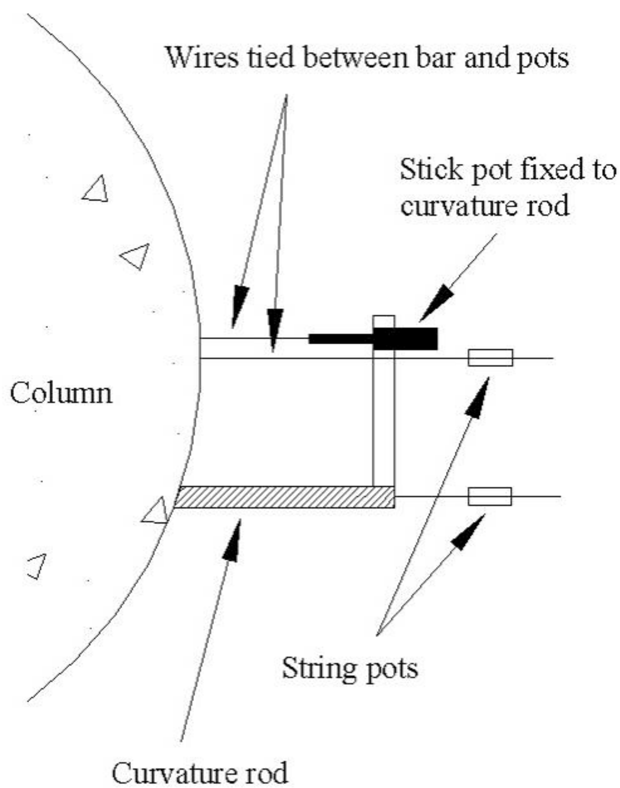

Fig. 3.26 Diagram showing methods for measuring lateral bar displacement.

In some cases only Method 1 was used, in others only Method 2 was used, in yet others both were used to get a comparison between the two methods. Figure 3.27 shows a photo of both methods implemented.

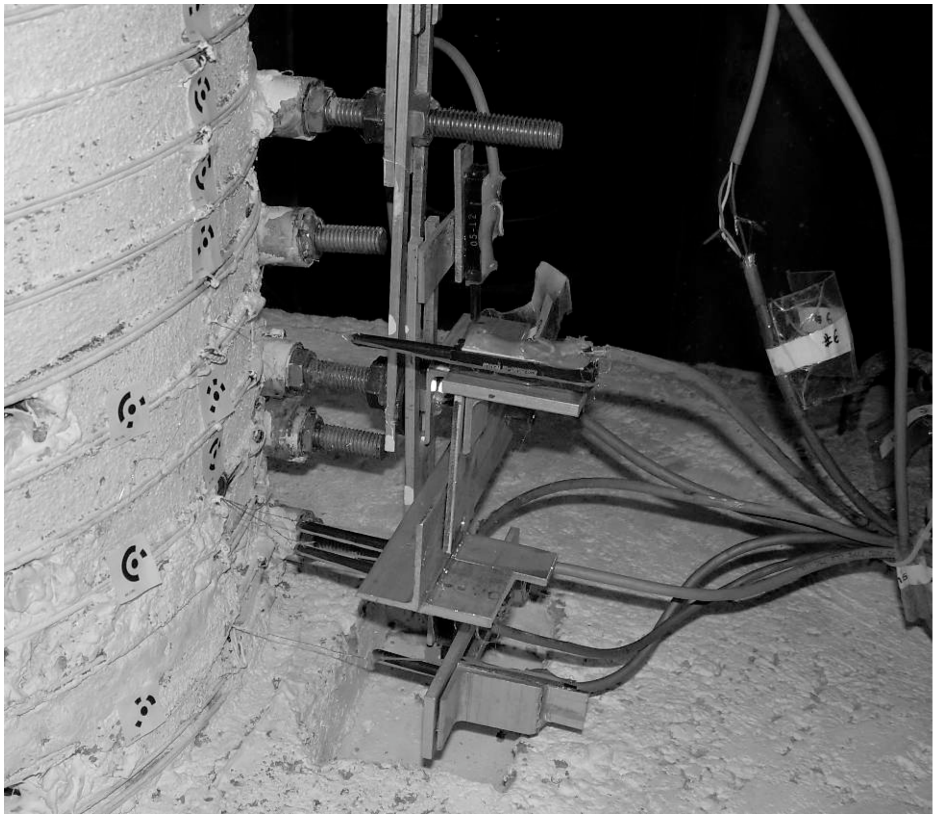

Fig. 3.27 Photo of lateral bar displacement measurement setup.

3.5.5 Core Expansion

The expansion of the concrete core was measured close to the same locations at which the bar lateral displacements were measured. The device use to measure core expansion is shown schematically in Figure 3.28. To avoid congestion, these devices were located about 3″ away from the center of the column, on the opposite side to the curvature rods.

Prior to casting the column, ½″ PVC pipes were greased and wrapped with duct tape "sticky-side out" and inserted into the forming tube between the spirals. After concrete curing, the PVC pipe could easily be removed, leaving a hole through the concrete core. The end of a ½″ threaded rod was glued to the inside of a 2″ long aluminum tube that had a slightly larger diameter than the rod. This aluminum tube was then glued to the inside of the hole in the concrete at the end. Another piece of aluminum tube was placed around the rod and inserted into the hole. This piece was then glued to the concrete at the other end of the rod, but not to the rod itself. A pot was then fixed to this aluminum tube and placed against the end of the rod (see Fig.

3.28). This allowed the rod in the aluminum tube to move independently thus measuring the expansion of the concrete core. Figure 3.29 shows the pot attached to the aluminum tube and extending to the threaded rod. Earlier tests relied on taking string pots measurements on each side of the column and subtracting the readings to obtain the difference, but the accuracy of this approach was found to be poor. The device described here gave results that gave consistent readings at adjacent locations and correlated much better with spiral strains. These characteristics suggest that it was working reliably.

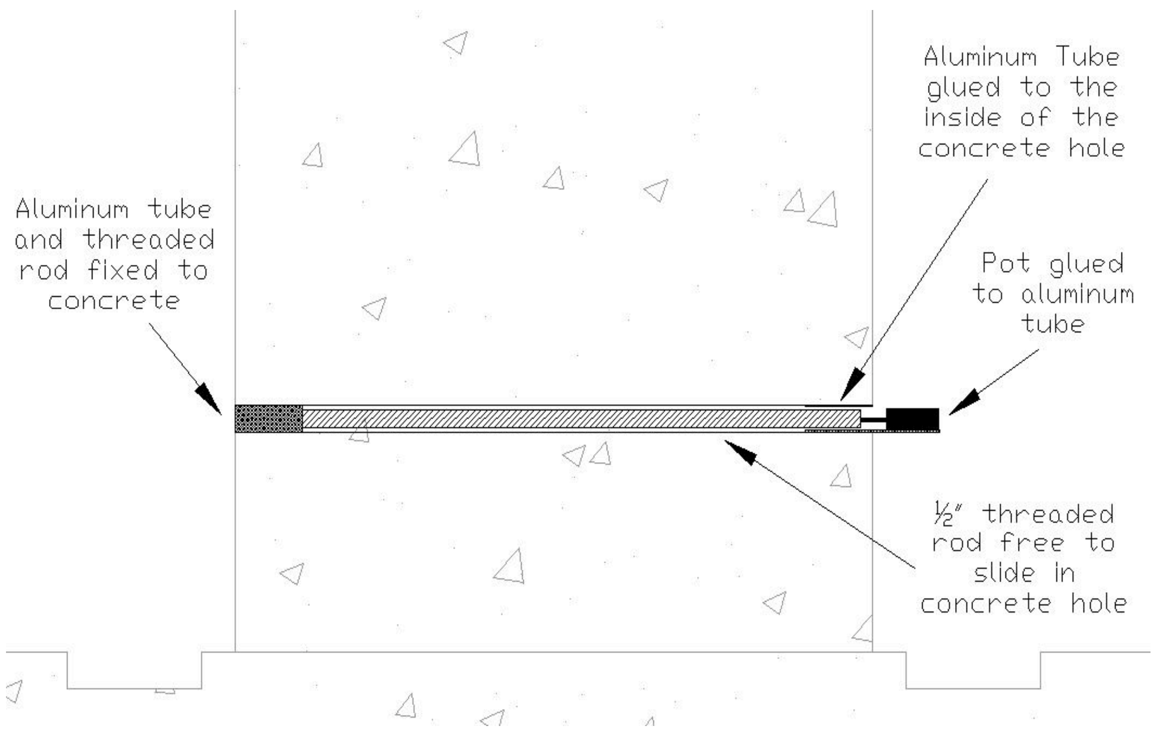

Fig. 3.28 Column section showing core expansion measurement technique.

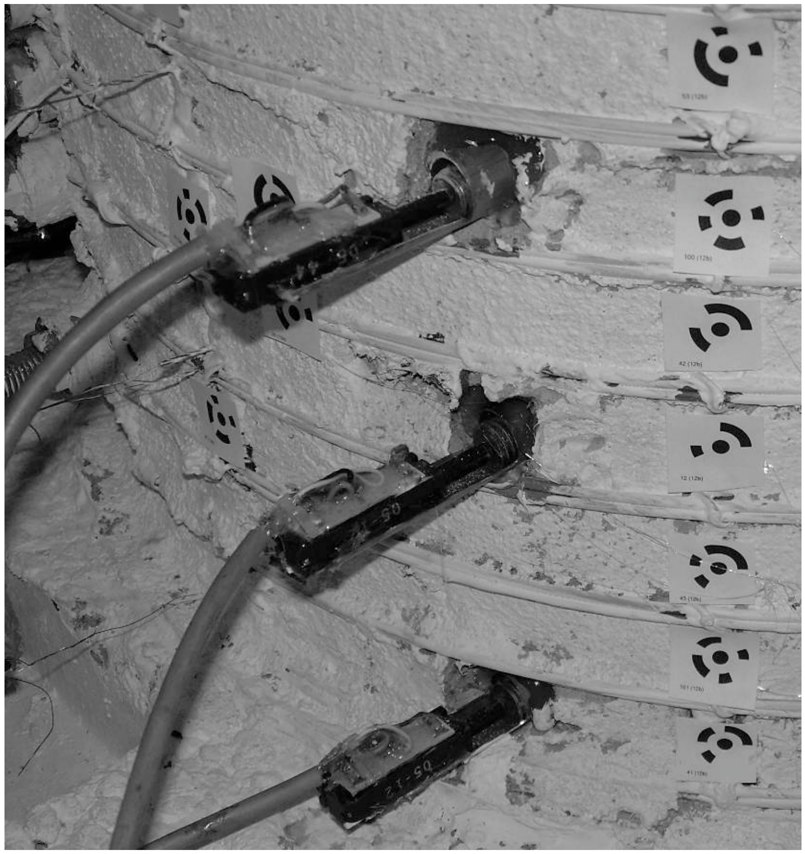

Fig. 3.29 Front side of core expansion measuring device.

3.5.6 Strain Gages

Strain gages were used to record the strain in both the longitudinal bars and the spirals in the buckling critical sections of the column. Strain gages were attached to the longitudinal bars as shown in Figure 3.30. Strain gages were placed on both the inside and outside of the bars to capture both axial strain and bending. Strain gages were placed on Bars 2–5 on Group 1 columns; however these did not provide very useful data and were omitted for Group 2 columns in the interests of economy. The location of spiral strain gages is shown in Figure 3.32; these gages were located approximately 3″, measured along the spirals, from Bars 1 and 6. Each spiral was equipped with a pair of strain gages to capture both axial strain and bending in the spirals. Figure 3.31 is a photo of both spirals and longitudinal bars with strain gages attached and coated prior to casting. The cage is for Specimen CT7, and shows the small-diameter wire used for the spiral.

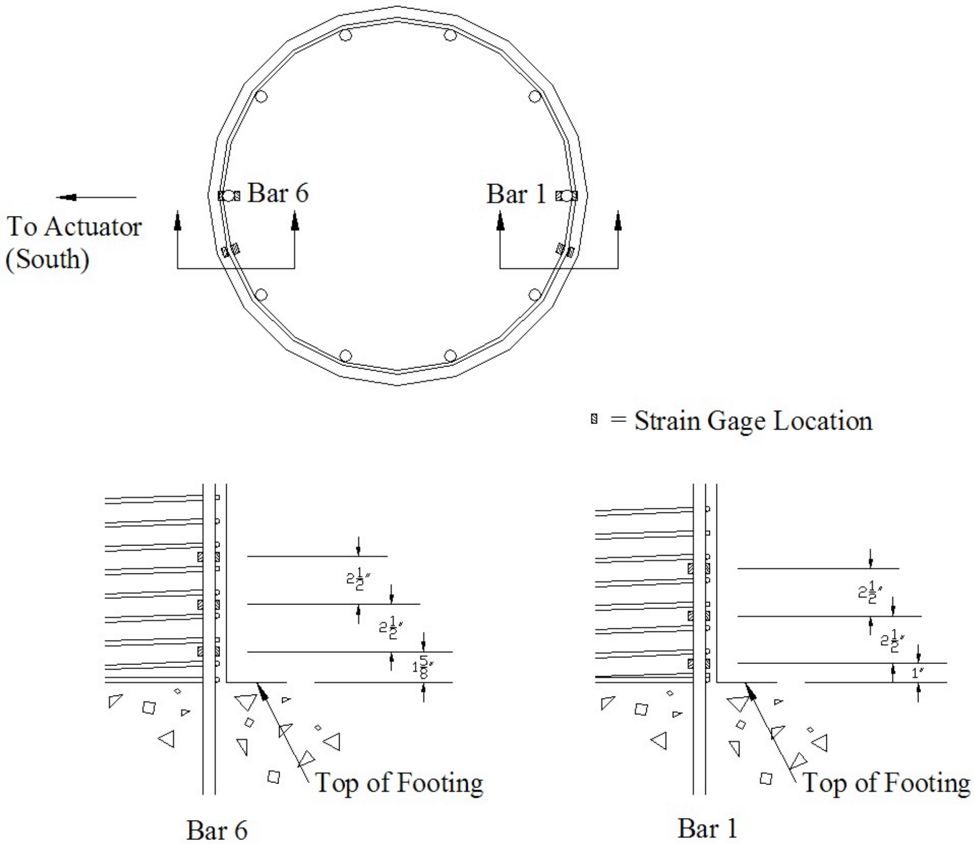

Fig. 3.30 Strain gage placement on longitudinal bars.

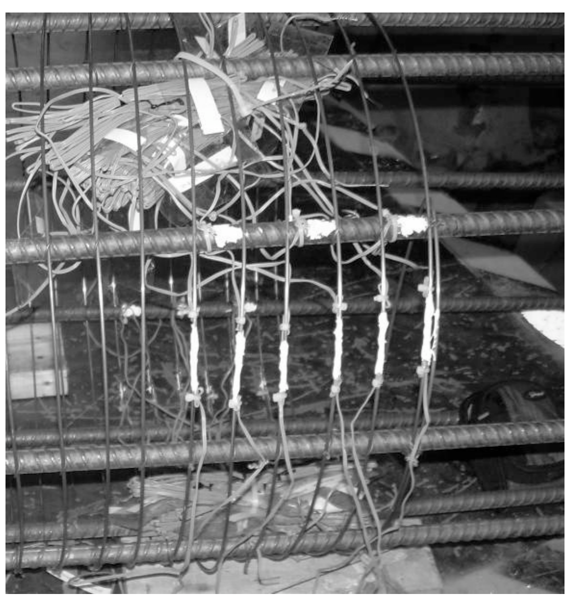

Fig. 3.31 Strain gages on both spiral and longitudinal bars shown on CT7.

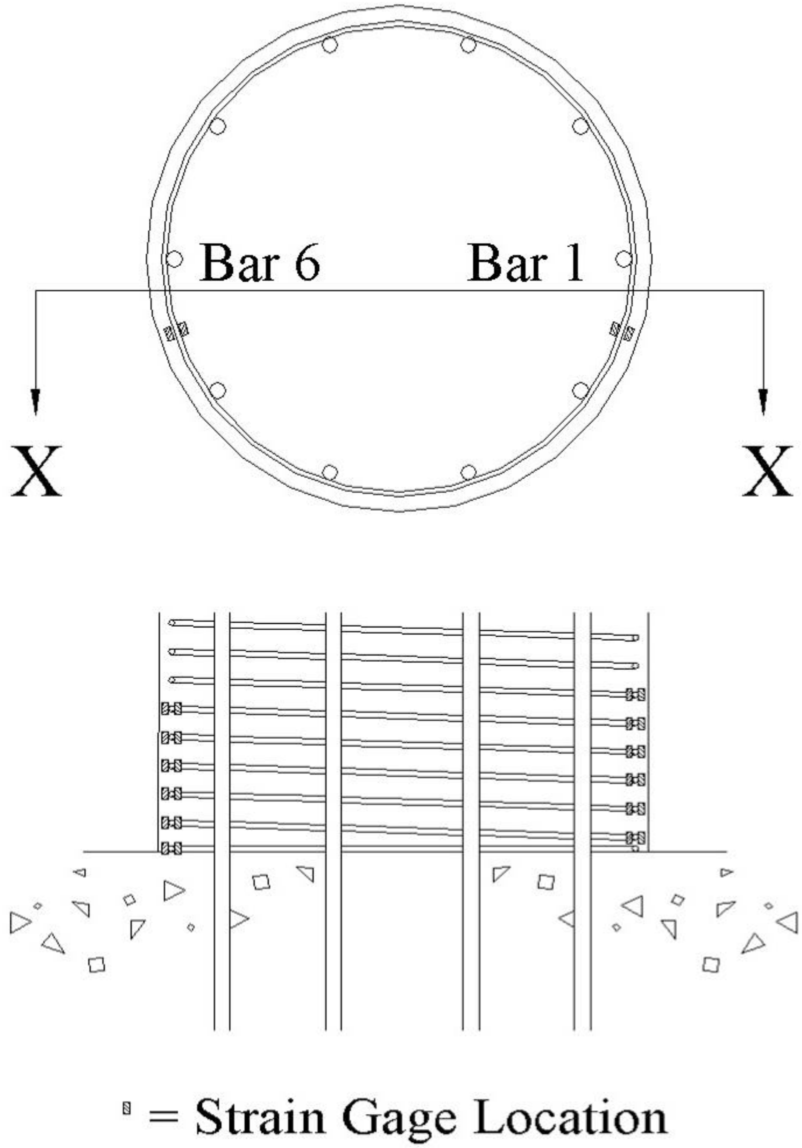

Fig. 3.32 Strain gage placement on spirals.

3.5.7 Photogrammetry

A digital photogrammetric system was used to capture three-dimensional displacements of the test columns. This system used four Canon EOS 20D digital cameras with 17–85mm zoom lenses. All four cameras were linked together such that they could take pictures simultaneously. Each camera was placed around the column as shown in Figure 3.33. Each point of interest was covered by two cameras, thus each point would show up clearly in at least two photographs. The view from each camera can be seen in Figure 3.34.

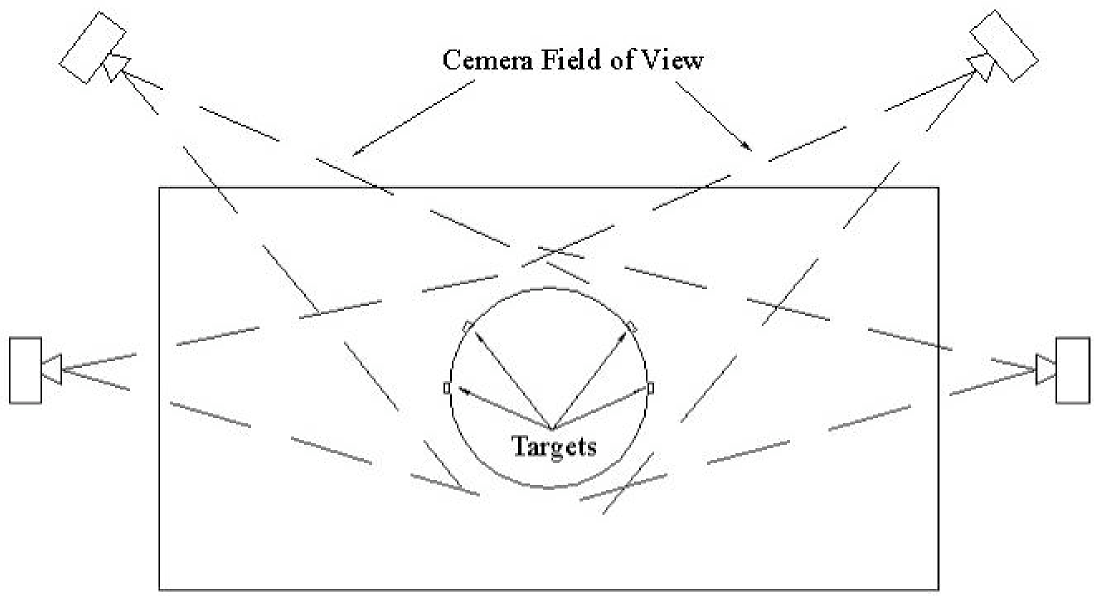

Fig. 3.33 Arial view of photogrammetry camera setup.

The software package Eos Systems' PhotoModeler Pro was used for image analysis. Special coded paper targets were attached to the column and tracked by the software. These targets are shown in Figures 3.33–3.34.

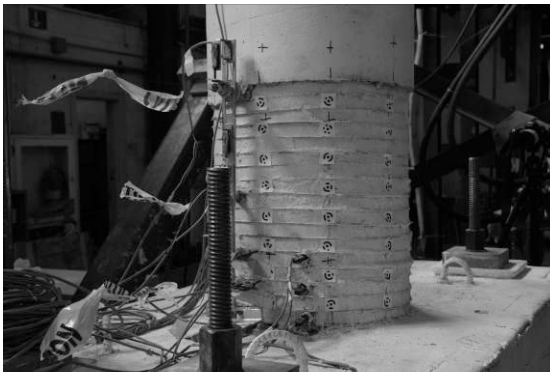

(a) Camera 1

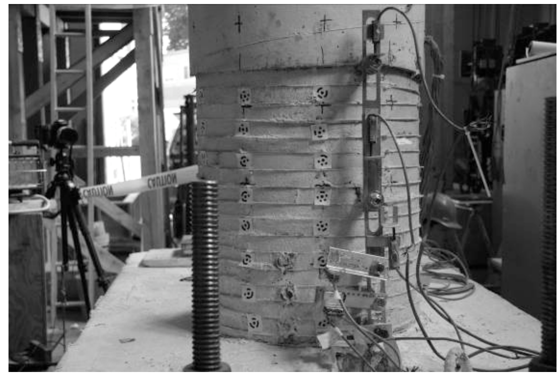

(c) Camera 3

(b) Camera 2

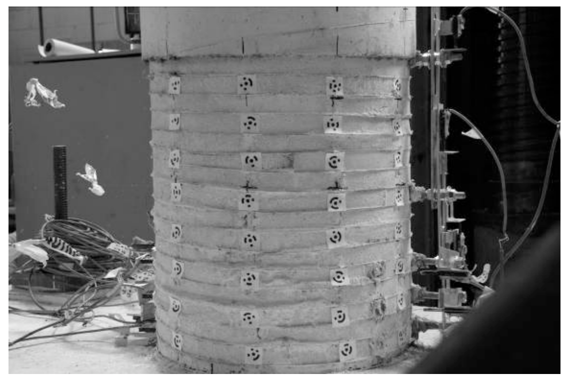

(d) Camera 4

Fig. 3.34 Examples of camera pictures from Specimen CT7.

Cameras were set to take 8.2 megapixel photos in black and white. The black and white setting permits the best resolution for a given file size because no color information is stored. The sharpness was set to minimum to help prevent data distortion. Manual focus was used and kept constant throughout the photos to ensure that all photos could be calibrated identically. Lens stabilization was also turned off to reduce errors. The cameras were placed on tripods which were stabilized by taping down the legs and hanging weights from them.

4 Test Observations

Observations were recorded throughout testing. The damage states most relevant to bar buckling were recorded for all of the columns, and are defined in Table 4.1.

Table 4.1 also shows the icons that are used to identify those same damage states on the plots of drift versus data point number for each column. For reference, the bar numbering designation of the test specimens is shown in Figure 4.1. This is needed because Bar 1 buckled during loading in the northerly direction, and Bar 6 buckled during loading in the southerly direction.

Table 4.2 shows the test matrix for all eight tests, and includes the target drift ratio histories for Specimens CT5–CT8, which were tested in this phase of the research and subjected to the RDH drift history (Fig. 4.2). Because of its extreme asymmetry, the definition of a cycle is not unique, and the history is instead defined in terms of half cycles. The test matrix also contains the actual values of strength and stiffness of the spirals from material tests.

Example photos of each damage state can be seen in Figure 4.3. Observations of Group 1 columns can be found in Freytag (2006).

Table 4.1 Damage milestone definitions.

Damage State	Criterion	Icon
Flexural cracking	First visible cracking	●
Diagonal cracking	Cracking angled 30 to 60	■
Yield of longitudinal bars	Strain gage reading at any location	▲
Yield of spiral	Strain gage reading at any location	◆
First visual sign of bar buckling	Longitudinal bar is no longer straight	★
First sign of spiral kinking	Plastic bend in spiral around bar	✚
Spiral fracture	Fracture of spiral at any point	▼
Bar fracture	Fracture of any longitudinal bar	♥
Loss of axial load capacity	Inability to resist applied load	☾

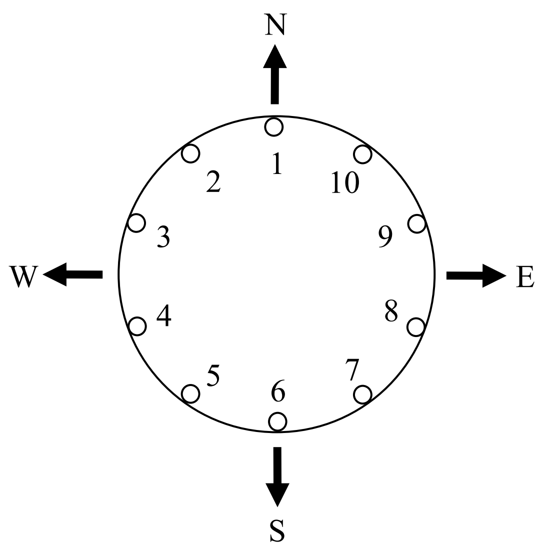

Fig. 4.1 Bar numbering designation.

Table 4.2 Test matrix.

Name	Cover	Drift History	$\rho E_s/f'_c$	$\rho f_y/f'_c$	Bar End Condition
CT1	1	BDH	30	0.036	Grouted Ducts
CT2	1/2	BDH	6	0.056	Grouted Ducts
CT3	0	ODH	34	0.106	Grouted Ducts
CT4	0	RDH	13	0.127	Grouted Ducts
CT5	0	RDH	34	0.105	Grouted Ducts
CT6	0	RDH	35	0.110	Standard Hooks
CT7	0	RDH	33	0.103	Grouted Ducts
CT8	0	RDH	35	0.110	Grouted Ducts

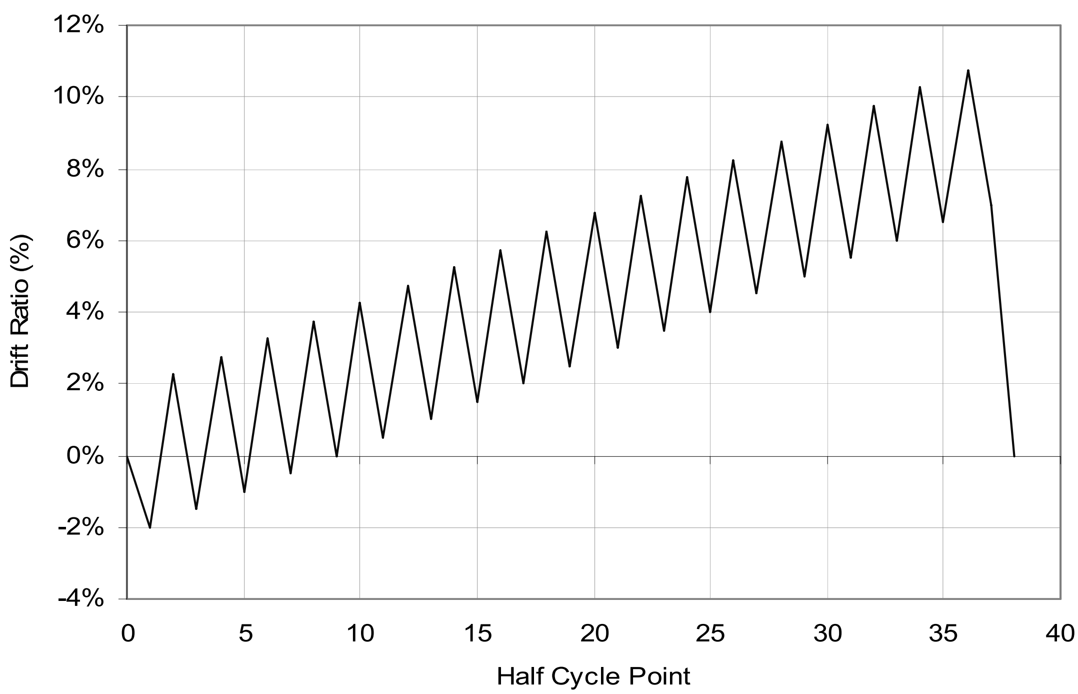

Fig. 4.2 Ratcheting drift history (RDH) target values.

(a) Cracking (b) Spiral kinking (c) Bar buckling

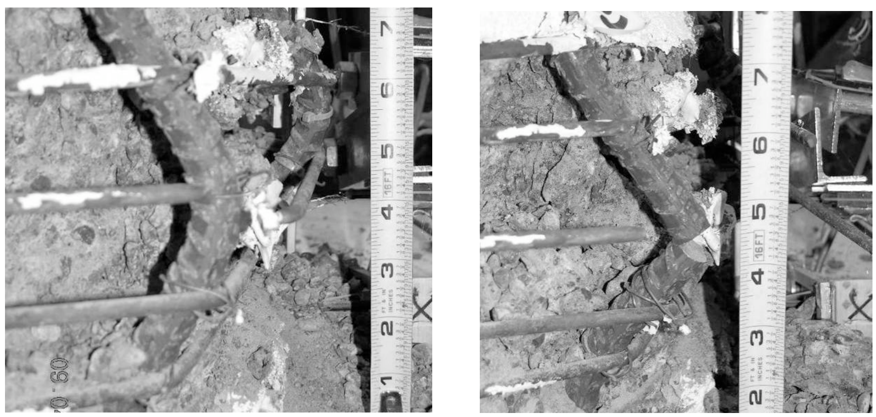

(d) Spiral fracture (e) Bar fracture

Fig. 4.3 Example photos of damage states.

4.1 SPECIMEN CT5

Specimen CT5 was cycled through the RDH displacement history, had low stiffness spiral, had no cover, and had longitudinal bars anchored in grouted ducts. The actual drift history showing the damage states for this specimen is shown in Figure 4.4, and Table 4.3 states the cycle and drift where each event occurred. The loading algorithm that was used for the RDH was not well established at the beginning of Specimen CT5; therefore there were some differences between the actual and target drift histories (Fig. 4.4). In all columns, the actual drifts were slightly smaller than the target values because the reaction rig had some flexibility and the displacement was controlled from the displacement sensor in the actuator.

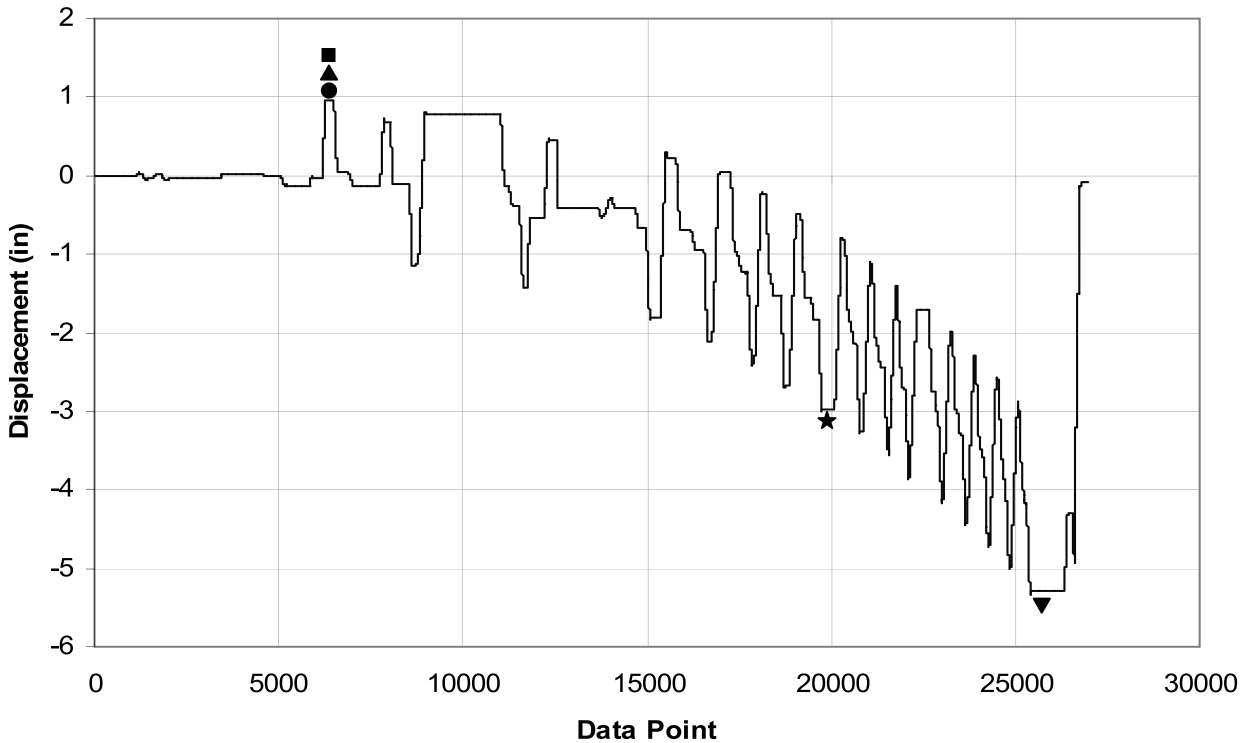

Fig. 4.4 Drift history for Specimen CT5 with damage states.

Table 4.3 Damage states for Specimen CT5.

Damage State	Cycle	Target Drift	Actual Drift	Icon
Flexural cracking	1	-2%	-1.6%	●
Diagonal cracking	1	-2%	-1.6%	■
Yield of longitudinal bars	1	-2%	-1.6%	▲
Yield of spiral	not recorded	---	---	◆
First visual sign of bar buckling	14	5.25%	5.0%	★
First sign of spiral kinking	not recorded	---	---	✚
Spiral fracture	30	9.25%	8.9%	▼
Bar fracture	Not reached	---	---	✖
Loss of axial load capacity	Not reached	---	---	☾

Cracking was first observed in Cycle 1 and was well distributed over the plastic hinge region; both flexural cracks and diagonal cracks were present. A crack also formed at the column-footing interface during Cycle 1. Starting with Cycle 2 a crack within the hinge region and 9″ above the footing on the north side of the column was selected for tracking throughout the test. The width of this crack after various cycles is noted in Table 4.4; Cycles 2 and 4 brought about additional cracking and extension and widening of previous cracks but little else. No new damage was found after Cycles 3 and 5 because these cycles were at a lower drift than previous cycles.

Table 4.4 Width of measured crack for Specimen CT5.

Cycle	Crack Width
2	1.0 mm
4	1.5 mm
5	0.33 mm
6	2.0 mm
8	1.75 mm
10	1.75 mm
12	1.0 mm
14	1.0 mm

The longitudinal reinforcement began to debond within the column starting at Cycle 6. This was apparent from small diagonal cracks distributed around bars, as illustrated in Figure 4.9. After Cycle 8 the interface crack had widened to 0.20″, which was the largest crack at the time. At this point the pieces of the spiral about 11″ from the footing began to separate from each other (see Fig. 4.5) on the south face. This was the same height as a fairly large flexural-shear crack that had began to form in the column. The interface crack had significantly widened (see Fig. 4.6) as well at this point.

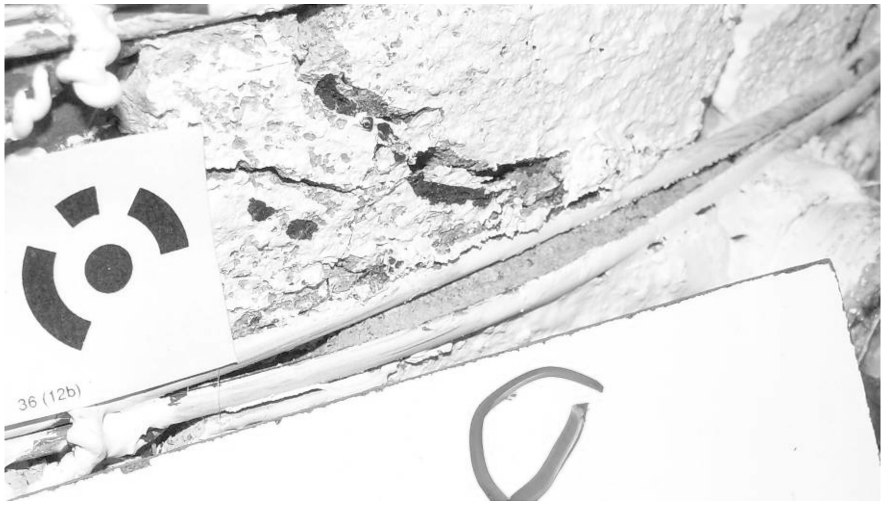

Fig. 4.5 CT5 spiral separation, Cycle 8.

Fig. 4.6 CT5 interface crack, Cycle 8.

At Cycle 12 the debonding cracks had grown considerably in size and number, and the crack at the interface continued to widen. At the large shear crack, there was significant movement of the upper section of the column compared to the lower section, as can be seen in Figure 4.7.

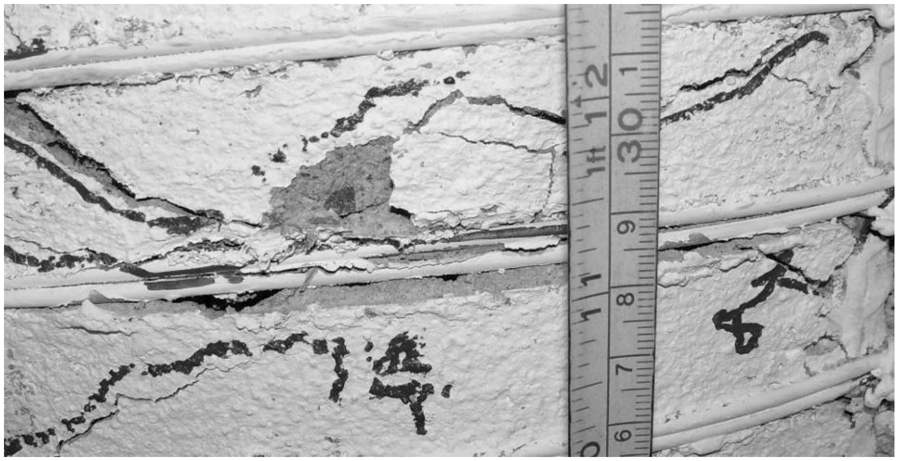

Fig. 4.7 CT5 large crack on south face, Cycle 12.

A slight buckling was noticed on the north side (Bar 6) after Cycle 14, as shown in Figure 4.8. After Cycle 15 a significant number of debonding cracks had appeared around Bars 1, 2, and 10. Some of these areas also displayed some crushing of the concrete around these cracks (see Fig. 4.9). Bar 1 had begun to buckle during Cycle 15 at two different points along its height. This was probably due to the fact that the large shear crack was wide enough for the spiral to fit inside it. The spiral could sink back into the column, and pull the bar back with it, thus giving the shape shown in Figure 4.10.

During Cycles 16 and 18, Bar 6 had a buckled length of 5 spiral spacings, or approximately 6″. Bars 1 and 10 both had some residual bending left over after returning to tension during Cycle 18.

Beginning with Cycle 18, the spirals on the south side 11″ from the base started to drop into the large shear crack. This caused the spirals to bend into straight lines between the longitudinal bars instead of the original circular shape; this can be seen in Figure 4.11.

Fig. 4.8 CT5 beginning of buckling on Bar 6, Cycle 14.

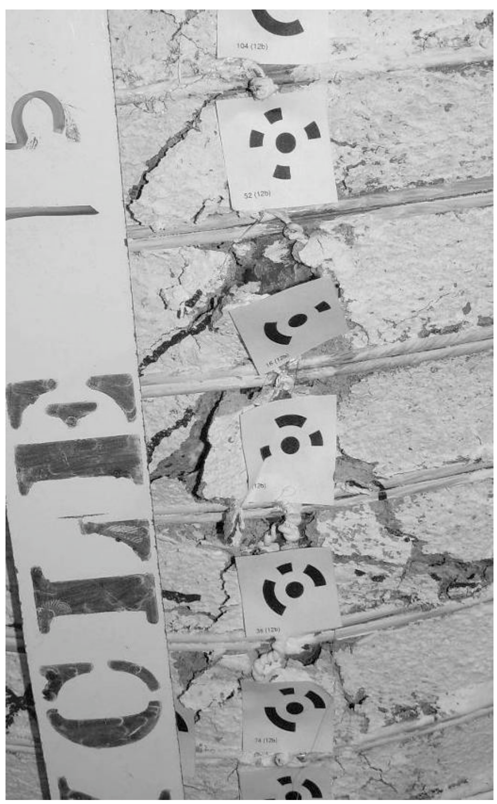

Fig. 4.9 CT5 debonding around Bar 10, Cycle 15.

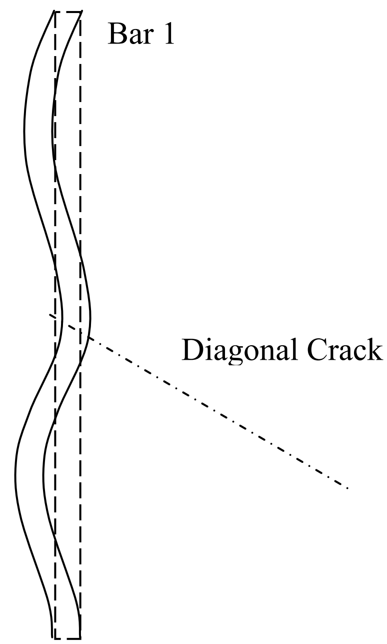

Fig. 4.10 Double buckling of Bar 1 for CT5.

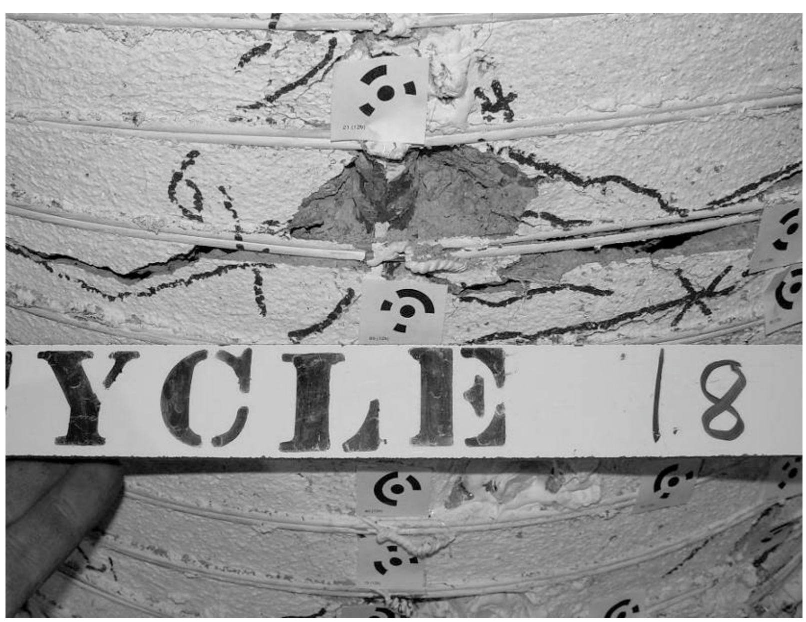

Fig. 4.11 CT5 large crack on south face, Cycle 18.

Figure 4.12 shows the buckling of Bar 6 after Cycle 20, and at this point the spiral is noticeably kinked. By Cycle 24 the amount of buckling in Bar 6 and the kinking of the spiral had increased even further (see Fig. 4.13). The shear crack at this point was very wide and extended at least 2/3 of the column depth. Almost all of the column rotation appeared to be coming from the shear crack and the interface crack.

During Cycle 30, the spirals 3″ above the footing fractured close to Bar 6. The failure was sudden and quite brittle. The spiral unwrapped itself for about 2 turns both up and down the column from the fracture point (see Fig. 4.14). When the drift returned to zero, all of the bars on the south side, now unrestrained by the spiral, buckled freely as shown in Figure 4.16. Figure 4.15 shows the residual bending in Bar 1 after returning to zero after spiral fracture.

During the later cycles it was noticed that the applied rotation was greater than the rotation capacity of the spherical bearing on top of the column, which was undergoing metal-to-metal contact. It was later discovered that this greatly affected the load supplied by the actuator. The bearing was then machined down to allow more rotation before Specimens CT7 and CT8.

Fig. 4.12 CT5 kinking of spiral around Bar 6, Cycle 20.

Fig. 4.13 CT5 Bar 6 buckling over multiple spirals, Cycle 24.

Fig. 4.14 CT5 spiral fracture, Cycle 30.

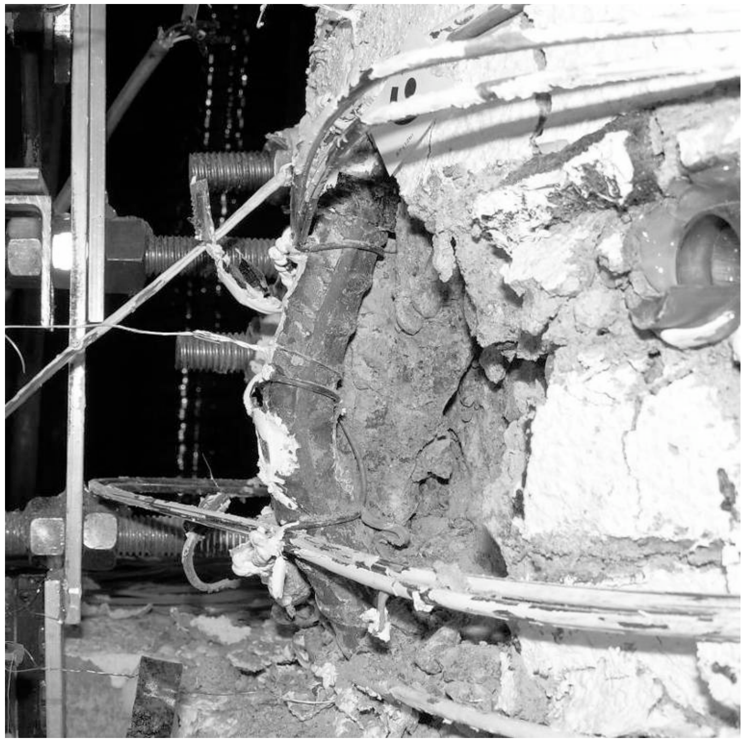

Fig. 4.15 CT5 Bar 6 buckling in final damage state.

Fig. 4.16 CT5 Bars 1, 2, and 20 buckling in final damage state.

4.2 SPECIMEN CT6

Specimen CT6 was cycled through the RDH displacement history, had normal spiral stiffness, had no cover, and was anchored with standard hooks. The actual drift history showing the damage states for this specimen is shown in Figure 4.17, and Table 4.5 states the cycle and drift where each event occurred.

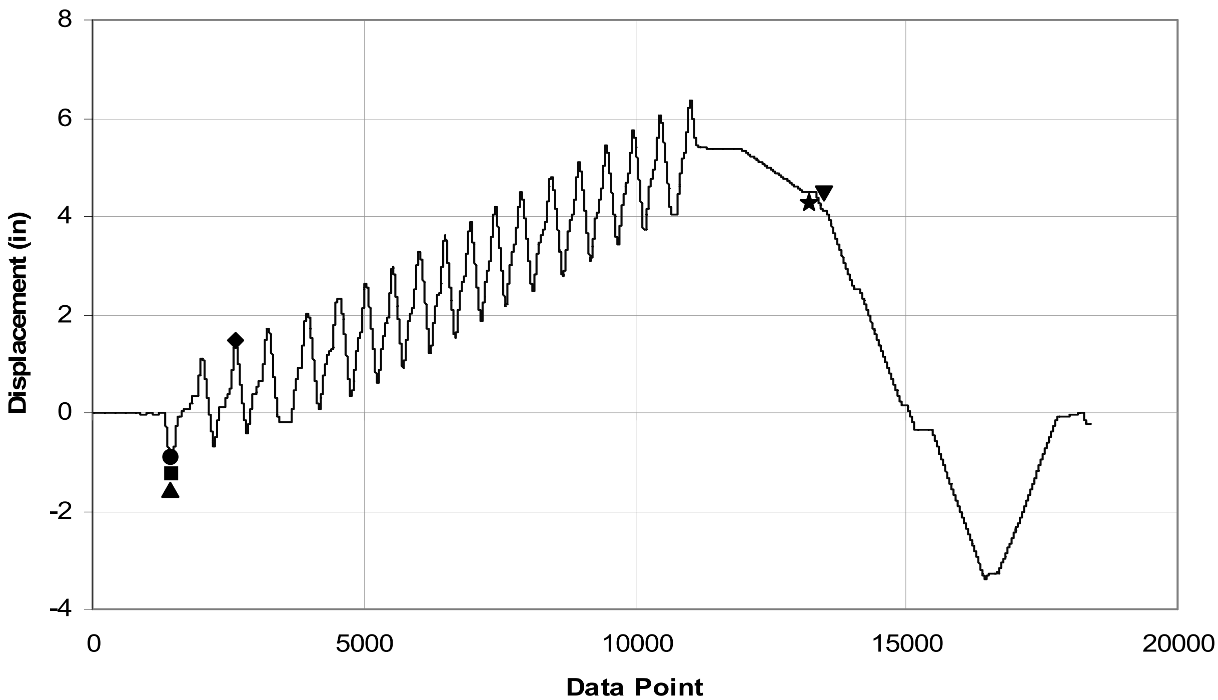

Fig. 4.17 Drift history for Specimen CT6 with damage states.

Table 4.5 Damage states for Specimen CT6.

Damage State	Cycle Point	Target Drift	Actual Drift	Icon
Flexural cracking	1	-2%	-1.6%	●
Diagonal cracking	1	-2%	-1.6%	■
Yield of longitudinal bars	1	-2%	-1.6%	▲
Yield of spiral	4	2.75%	2.3%	◆
First visual sign of bar buckling	37	N/A	5.6%	★
First sign of spiral kinking	Not recorded	---	---	✚
Spiral fracture	37	N/A	5.6%	▼
Bar fracture	Not reached	---	---	✖
Loss of axial load capacity	Not reached	---	---	☾

Cracking in the column began on Cycle 1. Throughout the majority of the test, the crack widths of an arbitrarily chosen crack ("measured crack" in the table) and the interface crack were recorded in Table 4.6. The measured crack was at an elevation of 11″ above the footing. The beginning of this test was very similar to CT5 except that the interface crack was larger than in CT5. Flexural and shear cracks developed early and continued to grow in width, length, and number through Cycle 12. Figure 4.18 shows the cracking on the west face of the column. Cycle 14 produced a few small radial cracks in the footing. There were a few very wide cracks within the bottom 1.5″ of the column (see Fig. 4.19).

Between Cycles 16–30 no additional damage occurred besides slight lengthening and widening of cracks. During Cycles 30 and 32 some flaking occurred (see Fig. 4.20) in the compression zone. At Cycle 32 one of the spirals began to drop into a flexural crack (Fig. 4.21), as happened in CT5. At Cycle 36 the stroke limit of the actuator was reached. With no significant damage to the column and no visible sign of bar buckling, it was decided that the column would then be cycled at the maximum drift.

Table 4.6 Widths of measured and interface cracks for Specimen CT6.

Cycle	Measured Crack	Interface Crack
2	1.0 mm	---
4	1.5 mm	---
6	1.5 mm	---
8	1.5 mm	1.5 mm
10	2.0 mm	---
12	2.5 mm	2.0 mm
14	3.5 mm	3.5 mm
16	3.5 mm	4.0 mm
18	3.5 mm	5.0 mm
20	3.5 mm	5.0 mm
22	5.0 mm	6.0 mm
24	5.0 mm	6.0 mm
28	4.0 mm	9.0 mm
30	7.0 mm	6.0 mm
32	3.0 mm	5.0 mm

Fig. 4.18 CT6 cracking on west face, Cycle 12.

Fig. 4.19 CT6 large cracks at column base, Cycle 16.

Fig. 4.20 CT6 flaking in compression zone, Cycle 32.

Fig. 4.21 CT6 spiral dropping into crack, Cycle 32.

On the return to zero displacement after Cycle 36, Bar 1 began to buckle (Fig. 4.22). Soon after the buckling of Bar 1, the spiral fractured at Bar 1 at the fourth turn up from the footing (Fig. 4.23). Unlike the spiral fracture in CT5, this spiral did not unwrap at all but seemed to remain bonded to the core concrete around the sides. The third and fifth turns of the spirals around Bar 1 were significantly kinked. Bar 2 was also showing signs of buckling and the third turn of the spiral was kinked where it was in contact with Bar 2.

As the column was pushed closer to zero drift Bar 10 began to buckle and fractured the spiral surrounding it at the second turn from the footing. The curvature of Bars 1 and 2 became more pronounced as they were no longer restrained by the spirals. Once the column reached a drift of about -5%, it was returned to zero displacement and Bars 5, 6, and 7 all buckled, as they were not restrained by the spirals either.

Fig. 4.22 CT6 buckling and spiral fracture.

Fig. 4.23 CT6 buckling of Bar 1.

4.3 SPECIMEN CT7

Specimen CT7 was cycled through the RDH displacement history, had low strength and stiffness spiral, had no cover, and was anchored in grouted ducts. The actual drift history showing the damage states for this specimen is shown in Figure 4.24, and Table 4.7 states the cycle and drift where each event occurred.

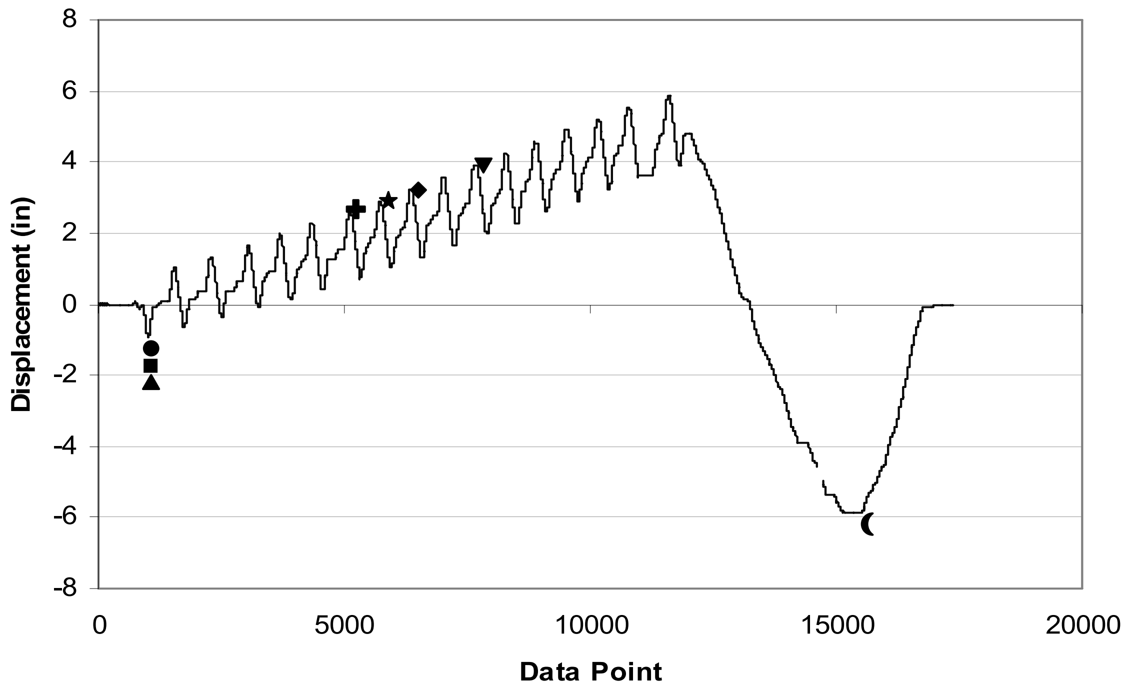

Fig. 4.24 Drift history for Specimen CT7 with damage states.

Table 4.7 Damage states for Specimen CT7.

Damage State	Cycle Point	Target Drift	Actual Drift	Icon
Flexural cracking	1	-2%	-1.5%	●
Diagonal cracking	1	-2%	-1.5%	■
Yield of longitudinal bars	1	-2%	-1.5%	▲
Yield of spiral	16	5.75%	5.25%	◆
First visual sign of bar buckling	14	5.25%	4.75%	★
First sign of spiral kinking	12	4.75%	4.25%	✚
Spiral fracture	20	6.75%	6.5%	▼
Bar fracture	Not reached	---	---	✖
Loss of axial load capacity	Data# 15128	N/A	-9.7%	☾

An arbitrary crack was selected and its width was recorded in Table 4.8 for various cycles, it was located at an elevation of 12″ above the footing. Cracking began forming starting with Cycle 1. By Cycle 4 diagonal cracking began to form similar to CT5. By the end of Cycle 8 the spirals that had to be patched with grout (as discussed in Section 3.3.6) began to slice though the grout patches behind them (Fig. 4.25). During Cycle 10 a large shear crack started to develop at about the same height as the shear crack in CT5.

During Cycle 12 the spiral around Bar 6 started to kink indicating that buckling would soon follow. (However, note that the spiral wire used here was much thinner than the standard material, and had a lower yield moment). The crack width at the interface was virtually zero at these cycles. Cycle 14 brought about visible buckling in Bar 6 (see Fig. 4.26). At this point the shear crack was quite wide, as can be seen in Figure 4.27. At Cycle 15, Bar 1 began to buckle, with the wave centered about 12″ above the footing (see Fig. 4.28). It was noted that the bar was buckling at the same point where the shear crack intersected the bar; this is quite the opposite of the behavior shown in Figure 4.10. This behavior could be caused by the wide crack that intersected the bar at this point; most of the deformation was concentrated at this point and thus the bar underwent the most yielding in tension at this point. The large amount of tension strain in the bar at this point would greatly encourage buckling. The difference between Figure 4.27 and Figure 4.29 shows how much the crack widened over one full cycle. The concrete directly surrounding the Bar 1 buckled length was crushed (see Fig. 4.30), probably due to the debonding of the bar and the local loss of confinement from the bar buckling. During Cycle 19, Bar 1 remained in a buckled shape even though it was located on the tension face of the column.

Table 4.8 Width of measured crack for Specimen CT7.

Cycle	Crack Width
4	1.5 mm
8	0.125″
10	0.125″
12	0.125″
14	0.1875″
16	0.25″
18	0.4375″

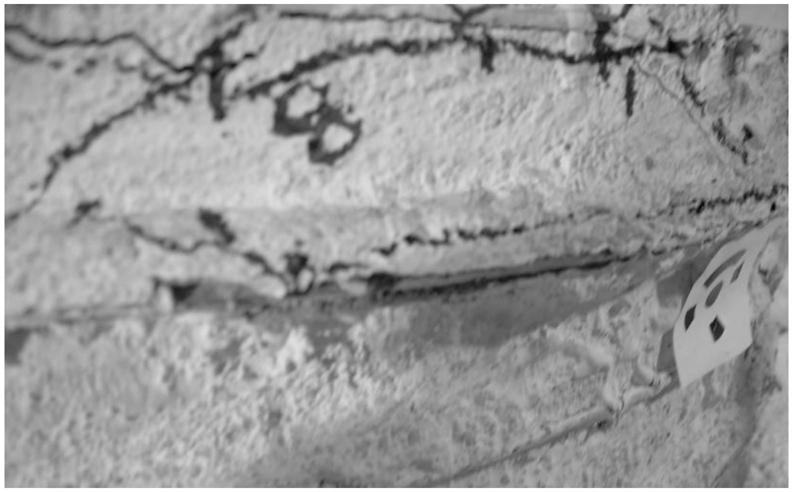

Fig. 4.25 CT7 spiral slicing through grout patching, Cycle 8.

Fig. 4.26 CT7 buckling of Bar 6, Cycle 14.

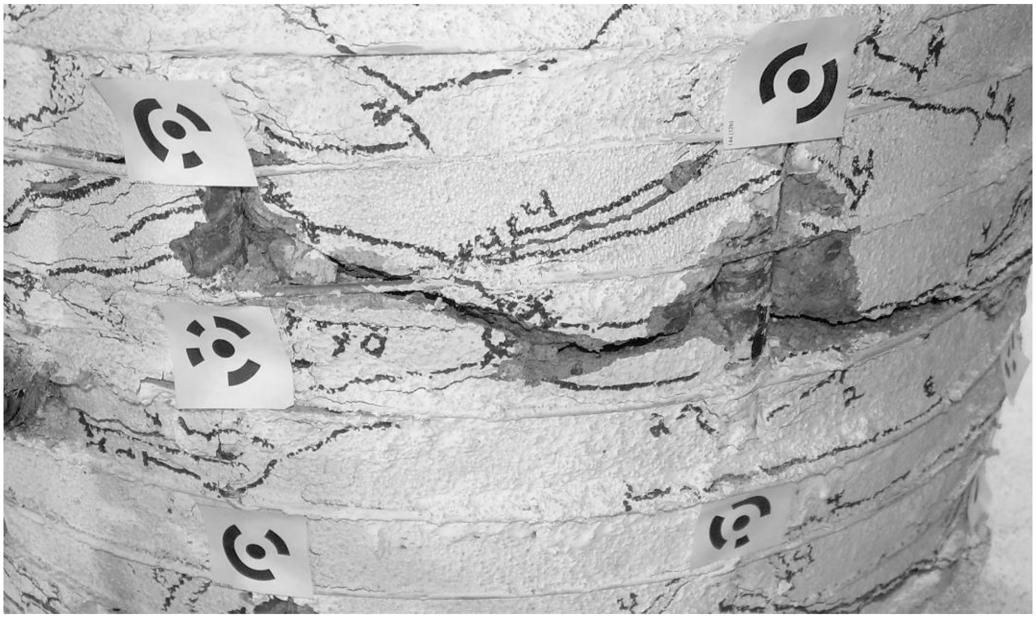

Fig. 4.27 CT7 wide shear crack on north face, Cycle 14.

Fig. 4.28 CT7 buckling of Bar 1, Cycle 15.

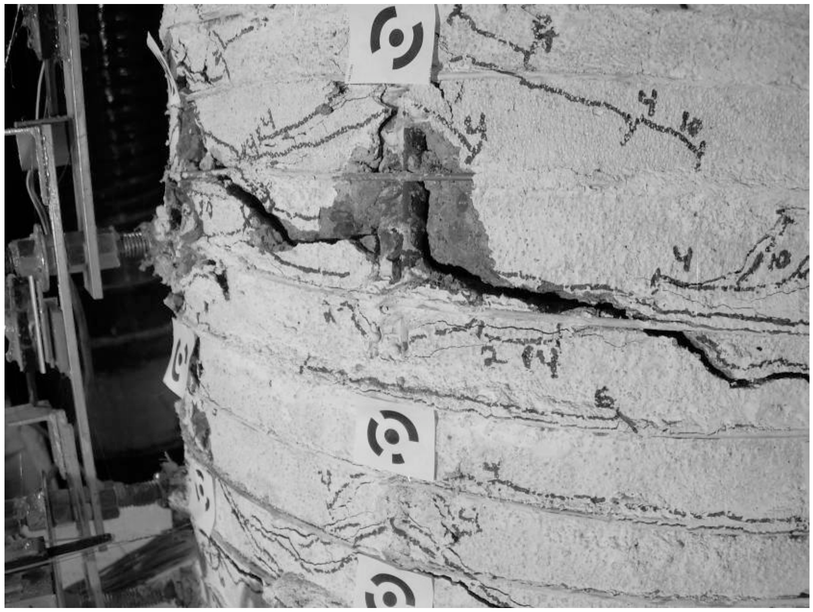

Fig. 4.29 CT7 large shear on north column face, Cycle 16.

Fig. 4.30 CT7 Bar 1 buckling, Cycle 17.

After Cycle 20 the spiral fractured at the fourth turn from the base, near Bar 6. This spiral fracture caused the spiral to unwrap for several turns and occurred quite suddenly just as in CT5, in which the same high-strength, small-diameter wire was used. Bars 5 and 7 also began to buckle at this point. The fourth, fifth, and sixth turns of the spiral around Bar 5 and the third, fourth, and fifth turns around Bar 7 were also kinked. Figure 4.31 shows the north face (Bar 1) of the column after spiral fracture, and Figure 4.32 shows the buckling of Bar 6 where the spiral had fractured. At Cycle 23 Bar 2 began to buckle within the bottom 6″ of the column.

During Cycles 24–33 all of the bars that had buckled previously buckled more, and much of the core concrete began to crush significantly. After reaching the displacement limit of the test apparatus the column was returned to zero drift. Upon returning to zero drift (see Fig. 4.33) Bars 1, 2, and 10 were all significantly buckled over 8 spiral spacings, Bar 9 had buckled radially, and Bars 5, 6, and 7 straightened. It was then decided that the column would be cycled at approximately 10% drift in order to attempt to fracture the longitudinal bars; however after one cycle of this procedure, the core became very crushed and it was no longer possible to apply the prescribed axial load (see Fig. 4.34) at which time testing was stopped.

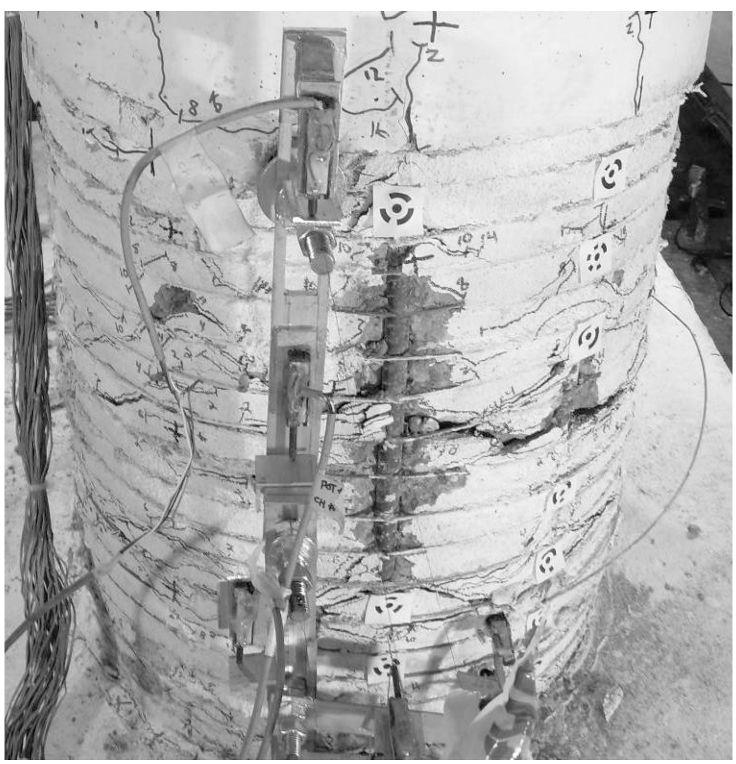

Fig. 4.31 CT7 north face after spiral fracture, Cycle 20.

Fig. 4.32 CT7 buckling on Bar 6, Cycle 22.

Fig. 4.33 CT7 residual buckling on north face at zero drift.

Fig. 4.34 CT7 damage after additional cycles.

4.4 SPECIMEN CT8

Specimen CT8 was cycled through the RDH displacement history, had spiral of low strength but normal stiffness, had no cover, and was anchored in grouted ducts. The actual drift history showing the damage states for this specimen is shown in Figure 4.35, and Table 4.9 states the cycle and drift where each event occurred. Note that in the later part of the displacement history damage states were recorded by data point number rather than by cycle number because the planned drift history was exceeded.

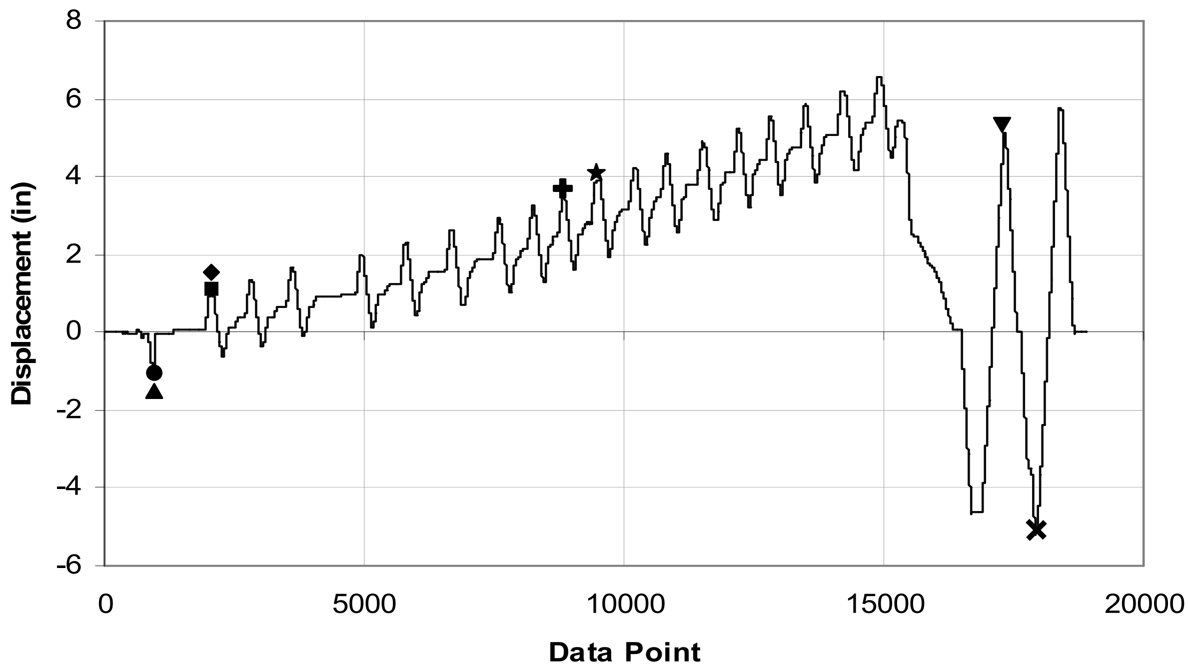

Fig. 4.35 Drift history for Specimen CT8 with damage states.

Table 4.9 Damage states for Specimen CT8.

Damage State	Cycle Point	Target Drift	Actual Drift	Icon
Flexural cracking	1	-2%	-1.5%	●
Diagonal cracking	2	2.25%	1.6%	■
Yield of longitudinal bars	1	-2%	-1.5%	▲
Yield of spiral	2	2.25%	1.6%	◆
First visual sign of bar buckling	20	6.75%	6.4%	★
First sign of spiral kinking	18	6.25%	5.6%	✚
Spiral fracture	Data# 17328	N/A	8.6%	▼
Bar fracture	Data# 17821	N/A	-8.6%	✖
Loss of axial load capacity	Not reached	---	---	☾

Cycle 1 induced cracking on the specimen; however the extent of cracking was unknown. This was due to an actuator malfunction, where the column was returned to zero drift prematurely, so data were not recorded for the return to zero. In Cycles 2–11 additional cracking and some spalling of the excess concrete occurred. During most of these cycles crack widths were measured and recorded in Table 4.10. The arbitrary crack was located approximately 8″ from the base and the shear crack was located about 13″ from the base. By Cycle 12 the flexural cracking was well distributed over the plastic hinge region, as shown in Figure 4.36, and the crack map, as shown in Figure 4.37. This cracking was much more distributed than in the past three specimens.

The excess concrete that surrounded the spirals had spalled off by Cycle 15, as shown in Figure 4.38. The fourth and fifth turns of the spiral on the south side of the column began to kink significantly in Cycle 18. During Cycle 20 buckling of Bar 6 was observed. When Bar 6 partially straightened in Cycle 21, the spiral did not rebound with the bar as it had in all of the other specimens, but instead remained bent and separated from the bar about 1/8″. This behavior was even more obvious in Cycle 23 (Fig. 4.39) during which the separation distance increased to ¼″.

Table 4.10 Width of various cracks for Specimen CT8.

Cycle	Arbitrary Crack	Interface Crack	Shear Crack
4	---	2 mm	---
6	---	2 mm	---
8	1.5 mm	1/8″	---
10	2.0 mm	1/8″	3/32″
12	1/8″	3/32″	3/32″
14	1/4″	1/8″	5/32″
16	9/32″	5/32″	5/32″
18	5/16″	5/32″	3/16″
20	11/32″	5/32″	3/16″
22	3/8″	3/16″	3/16″
26	1/2″	3/16″	3/16″
30	19/32″	3/16″	3/16″
36	5/8″	3/16″	3/16″

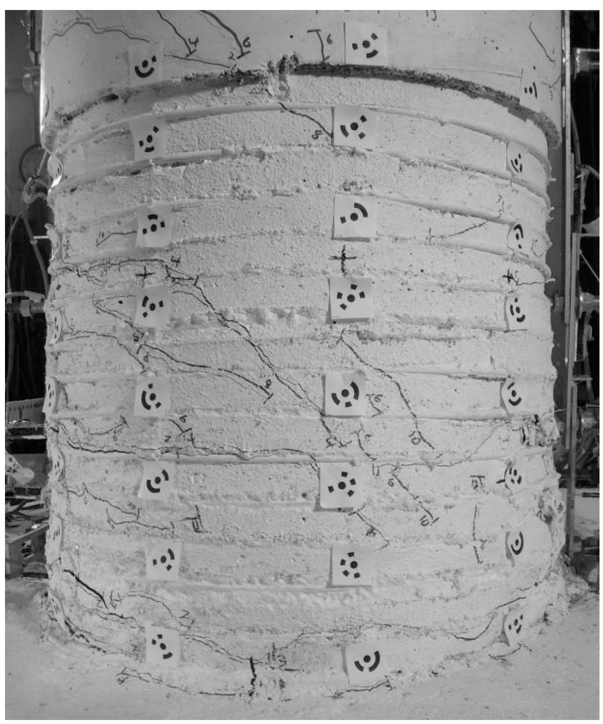

Fig. 4.36 CT8 diagonal cracking on west face, Cycle 12.

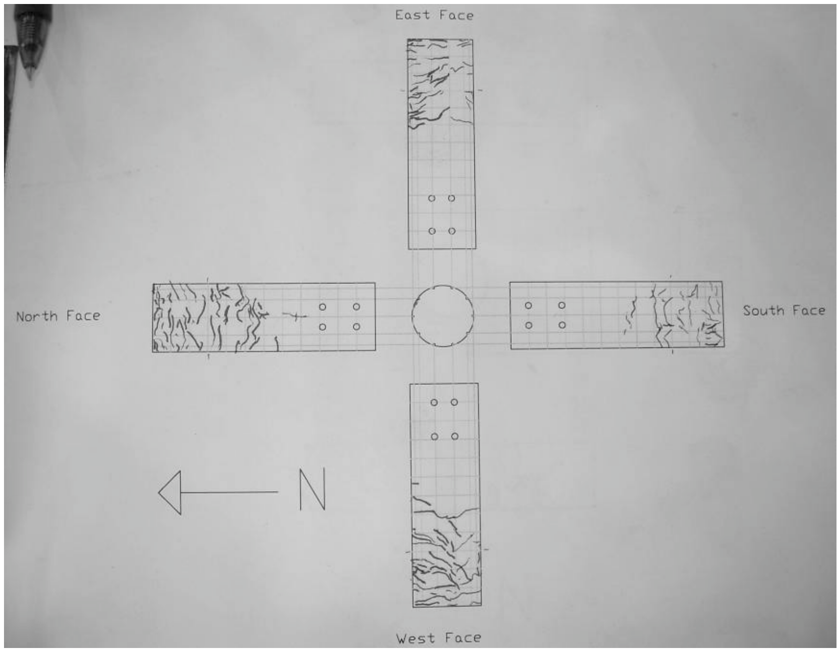

Fig. 4.37 Crack diagram for Specimen CT8 at Cycle 12.

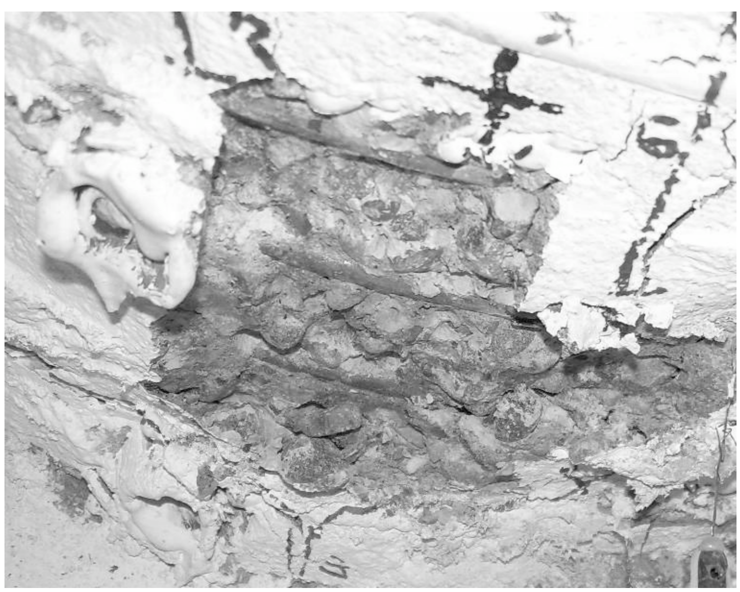

Fig. 4.38 CT8 spalling of excess concrete, Cycle 15.

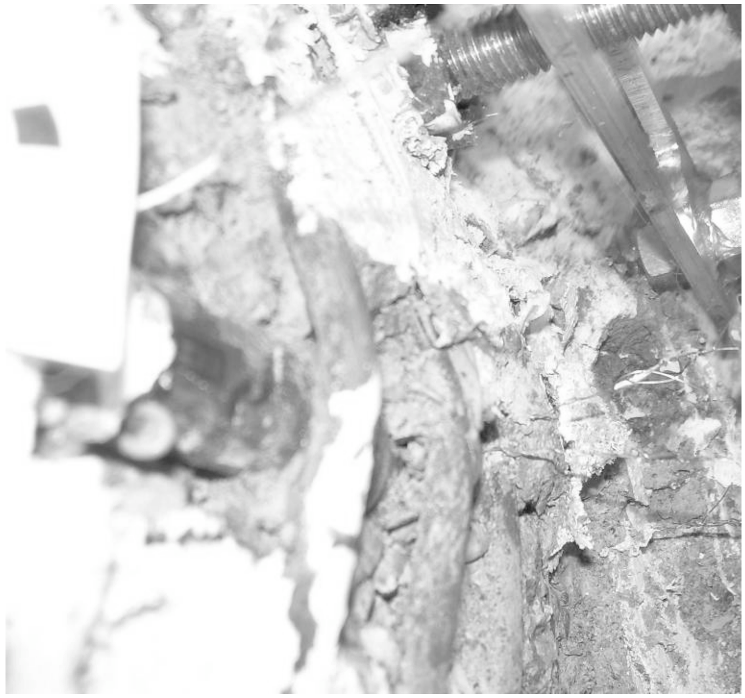

Fig. 4.39 CT8 spiral kinking and separation on Bar 6, Cycle 23.

Bar 7 was visibly buckled by Cycle 24 and the buckling of Bar 6 significantly increased (see Fig. 4.40). By Cycle 26, Bar 6 had undergone a large buckling displacement and a significant permanent kink was present in the spiral. Bar 5 also began to buckle during Cycle 30. By Cycle 31, Bar 6 was in tension but had not straightened. Figure 4.41 shows the residual buckled shape of Bar 6, as well as the distance between the spiral and the bar at this point.

Bar 1 began to buckle over a few spiral spacings centered about 12″ from the base at data point 15546, as seen in Figure 4.42. This buckling behavior is similar to what was seen in CT7 Bar 6 where the buckled shape was located about 12″ up from the footing. Bar 6 had almost completely straightened at this point as well. The column was then brought back to zero displacement at data point 16343. Bars 1 and 2 were buckled both at 12″ and 3″ from the footing, Bar 10 was buckled about 4″ from the footing, Bar 9 began to show signs of buckling, and Bars 5, 6, and 7 all appeared to be straight at this point. Bars 5, 6, and 7 each had a space between them and their respective spirals of 1/4″, 1/2″, and 1/8″, respectively.

Fig. 4.40 CT8 buckling of Bar 6, Cycle 24.

Fig. 4.41 CT8 residual buckling of Bar 6, Cycle 31.

Fig. 4.42 CT8 buckling of Bar 1, data point 15546.

When the column was pushed back to approximately +5″ (data point 16773), Bars 1 and 2 had buckled lengths of about 3 spiral spacings (Fig. 4.44) approximately 12″ up from the base of the footing. At this drift level all of the bars on the south side of the column had become very straight, and the distance between the straight bar and the spiral was up to an inch (see Fig. 4.43). The spirals surrounding the buckled bars were no longer circular but instead were polygons with vertices at the locations of the longitudinal bars, as shown in Figure 4.45. It was concluded that they were working primarily in tension rather than bending. This change in shape of the spiral was much more extreme than in any of the other specimens, and is attributed to the large ductility capacity of the annealed spiral.

Fig. 4.43 CT8 gap between spiral and Bar 6, data point 16773.

Fig. 4.44 CT8 buckling of Bars 1 and 2, data point 16773.

The column was then pushed to a drift of approximately -5″ (data point 17328). At this drift level, fracture of the fifth spiral turn up from the base occurred around Bar 5 as shown in Figure 4.46. Bars 5, 6, and 7 were buckled over approximately 5 spiral spacings when the spiral fractured. At data point 17821 another spiral turn fracture occurred, this time located at Bar 2, 10 turns up from the base (see Fig. 4.47). At this point Bar 6 also fractured at about 6″ from the footing (see Fig. 4.48). Bar fracture occurred on Bar 5 about 5.5″ from the footing at data point 17928. Bars 1 and 2 also fractured on data point 18397 as can be seen in Figure 4.49. These bar fractures were also accompanied by a spiral fracture around Bar 5 when the two fractured ends of Bar 5 compressed together, pushed outwards and broke the spiral (see Fig. 4.50).

The behavior of Specimen CT8 differed markedly from that of Specimens CT5 and CT7. The difference was attributed to the spiral material. In Specimen CT8, the spiral was made from 0.25″ diameter wire, annealed to have a yield strength of approximately 30 ksi, whereas in the other two specimens the wire was 0.1″ diameter with a yield strength of approximately 300 ksi. The former kinked extensively at each longitudinal bar so that when the first spiral fracture occurred, the kinks acted as bends around the bars, which therefore provided anchorage and enabled the spiral turns distant from the fracture point to develop tension and provide some confinement to the core concrete. This ductile behavior was possible because the material has a large elongation at fracture and exhibits extensive strain hardening. By contrast the high-strength, small-diameter material remained essentially elastic over most of its length, and sprang away from the column core as soon as the first fracture occurred. This occurred because the material has a relatively small ratio of ultimate strength to yield strength, as is typical of high-strength steels.

Fig. 4.45 CT8 residual bending of spirals, data point 17328.

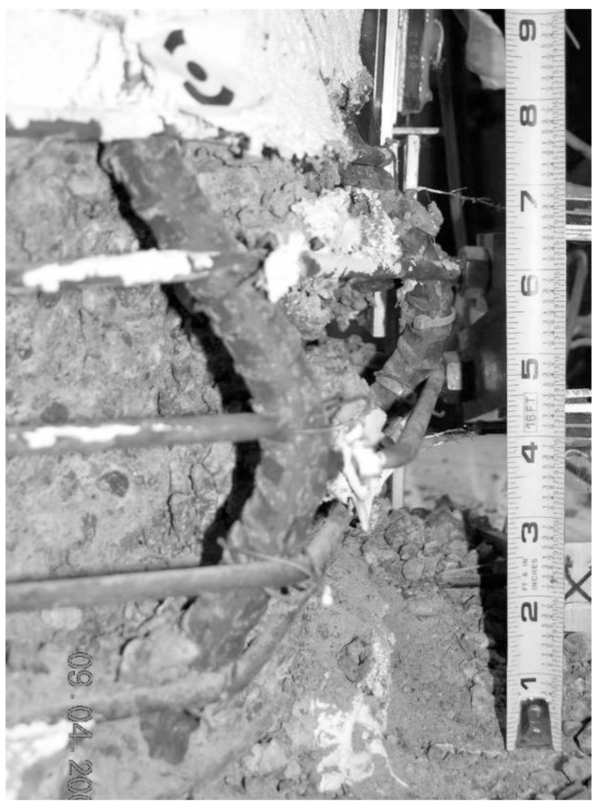

Fig. 4.46 CT8 spiral fracture around Bar 5, data point 17328.

Fig. 4.47 CT8 buckling of Bars 1 and 2 and spiral fracture, data point 17821.

Fig. 4.48 CT8 fracture of Bar 6, data point 17821.

Fig. 4.49 CT8 fracture of Bars 1 and 2, data point 18397.

Fig. 4.50 CT8 spiral fracture around Bar 5.

5 Measured Data

In addition to the observations made in the previous chapter, data were collected and analyzed to characterize the behavior of the bar-buckling mechanism. This chapter isolates the effects of different column parameters that may influence bar buckling and studies each. This section presents data from Group 2 columns only. Data from Group 1 columns can be found in Freytag (2006).

5.1 GLOBAL RESPONSE

The global response of the columns was recorded by instrumentation as presented in Section 3.5.2. The moment versus drift response of each column as well as the actual displacement history for each column is presented in this section. The applied moment was found using Equation 5.1 and illustrated by Figure 5.1,

$$M = LH + P\Delta \tag{5.1}$$

where M is the induced moment, P is the applied vertical load from the Baldwin Universal Testing Machine, Δ is the horizontal deflection at the top of the column, L is the applied lateral force from the MTS actuator, and H is the vertical distance from the top of the footing to the centroid of the lateral load. The vertical and lateral loads could not be applied in exactly the same place because of the size of the actuator swivels. Thus, parameter Δ was not measured directly, but it was estimated as the displacement at the point where the lateral load was applied multiplied by the ratio h/H, as shown in Figure 5.1. Here h is the vertical distance from the foundation to the point where the vertical load was applied.

Specimens CT5, CT6, CT7, and CT8 were all subjected to the RDH displacement history. The details of their displacement histories can be found in Figure 5.2, 5.4, 5.6, and 5.8, respectively. The displacements were controlled by the LVDT in the MTS actuator, which necessarily measured the distance between the specimen and the point of attachment of the actuator on the reaction frame. The specimen displacements were measured with the string pot and are thus independent of any deformation of the reaction rig. The moment-drift response of Specimens CT5, CT6, CT7, and CT8 are shown in Figure 5.3, 5.5, 5.7, and 5.9, respectively. The drift and displacement of the column at the point when bar buckling first occurred are also indicated on the graphs. The "Tens. Bar" is the bar that experiences the most tension from the test (Bar 1) and the "Comp. Bar" opposite this bar (Bar 6).

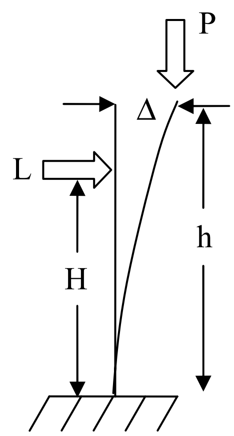

Fig. 5.1 Schematic showing values for moment calculations.

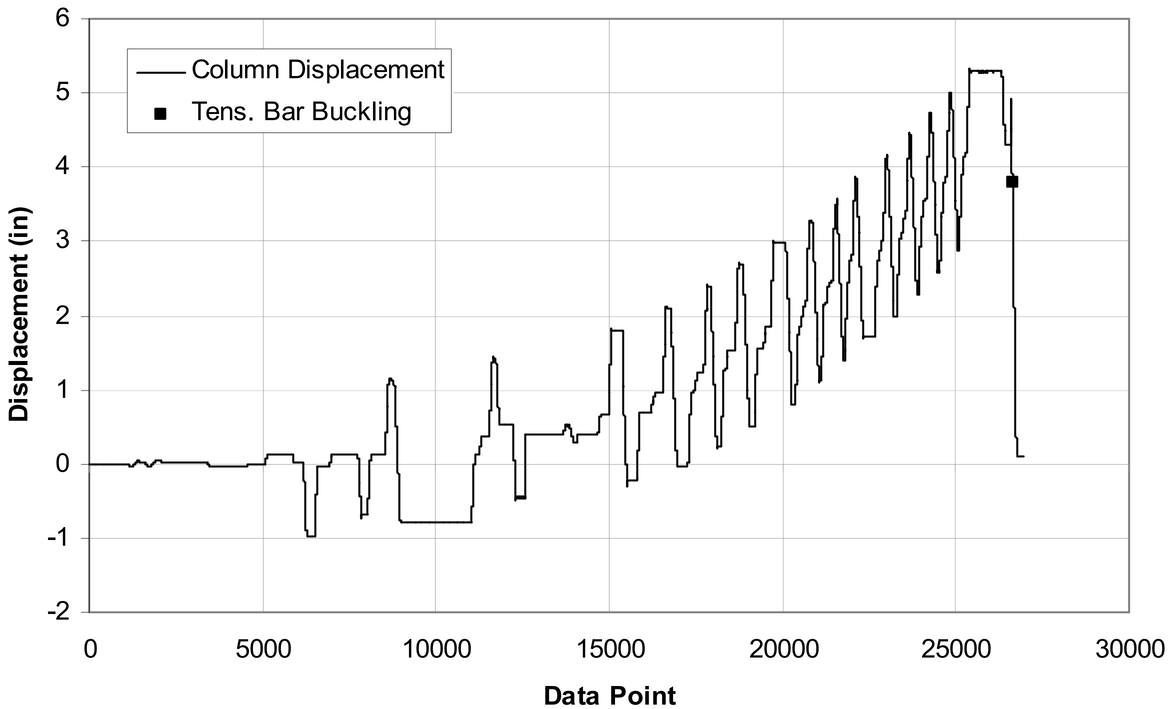

Fig. 5.2 Actual displacement history for CT5.

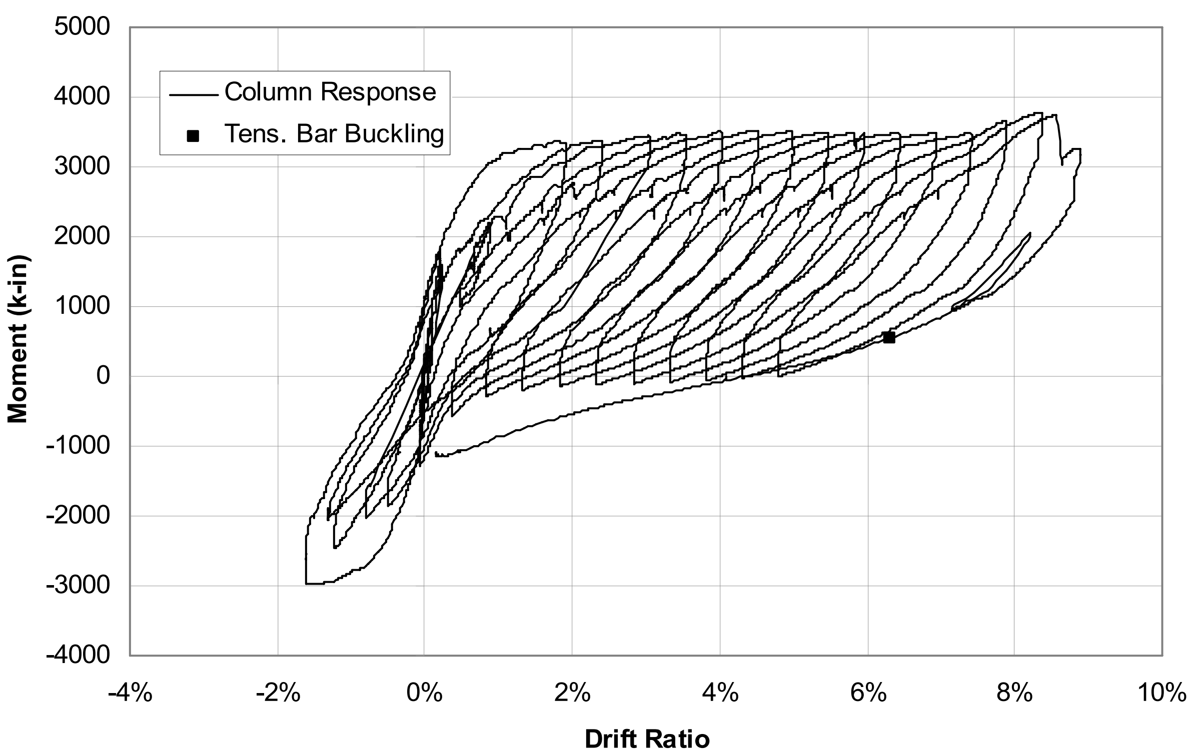

Fig. 5.3 Moment-drift curve including P-Δ effects for CT5.

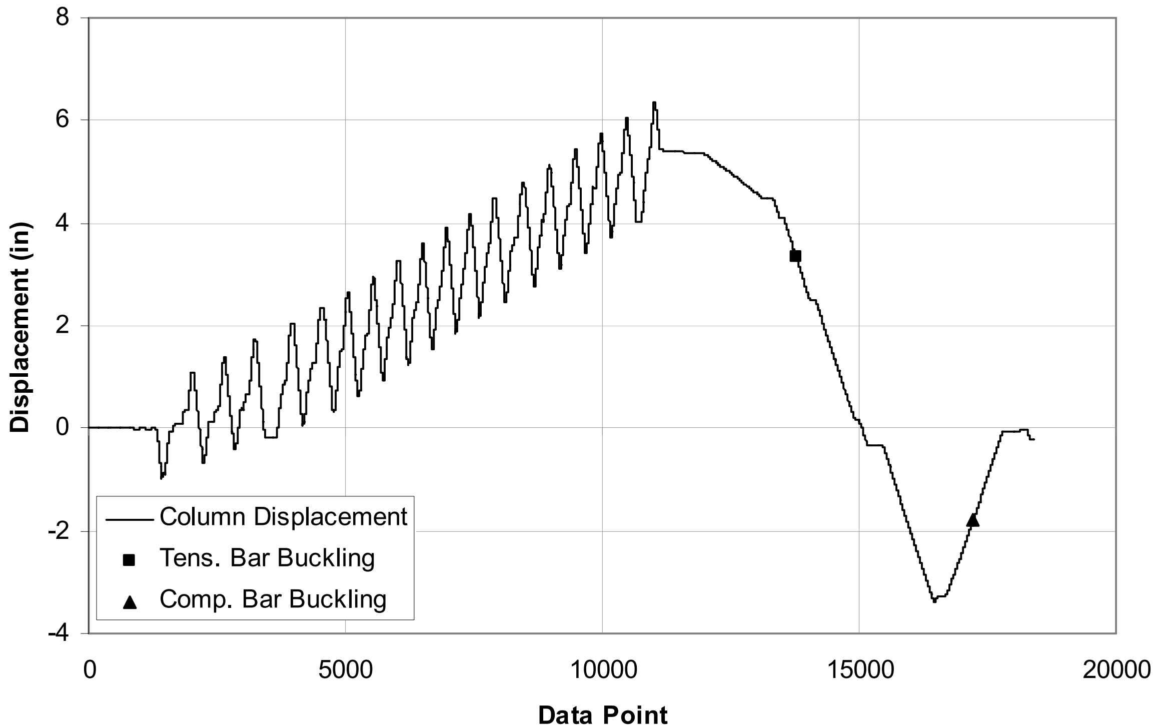

Fig. 5.4 Actual displacement history for CT6.

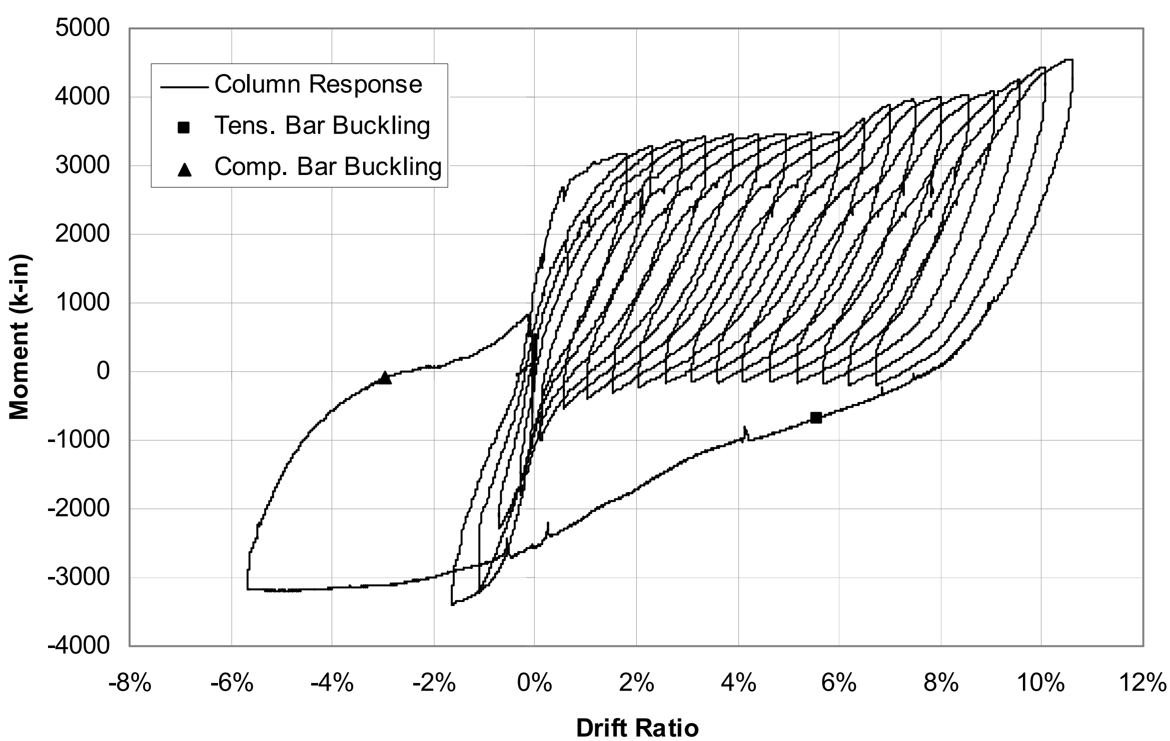

Fig. 5.5 Moment-drift curve including P-Δ effects for CT6.

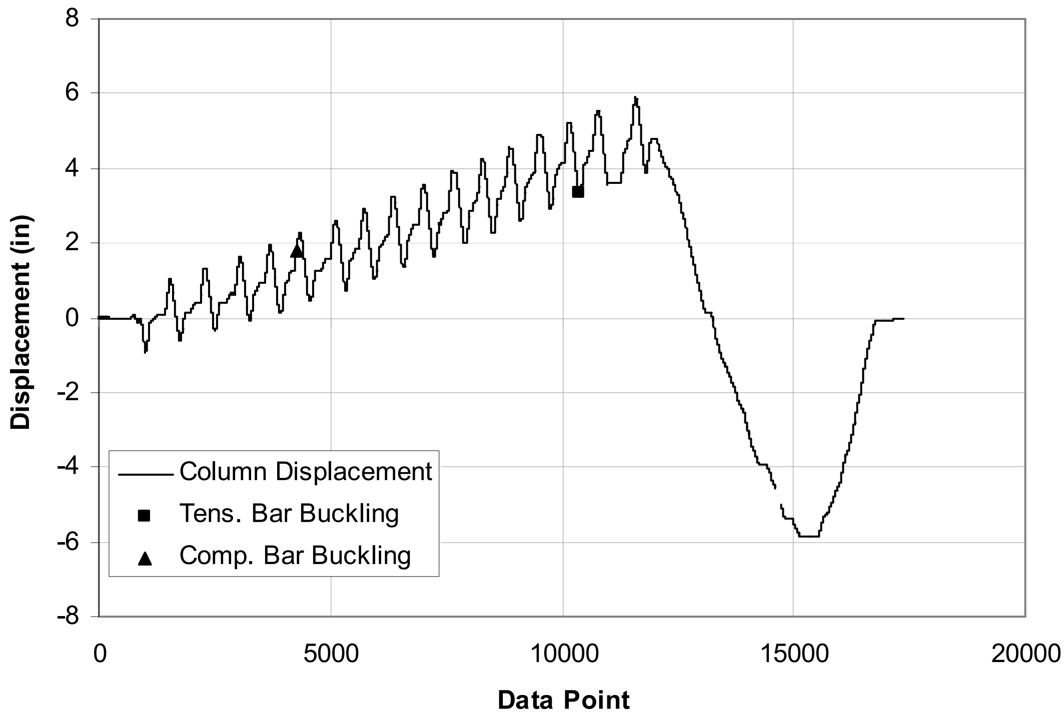

Fig. 5.6 Actual displacement history for CT7.

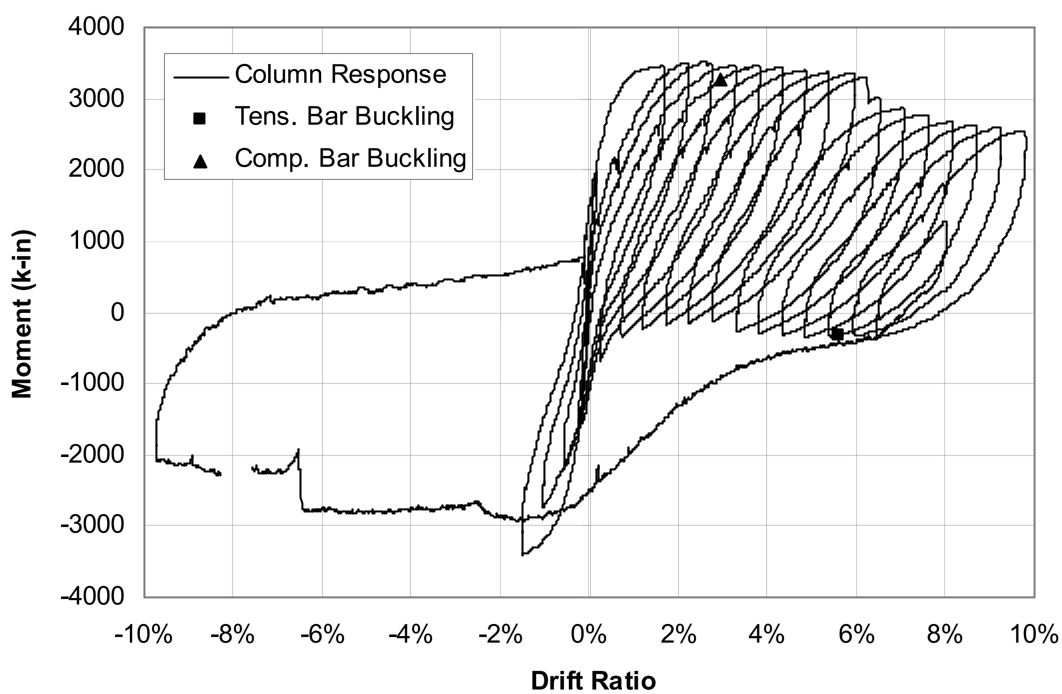

Fig. 5.7 Moment-drift curve including P-Δ effects for CT7.

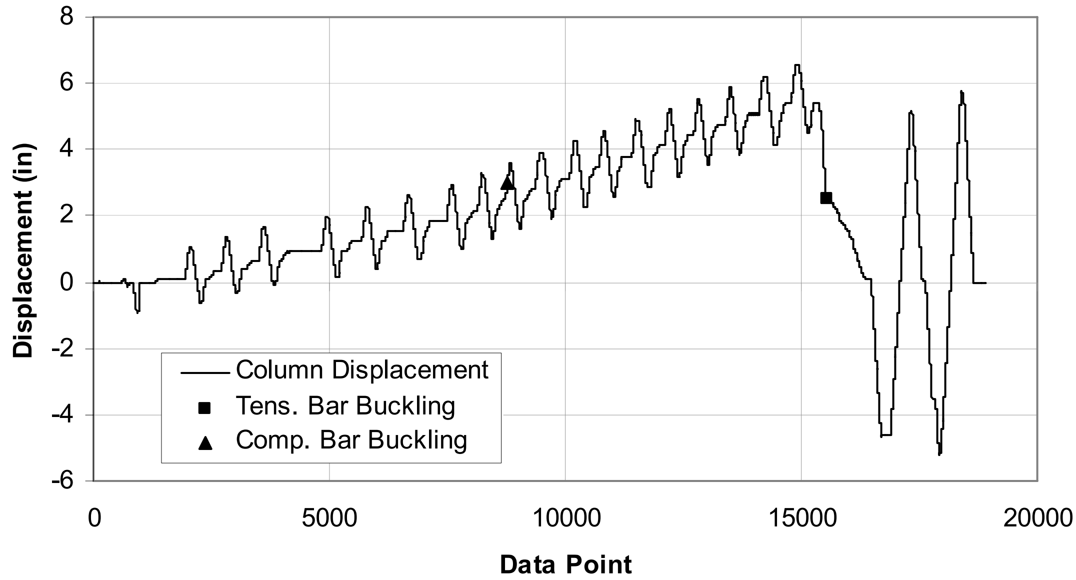

Fig. 5.8 Actual displacement history for CT8.

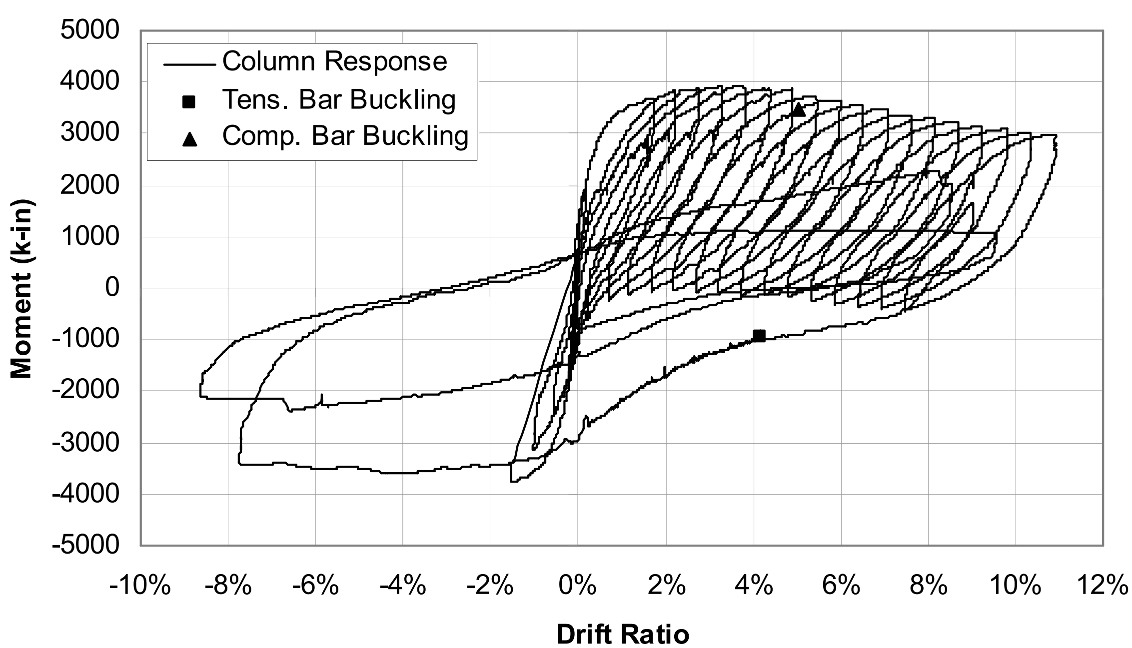

Fig. 5.9 Moment-drift curve including P-Δ effects for CT8.

The data points for each measured damage state are shown in Table 5.1. Many of the strain gages exceeded their range, broke or became detached from the bar before they recorded yield. This was primarily a problem for the spirals in Specimens CT5 and CT7 due to the high-strength, very small-diameter wires that was used. These points are indicated with an asterisk (*) in the table.

Table 5.1 Data points for each data point for each specimen.

CT5	Data Point	
Bar 1 yield	6206	
Bar 6 yield	8556	
Spiral 1 yield	22903	*
Spiral 6 yield	N/A	*
Bar 1 buckle	N/A	
Bar 6 buckle	26628	

CT6	Data Point
Bar 1 yield	1359
Bar 6 yield	1353
Spiral 1 yield	2619
Spiral 6 yield	5507
Bar 1 buckle	13774
Bar 6 buckle	17232

CT7	Data Point	
Bar 1 yield	945	
Bar 6 yield	938	
Spiral 1 yield	7640	*
Spiral 6 yield	6310	*
Bar 1 buckle	10349	
Bar 6 buckle	4269	

CT8	Data Point
Bar 1 yield	841
Bar 6 yield	861
Spiral 1 yield	2193
Spiral 6 yield	1962
Bar 1 buckle	15537
Bar 6 buckle	8778

* Strains were inaccurate for these spirals

5.2 BAR-BUCKLING DISPLACEMENTS

Lateral bar displacements were recorded as discussed in Section 3.5.4 using Method 2, in which a single potentiometer measured the displacement of the bar relative to the concrete core. Method 2 was used as the primary source of data because it was used on all specimens in Group 2, while Method 1 was used only in some Group 2 columns. (It was used there as a backup while Method 2 was first implemented). Figures 5.10–5.17 show the lateral bar displacement histories for Bars 1 and 6 in each column. For each bar the lateral bar displacement was measured at 1″, 3″, and 6″ above the footing. The "onset" of buckling is arbitrarily defined as a lateral bar displacement of 1% of the column diameter, or 0.20″ for these column specimens.

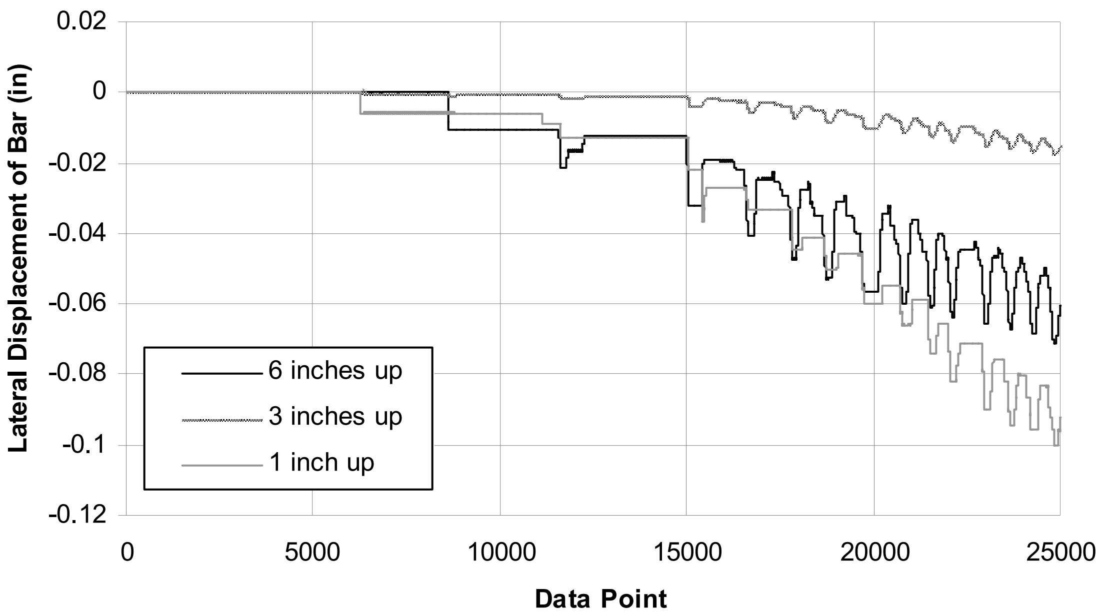

Fig. 5.10 Bar lateral displacement for Specimen CT5 Bar 1.

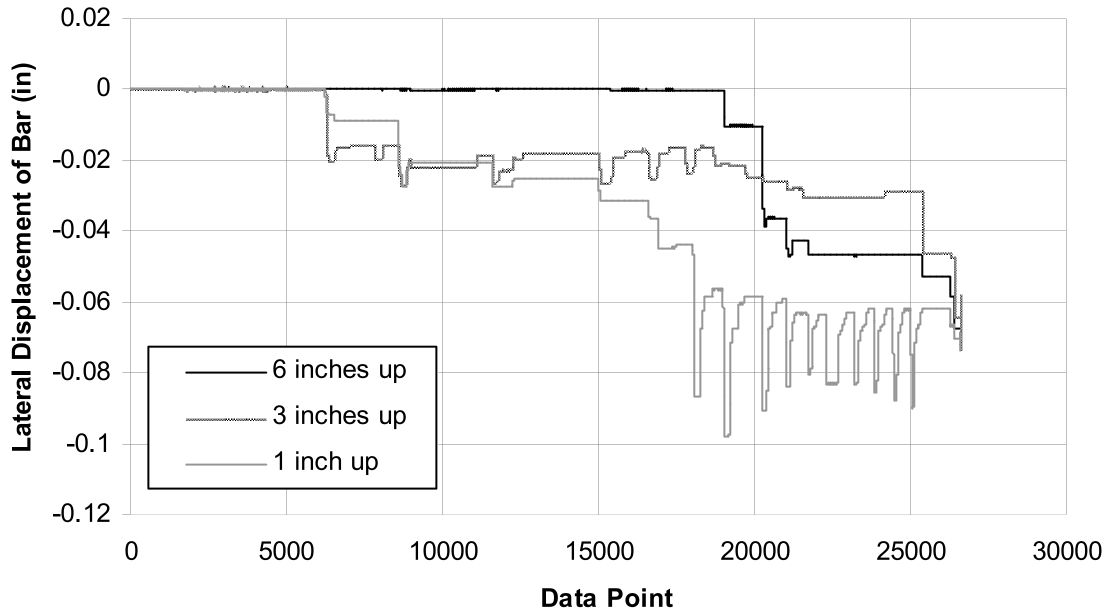

Fig. 5.11 Bar lateral displacement for Specimen CT5 Bar 6.

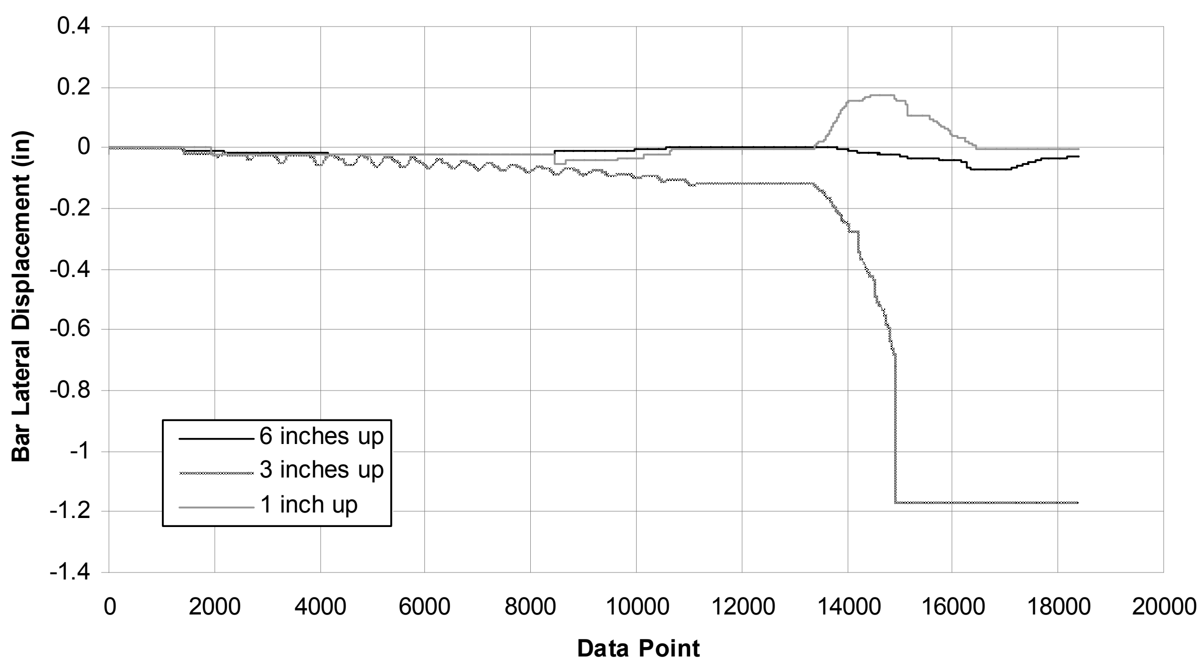

Fig. 5.12 Bar lateral displacement for Specimen CT6 Bar 1.

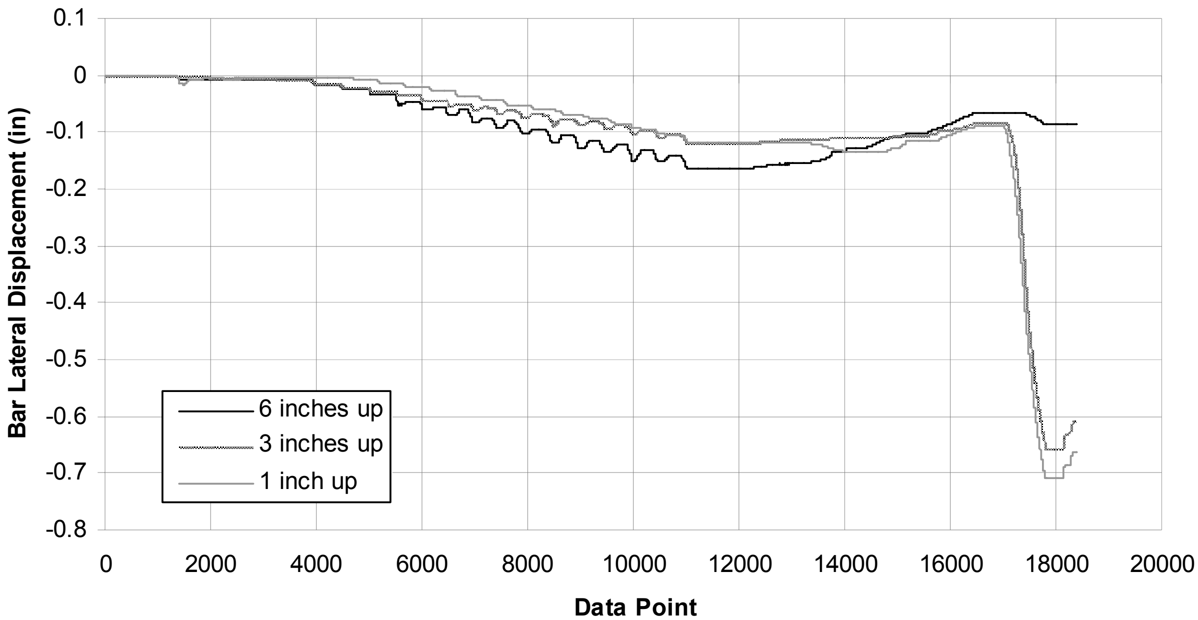

Fig. 5.13 Bar lateral displacement for Specimen CT6 Bar 6.

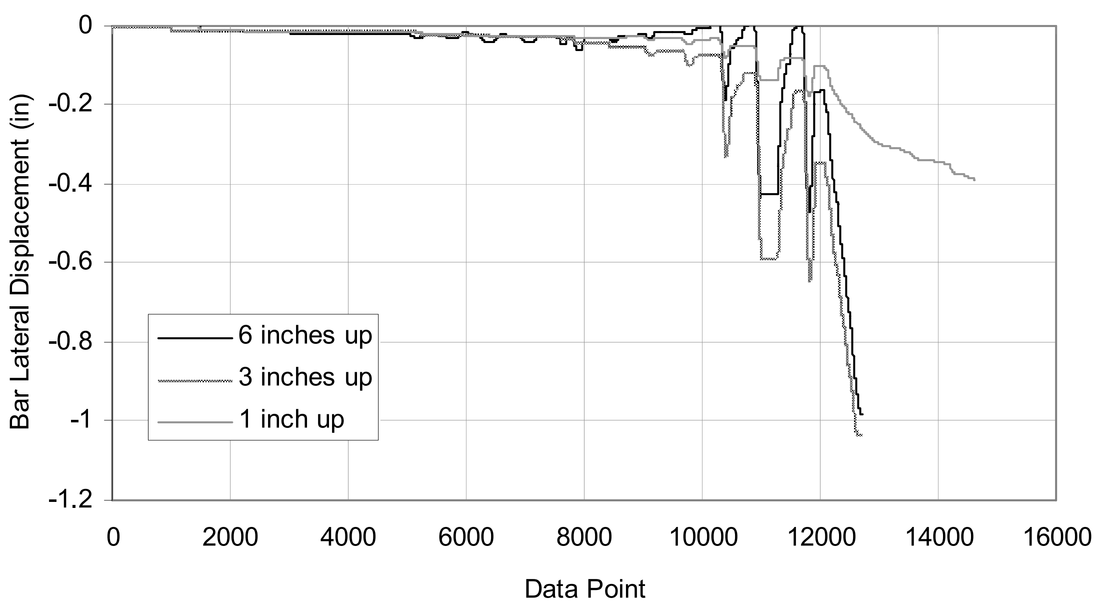

Fig. 5.14 Bar lateral displacement for Specimen CT7 Bar 1.

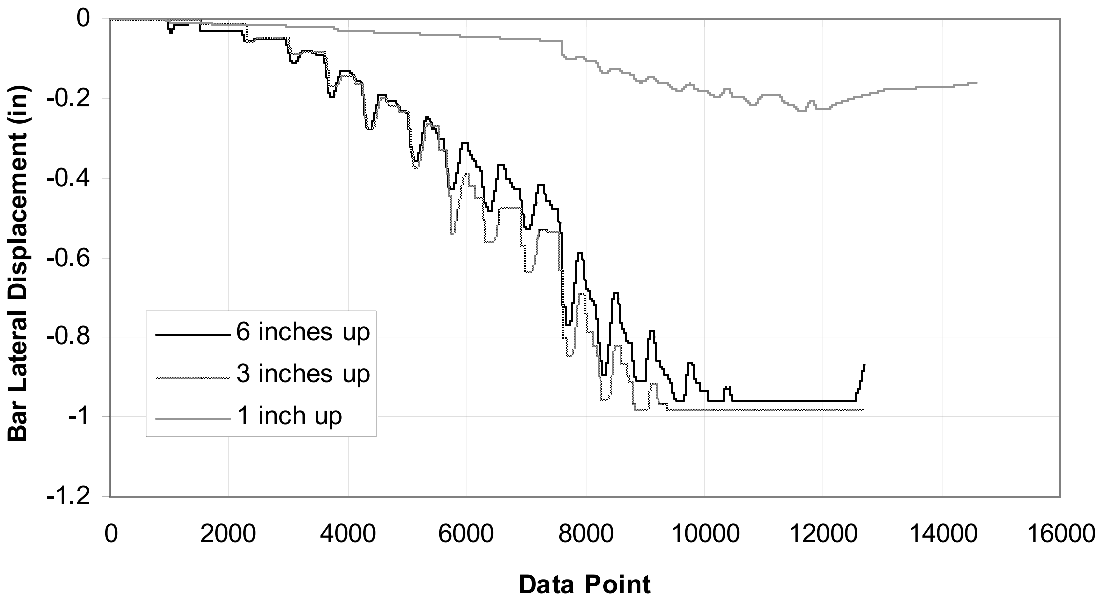

Fig. 5.15 Bar lateral displacement for Specimen CT7 Bar 6.

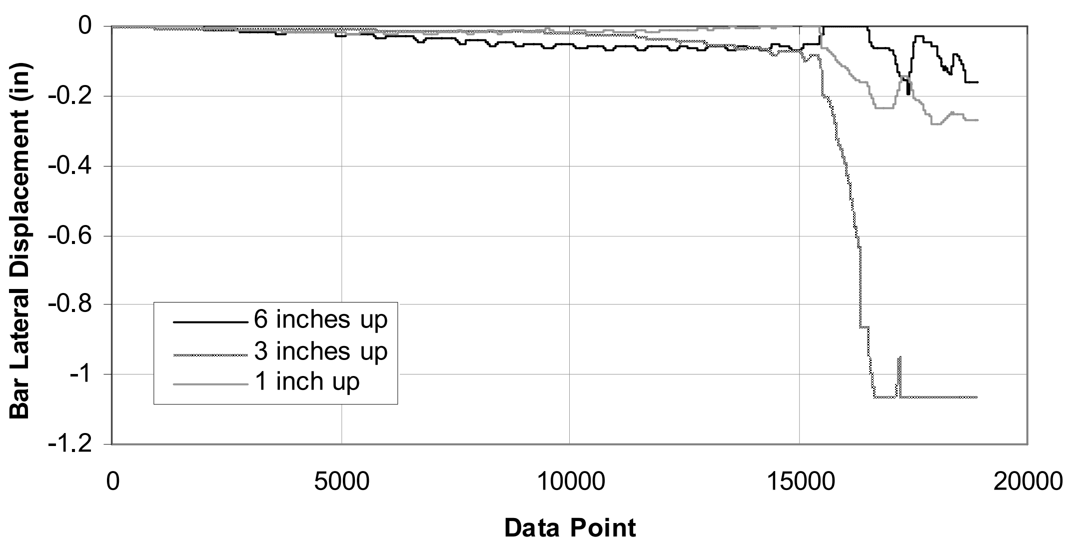

Fig. 5.16 Bar lateral displacement for Specimen CT8 Bar 1.

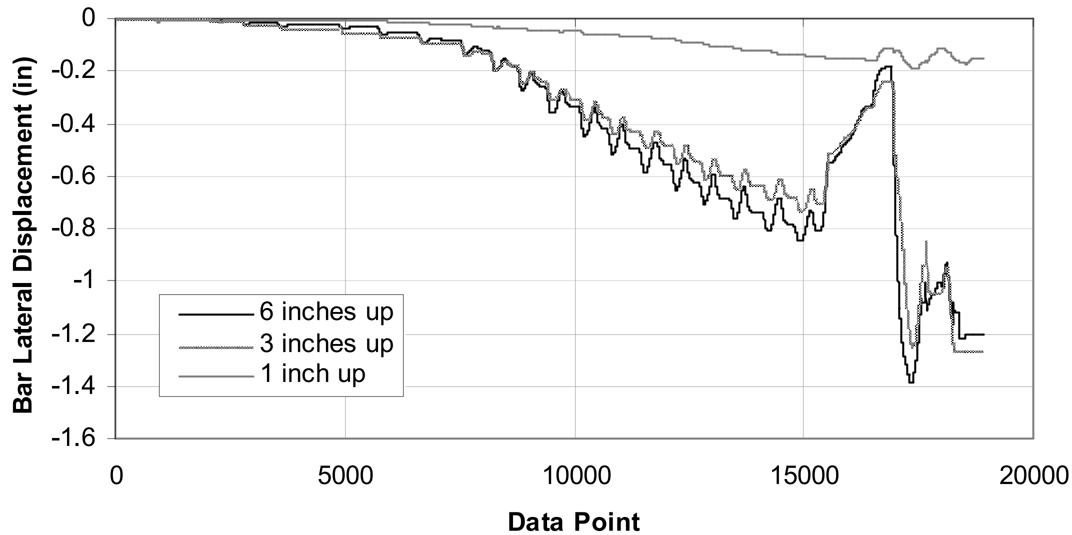

Fig. 5.17 Bar lateral displacement for Specimen CT8 Bar 6.

5.3 CONCRETE CORE EXPANSION

The radial expansion of the core concrete was measured as discussed in Section 3.5.5. Figures 5.18–5.21 show the measured core expansion for each specimen at 1″, 4″, and 7″ above the footing. The 1″ data for Specimen CT7 and the 4″ data for CT6 all read zero for the duration of the test, and thus were assumed to be faulty and were omitted. The magnitudes of the core expansions for Specimens CT5 and CT6 are quite different than those for Specimens CT7 and CT8. The magnitude of the core expansion from Specimens CT7 and CT8 are similar to those for Specimens CT3 and CT4 (Freytag, 2006).

As discussed in Section 2.3 the core concrete expands and pushes outwards on the bars and spirals, and may promote buckling of the longitudinal reinforcement. Figures 5.22–5.24 plot the calculated hoop strain due to the core expansion and the actual strain in the spirals as measured by strain gages. The calculated hoop strain is found by $\Delta d/D_{col}$ where Δd is the measured core expansion and D_{col} is the diameter of the column. These figures were plotted for Specimen CT8 at 7″, 4″, and 1″ above the footing.

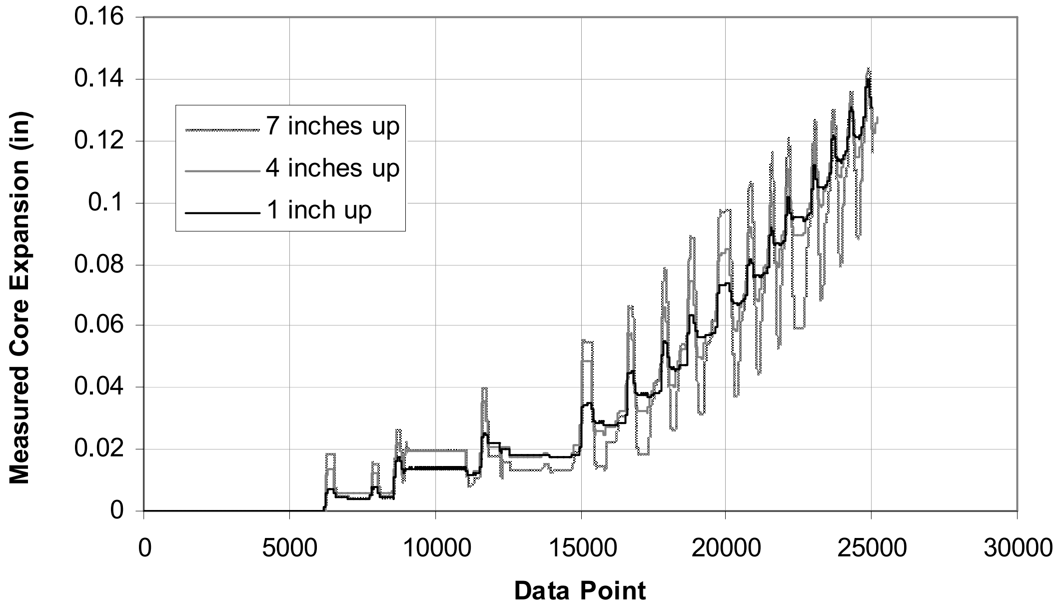

Fig. 5.18 Measured concrete core expansion for Specimen CT5.

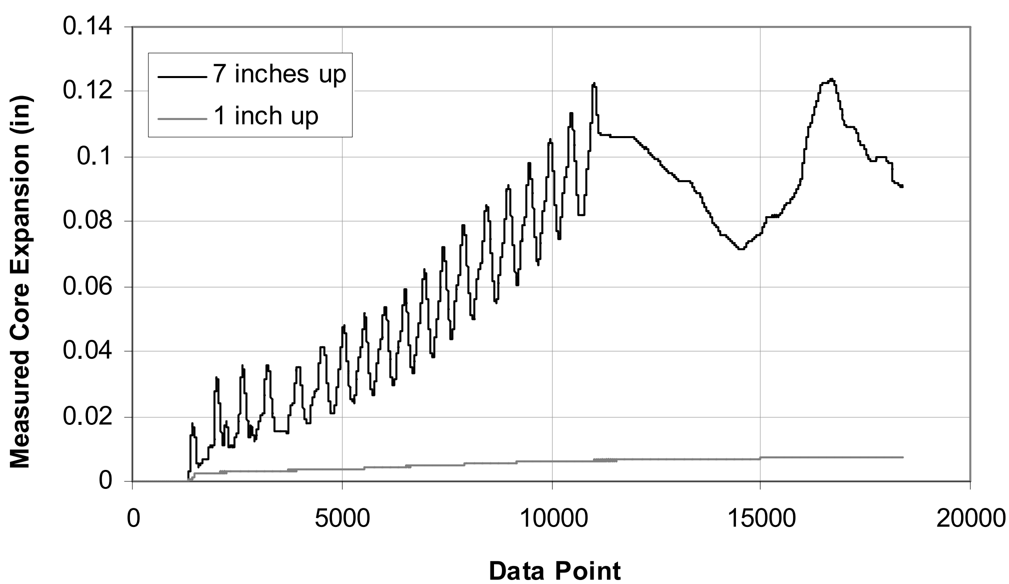

Fig. 5.19 Measured concrete core expansion for Specimen CT6.

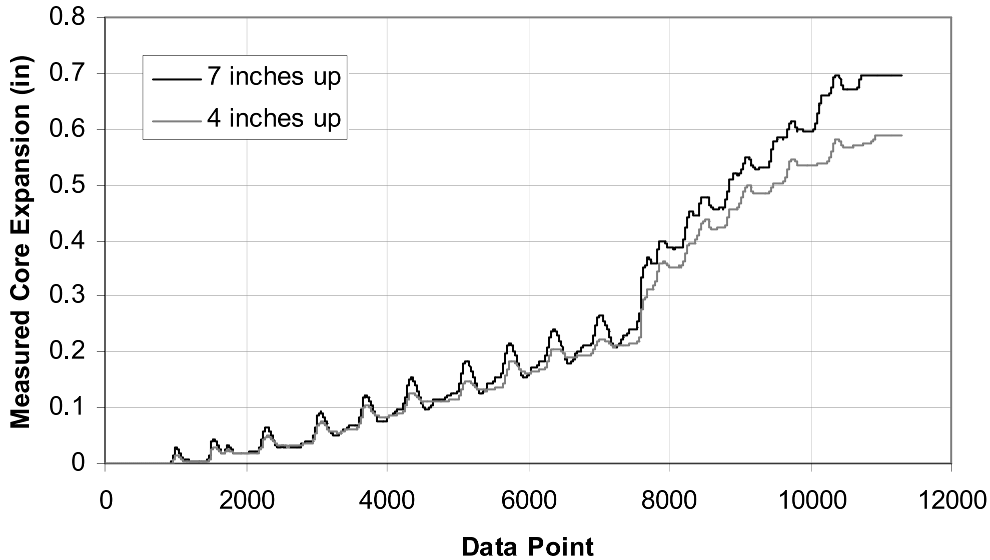

Fig. 5.20 Measured concrete core expansion for Specimen CT7.

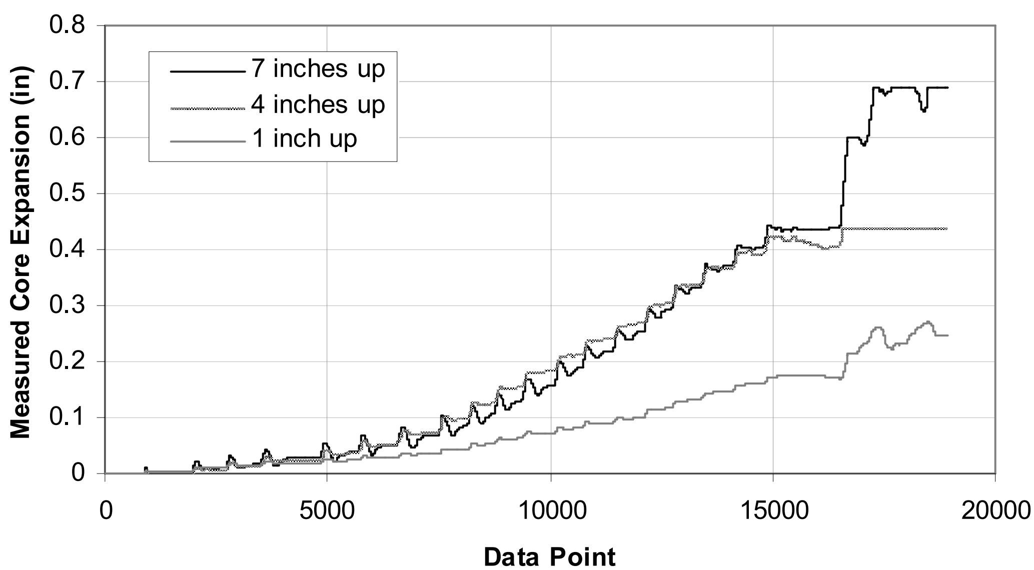

Fig. 5.21 Measured concrete core expansion for Specimen CT8.

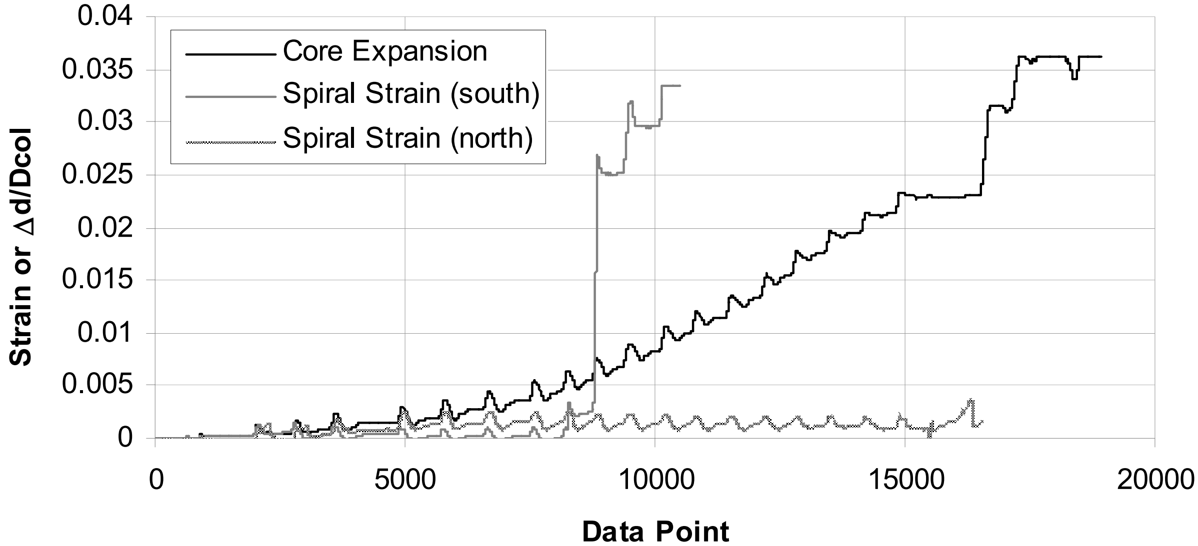

Fig. 5.22 Calculated hoop strain and measured hoop strain for CT8, 7″ up.

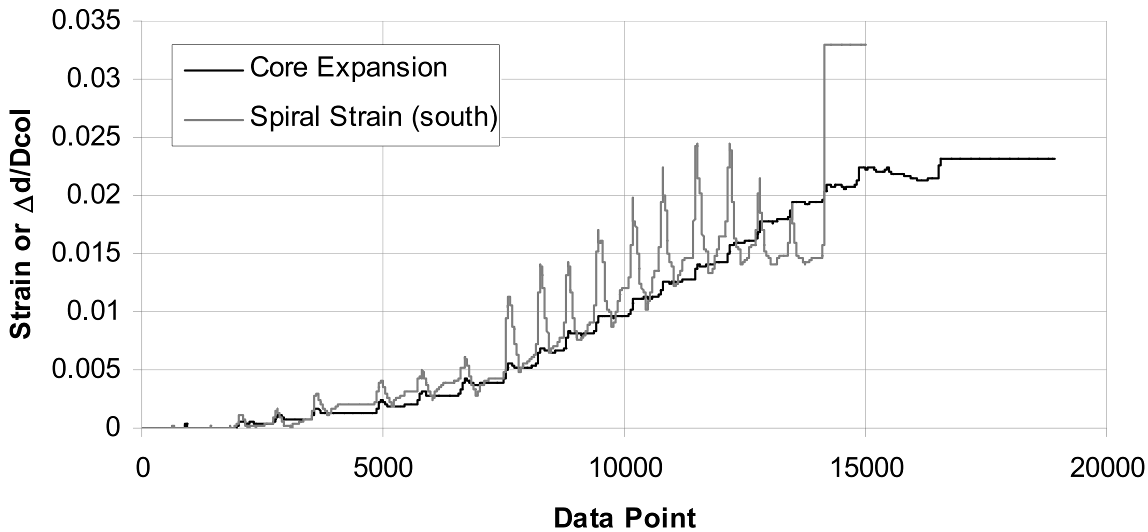

Fig. 5.23 Calculated hoop strain and measured hoop strain for CT8, 4″ up.

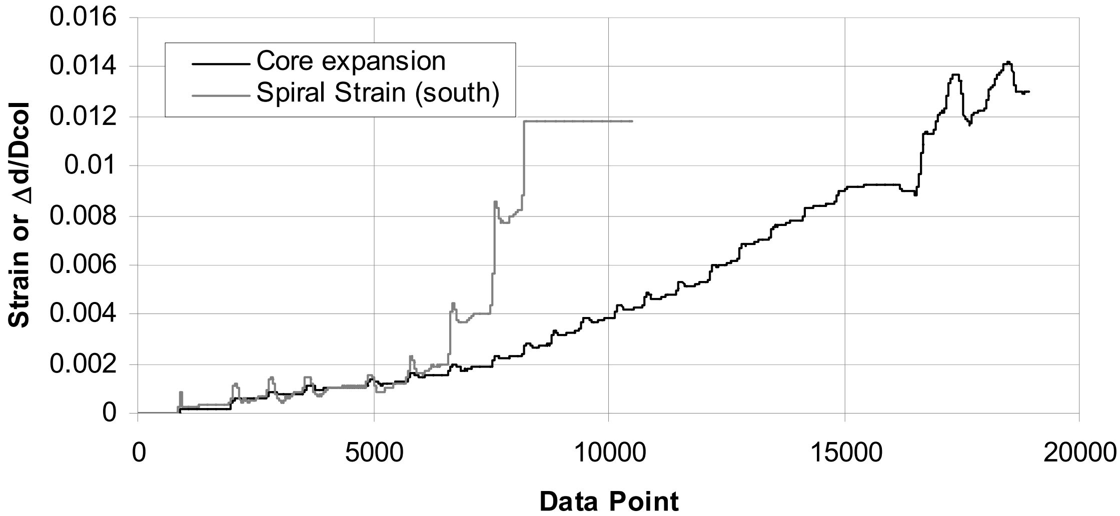

Fig. 5.24 Calculated hoop strain and measured hoop strain for CT8, 1″ up.

Figures 5.25–5.27 plot the total bar displacement history and the core expansion history. The total bar displacement is the sum of the two lateral bar displacements on opposite sides of the column at the same level. These plots show that at 1″ above the footing all of the lateral bar displacement was caused by the expansion of the core, while at higher points the total bar displacement was significantly greater than the expansion of the core indicating that the bar was displacing laterally due to other factors. These plots are only for Specimen CT8; however data from the other specimens were similar. Figure 5.26 also shows the total displacement of the spiral compared to the core concrete.

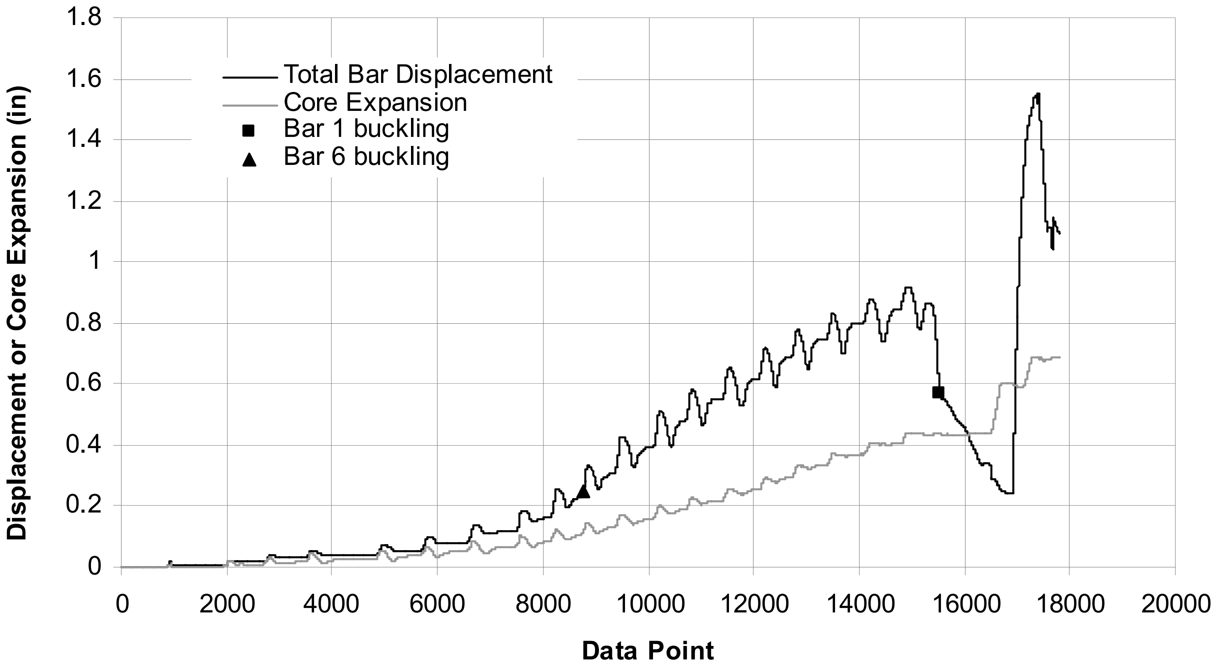

Fig. 5.25 Core expansion and lateral bar displacements for CT8, 7″ up.

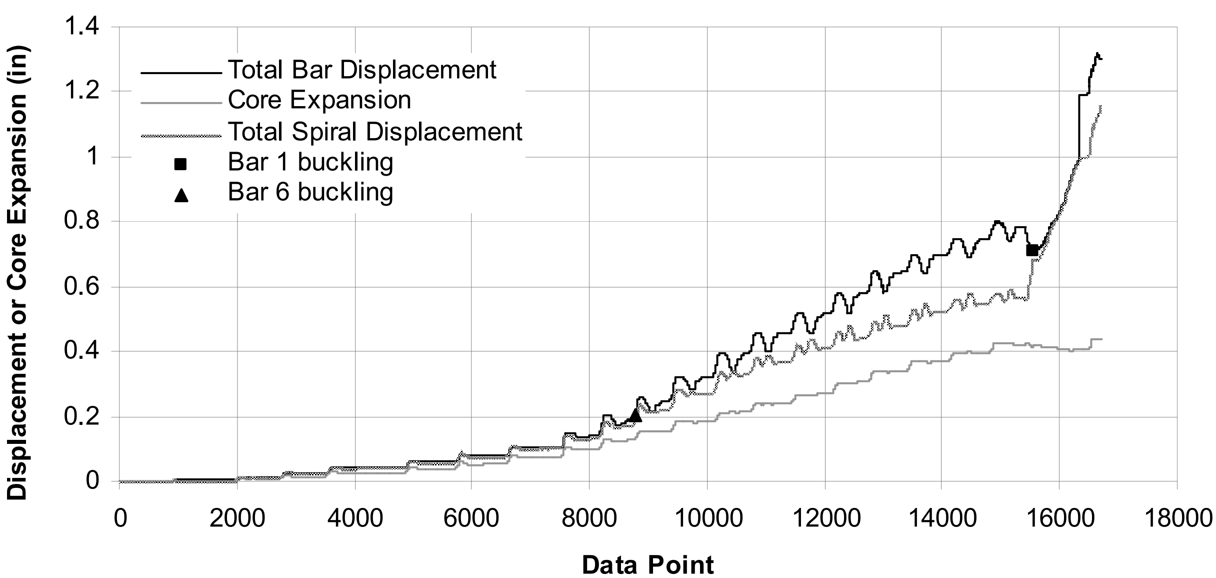

Fig. 5.26 Core expansion and lateral bar displacements for CT8, 4″ up.

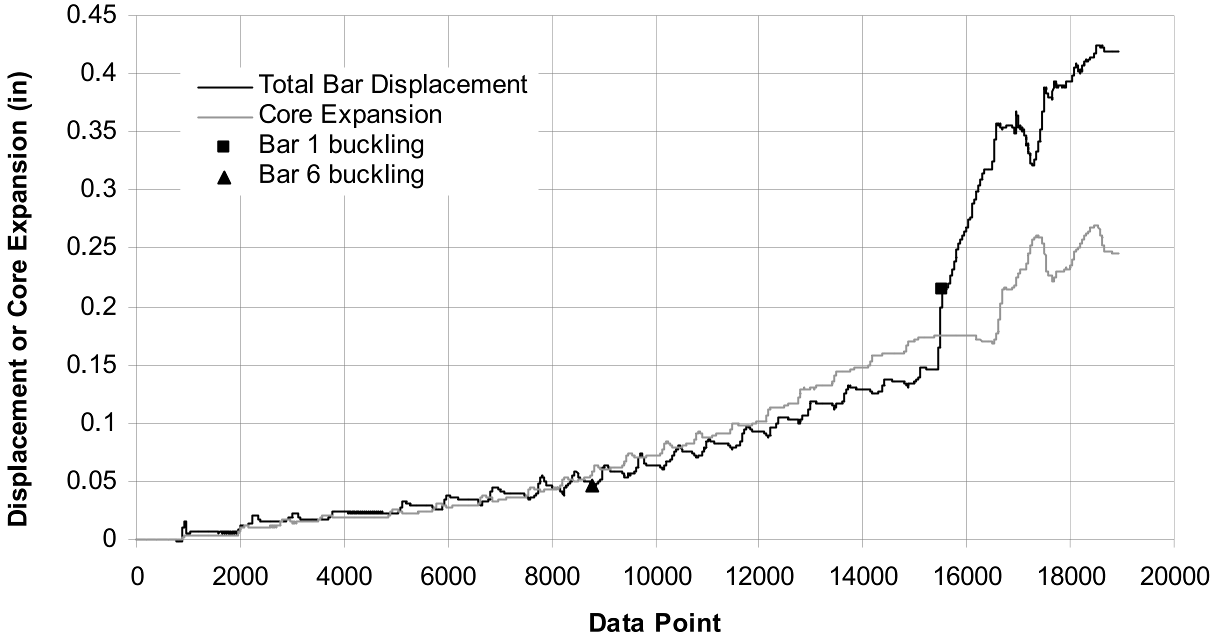

Fig. 5.27 Core expansion and lateral bar displacements for CT8, 1″ up.

6 Analysis of Data

6.1 LONGITUDINAL BAR STRAIN

Strain data from the longitudinal bars were analyzed to compare the strain responses with those predicted by the theories of previous researchers. While the bars remained elastic, the measured strains seemed consistent with the data from other instruments. However, after yielding had occurred the gage readings were erratic and suggested that most of the gages had failed, despite the use of high-yield gages. Thus little useful strain data are available at bar buckling, which occurred well after yielding.

On Specimen CT7 two gages on Bar 6 both survived through bar buckling, and a plot of the average of these two gages verses column drift is shown in Figure 6.1. The average strain provides a measure of the axial strain in the bar. It is interesting to note that during the cycling of the column the bar experiences a change in strain of about 0.004 which is 2 times the yield strain of the bar ($\Delta \varepsilon \approx 2\, \varepsilon_y$). This indicates that after some permanent plastic deformation near the beginning of the lateral loading, the bar experiences only elastic strain reversals and does not yield further. These gages were located approximately 1″ from the top of the footing and thus were located quite close to the inflection point of the buckled shape as shown in Figure 6.2. The implication is that the axial force in the bar was controlled by the flexural strength of the bar at the plastic hinges, and that that prevented the axial force from exceeding the yield level. As can be seen in the figure, the strain range reduces as the load history progresses. This is consistent with increasing buckling amplitudes because if the plastic moment strength is proportional to the product of axial force and displacement, a larger displacement implies a smaller force.

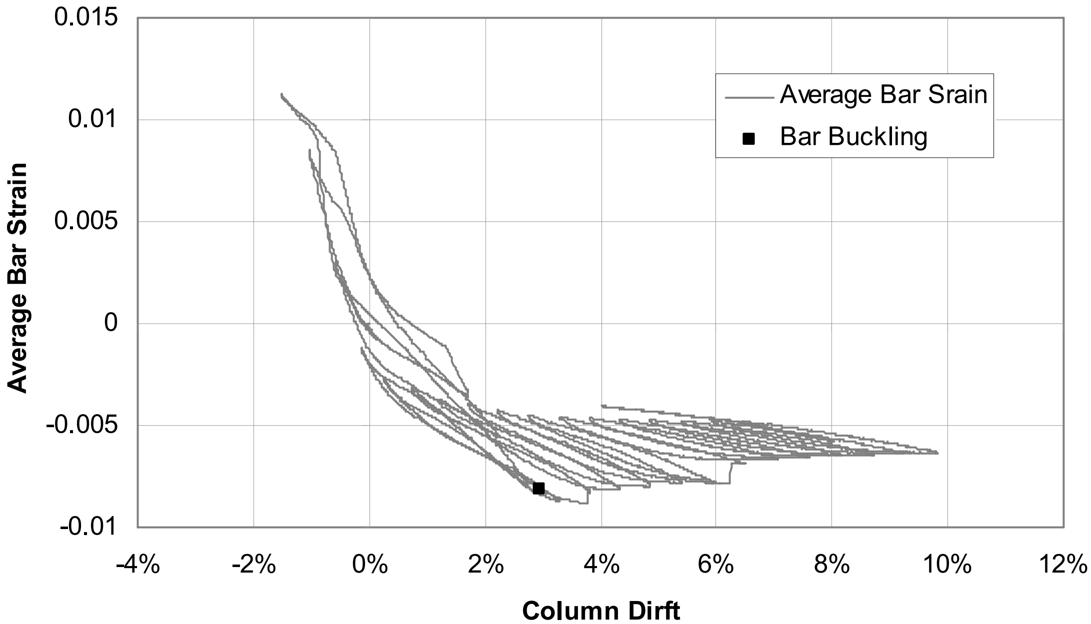

Fig. 6.1 Comp. Bar average measured strain history for Specimen CT7.

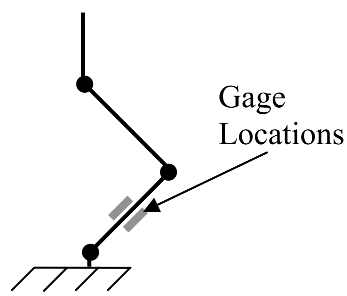

Fig. 6.2 Location of strain gages from Fig. 6.1.

6.2 BAR-BUCKLING DISPLACEMENTS

The drift at which bar buckling occurred is shown in Figures 6.3 and 6.4 plotted against the stiffness and strength of the spiral, respectively. Each of these figures shows a return drift for the Tens Bar and Comp. Bar; these return drifts are analogous to the return strain increments discussed by Rodriguez (1999). The Tens and Comp. Bars are defined in Chapter 5. The "Maximum Drift" is the largest drift that the column experiences in either direction prior to bar buckling and in some cases that drift was achieved when the bar was in tension. The "Comp. Bar Max" is the largest drift that the Comp. Bar experienced in tension. Figures 6.3 and 6.4 also show the drift at which Berry (2005) indicated that buckling would occur. The figures also show the trends for each group. Considerable scatter exists in both plots.

The definitions above were used because of the difficulty in defining a maximum drift with the RDH. The trends from Figure 6.3 show a slight increase in the drift at buckling with three of the four drift definitions. The one measure that showed no dependence on spiral stiffness was the return drift. This was surprising because Rodriguez et al. (1999) had identified the return strain as the key parameter in predicting bar buckling. Figure 6.4 shows no meaningful correlation between spiral strength and drift at buckling. The finding that spiral stiffness affects bar buckling but that spiral strength does not is in agreement with the concept of modeling the bar as an inelastic beam-column on an elastic foundation, as suggested by Dhakal (2002), but it is at odds with the dictates of design codes, most of which define the spiral requirements in terms of strength and not stiffness.

In Figure 6.4 the line marked "Berry (2005)" is based on observed buckling from a large database of column tests in most of which bar buckling was not the main focus. It is expected that buckling defined by a lateral displacement of 1% of the column diameter would occur slightly before it can be observed, especially if the column has concrete cover. Many of the points in Figures 6.3 and 6.4 represent drifts that are approximately 1% lower than those proposed by Berry (2005), and this could be attributed to the difference between measured and observed buckling. It is also important to note that the majority of the columns in the database from Berry (2005) used a symmetric displacement history, in which case the drift at buckling was much easier to define.

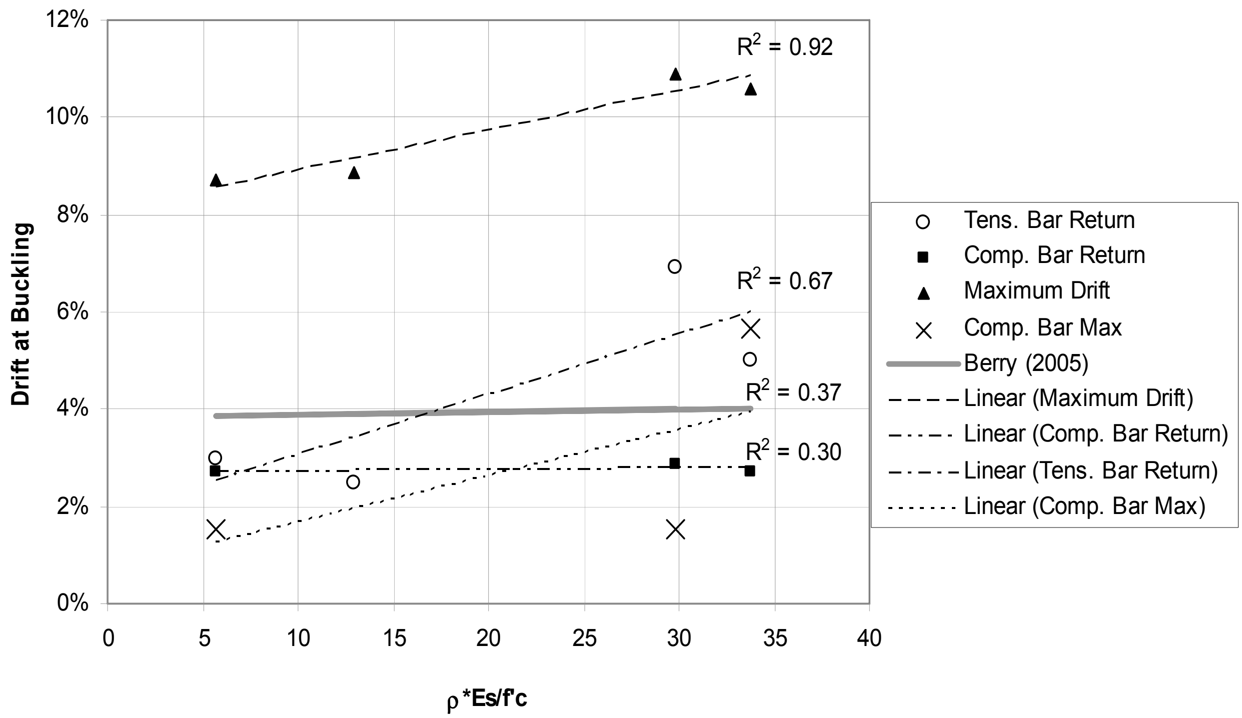

Fig. 6.3 Drift at bar buckling vs. spiral stiffness.

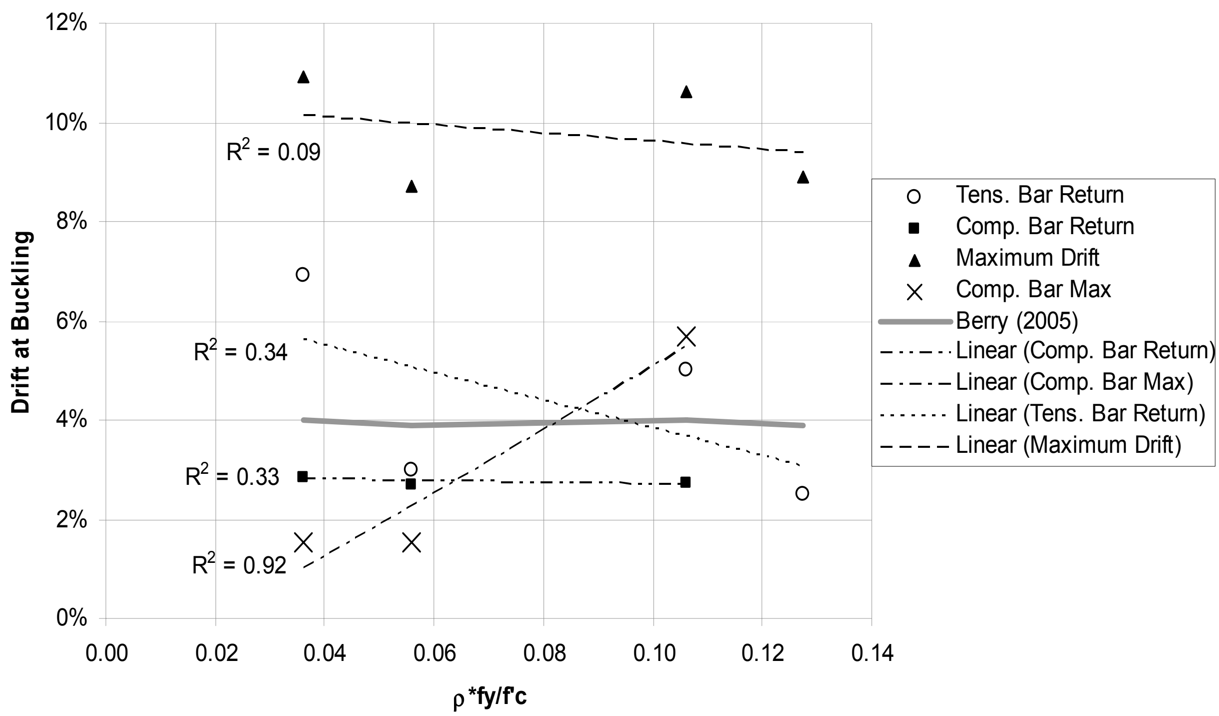

Fig. 6.4 Drift at bar buckling vs. spiral strength.

6.3 CORE EXPANSION

The core expansion measurements suggest that the definition for bar buckling adopted in this report was in good agreement with the observed behavior. The lateral displacements of Figures 5.25–5.26 show that near the point defined as bar buckling, the bar rapidly moved away from the concrete core. Figure 5.27 shows a similar behavior for the other bar; however that bar had buckled higher up and the instrument in Figure 5.27 measured only the bottom of the buckled shape.

The measured data show that the bar was deflecting laterally throughout the entire load history. Thus bar buckling was not a sudden bifurcation event, as defined in the classical Euler sense, but rather a gradual increase in lateral displacement with increasing loads. In that case there is no uniquely identifiable point during the load history at which the bar starts to buckle, and either the quest for a definition of buckling should be abandoned, or an arbitrary definition should be adopted that represents a point at which lateral bending of the bar starts to play a significant role in its behavior. The latter approach was adopted here, and the definition of buckling used in the study appears to be a viable indicator for the onset of rapidly increasing bar displacements.

Figures 5.25–5.27 also indicate that the core expansion is the primary cause of lateral movement of the longitudinal bar in the initial load stages, but that P-Δ effects exacerbate the displacement later. During the early stages of the drift history, the displacements of the core and bar are almost identical, indicating that they are in contact, but after a certain point the bar displacement starts to exceed the core expansion and the bar moves away from the core. This is consistent with the concept of the core expansion creating an initial eccentricity in the bar, which is then amplified by the axial load, especially when the steel starts to yield.

6.4 SPIRAL FRACTURE

The relationships between the drift at spiral fracture and the strength and stiffness of the spiral were also investigated. Figure 6.5 is a plot of the drift at spiral fracture versus spiral stiffness, and Figure 6.6 is a plot of the drift at spiral fracture versus spiral strength. In the figures "Actual" drift is the drift level at which spiral fracture occurred (independent of the previous history), "Return" is the return drift increment during the half cycle immediately before spiral fracture, and "Max Drift" is the maximum drift that the column reached prior to spiral fracture. The data in these plots exhibit large scatter and suggest that no statistically significant relationship exists between the strength and stiffness of the spirals and the drift at which spiral fracture occurs. These two plots contain all points from Groups 1 and 2. However, omitting the points from either group caused only a very small change in the trends, and the correlation coefficients remained low.

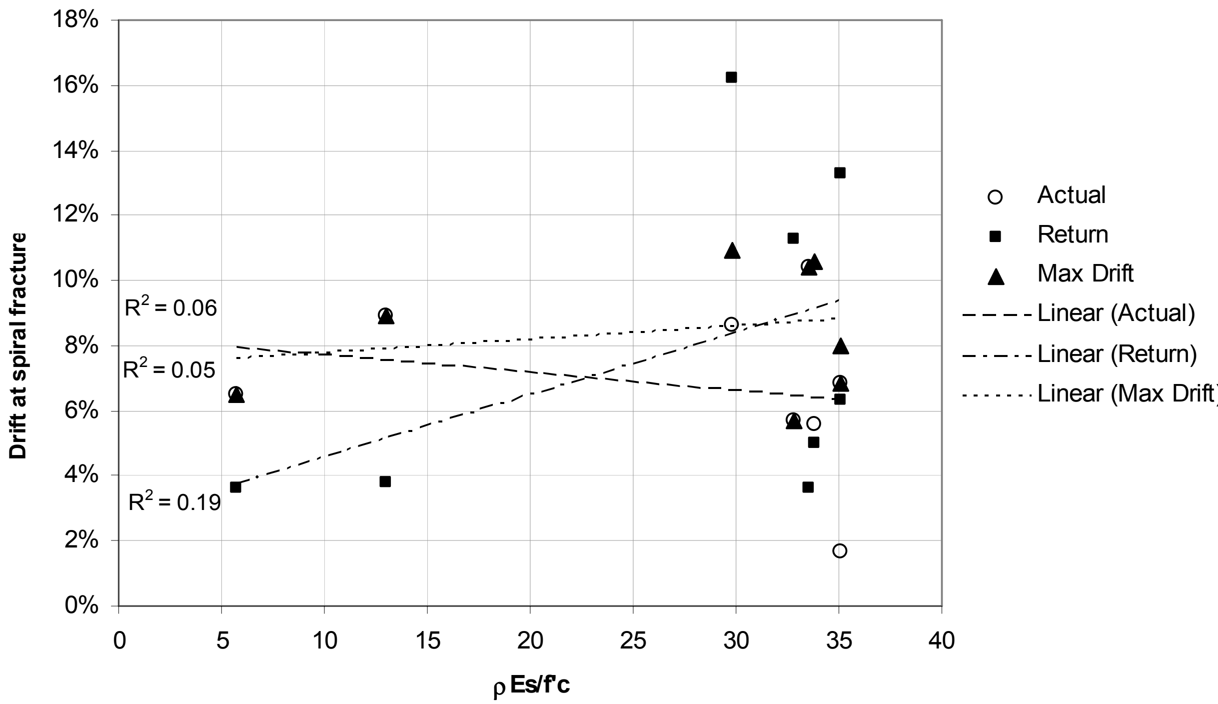

Fig. 6.5 Drift at spiral fracture vs. spiral stiffness.

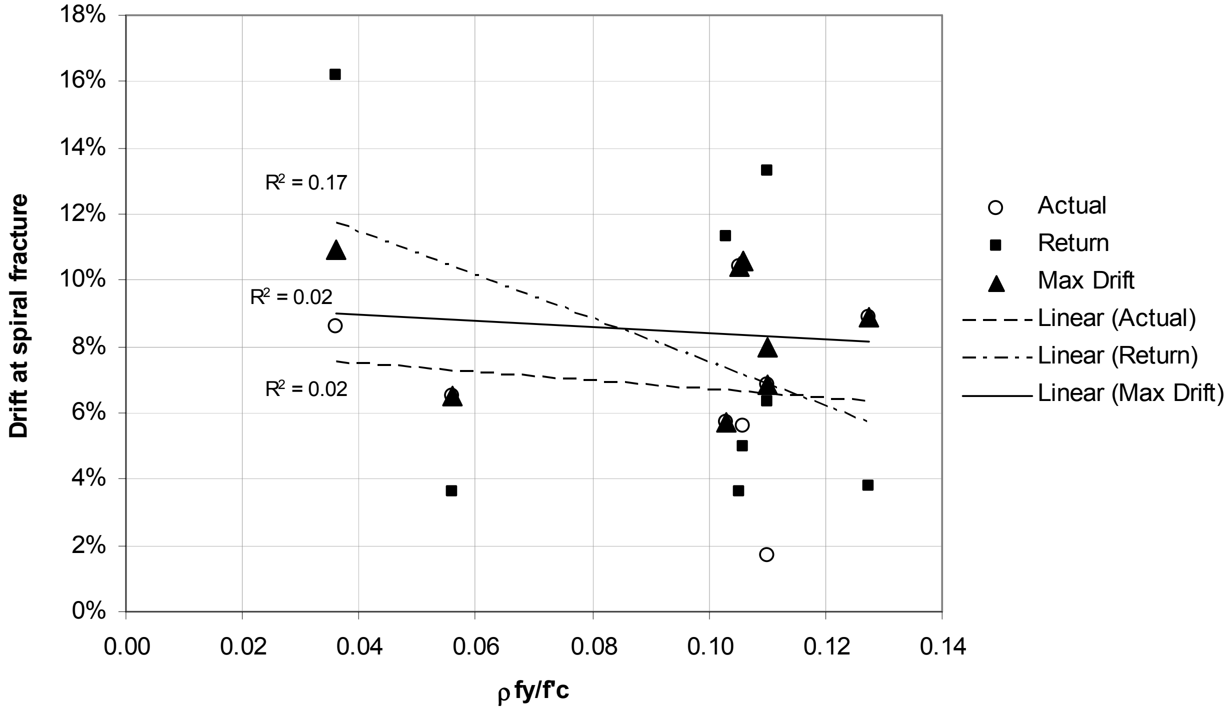

Fig. 6.6 Drift at spiral fracture vs. spiral strength.

7 Conclusions

7.1 SUMMARY

The research described in this report was intended to advance understanding of bar buckling in reinforced concrete columns by generating appropriate experimental data. Eight circular columns, reinforced with longitudinal bars and circumferential spirals, were constructed and tested by applying constant compressive axial load and cyclic lateral displacements. The specimens were divided into two groups. The displacement history and the properties of the spiral reinforcement were the primary variables studied in Groups 1 and 2, respectively. In six of the eight specimens the lateral displacement history was highly asymmetric. In the Group 2 specimens, the strength and stiffness of the spiral were varied independently. This was achieved by maintaining a constant spiral pitch, but using wires with different yield strengths and diameters.

The columns were heavily instrumented, and special measures were adopted to detect the onset of bar buckling. For example, six of the eight columns had no cover (which improved visual observations), and the bars furthest from the axis of bending were equipped with instruments with which to determine their lateral displacement profile over a height equal to the estimated plastic hinge length. Radial expansion of the column core was also measured using a specially constructed device.

In each test, loading proceeded until bars on at least one side of the column buckled. Loading continued thereafter and in most cases the bars on the other side buckled as well, and some bars fractured.

The typical response was as follows. Application of axial load caused the column core to expand. That core expansion continued, and the longitudinal bars and spiral displaced radially with the core as the initial drift cycles were applied. After a number of cycles, the bars and spiral started to displace radially away from the column core, and the bars pushed against the spiral, causing a kink in it. The bars then started to buckle, and the spiral fractured. In most cases, further cycling caused the bars that had buckled to straighten and fracture.

7.2 CONCLUSIONS

The following are the primary conclusions that can be drawn from the work:

1. Bar buckling under monotonic differs from buckling under cyclic loading for two reasons.

   First, under monotonic load, the strains in the compressed bars remain relatively small, and buckling is thus suppressed, until large drifts are imposed, because the concrete carries most of the compression force. By contrast, under cyclic loading, a large flexural crack may be present after one, say, eastbound half-cycle of displacement. During the next westbound displacement, a large strain increment may be applied and cause bar buckling before the crack even closes.

   Second, the Bauschinger effect caused by cyclic loading changes the local stress-strain properties of the steel. Lowering the tangent modulus of the material reduces the inelastic buckling load of the bar.

2. The onset of bar buckling was defined, arbitrarily, as a lateral bar displacement equal to 1% of the column diameter, or 0.20″ in this case. That definition proved to be a good indicator of the start of rapid increases in lateral bar displacements.

3. In almost all cases, buckling initiated at a drift that was smaller than that predicted by Berry (2005). In the comparison, the drift increment measured in the tests was compared with the (absolute) peak drift predicted by Berry (2005). This was necessary because the highly asymmetric displacement history used in these tests caused the absolute drift to be relatively meaningless as an indicator of buckling.

4. The apparent early onset of buckling is attributed in part to the fact that buckling was detected using instruments in these tests, whereas, in the tests from which the method in

Berry (2005) was derived, detection was usually visual and incidental to the main purpose of the tests.

5. Use of asymmetric drift histories demonstrated that attempts to define an absolute maximum drift, rather than a drift increment, at which buckling occurs face considerable difficulty. The criterion for the onset of buckling must therefore be based on an incremental, rather than an absolute, column drift or bar strain.
6. Within the range studied, the strength of the spiral reinforcement has no effect on the drift increment at which the longitudinal bars start to buckle.
7. Within the range studied, some of the data show a correlation between the stiffness of the spiral reinforcement and the drift increment at which the longitudinal bars buckle. Other data show no correlation.
8. Within the range studied, the strength and stiffness of the spiral reinforcement have no effect on the drift increment at which the transverse reinforcement spiral fractured.
9. Bar buckling always occurred before spiral fracture. Buckling of the bar tended to cause a kink in the spiral, which yielded soon after the main bars started to buckle.

7.3 RECOMMENDATIONS

1. The tests conducted here provide experimental data that can be used to develop an analytical model. The test results alone do not constitute an adequate basis for developing design recommendations.
2. Further research, particularly in the field of numerical modeling, is necessary for a complete understanding of a phenomenon as complex as bar buckling. No all-encompassing model is known to exist. Any model that is to be successful must address the following trends in behavior that were observed in these experiments:

   The buckling half-wavelength is equal to several turns of spiral, in which case the stiffness of the spiral may be expected to play a role in the inelastic (reduced modulus) buckling,

   The bar is not initially straight due to column core expansion,

   The bonded length of the bar is unknown, which affects the strain-displacement relationship, and

Cyclic loading causes the constitutive behavior to change with every cycle, which requires a representative constitutive law.

Previous researchers have addressed some of these issues individually, but no one has incorporated them all.

3. In any future experiments, the behavior of critical components that affect bar buckling should be monitored by instrumentation devoted specially to that purpose. The critical response quantities include the bar displacement, the spiral displacement (and if possible the spiral strain), and the concrete core expansion. The core expansion device developed for these tests was convenient to use, and indirect evidence suggests that it was accurate.

4. Test parameters that warrant further investigation include:

   Column aspect ratio. This will affect the shear-to-moment ratio and the core deformation caused by shear cracking.

   Longitudinal bars. Investigate the effects of using different bar sizes and different reinforcement ratios by varying each independently.

   Transverse reinforcement. Investigate the effects of a wider range of spiral stiffness and strength than was possible here, and the effects of using individual circular hoops rather than continuous spirals. The lack of correlation found here between the spiral properties and the bar buckling was unexpected.

   Displacement history. Conduct further tests with both symmetric (e.g., BDH) and asymmetric (e.g., RDH) drift histories to further examine the relationship between drift (or strain) increment and bar buckling.

REFERENCES

AASHTO (1998). *AASHTO LRFD Bridge Specifications for Highway Bridges* 2nd ed. American Association of Highway and Transportation Officials, Washington D.C.

ACI Committee 318 (2005). *Building Code Requirements for Structural Concrete*. American Concrete Institute.

Bae, S., A. Mieses, and O. Bayrak (2005). Inelastic Buckling of Reinforcing Bars. *Journal of Structural Engineering, ASCE.* 131(2), 314–321.

Berry, M. and M. Eberhard (2005). Practical Performance Model for Bar Buckling. *Journal of Structural Engineering, ASCE.* 131(4), 1060–1070.

Dhakal, P. and K. Maekawa (2002). Reinforcement Stability and Fracture of Cover Concrete in Reinforced Concrete Members. *Journal of Structural Engineering, ASCE.* 128(10), 1253–1262.

Freytag, D. (2006). *Bar Buckling in Reinforced Concrete Bridge Columns*. MSCE thesis, University of Washington, Seattle, WA.

Gomes, A. and J. Appleton (1997). Nonlinear cyclic stress-strain relationship of reinforcing bars including buckling. *Engineering Structures.* 19(10), 822–826.

Dhakal, R. P. and K. Maekawa (2002). Reinforcement Stability and Fracture of Cover Concrete in Reinforced Concrete Members. *Journal of Structural Engineering, ASCE.* 128(10), 1253–1262.

Mau, S. (1990). Effect of Tie Spacing on Inelastic Buckling of Reinforcing Bars. *ACI Structural Journal.* 87(6), 671–677.

Monti, G. and C. Nuti (1992). Nonlinear Cyclic Behavior of Reinforcing Bars Including Buckling. *Journal of Structural Engineering, ASCE.* 118(12), 3268–3284.

Moyer, M. and M. Kowalsky (2003). Influence of Tension Strain on Buckling of Reinforcement in Concrete Columns. *ACI Structural Journal.* 100(1), 75–85.

Pantazopolou, S. (1998). Detailing for Reinforcement Stability in RC Members. *Journal of Structural Engineering, ASCE.* 124(6), 623–632.

Papia, M., G. Russo, and G. Zingone (1988). Instability of Longitudinal Bars in RC Columns. *Journal of Structural Engineering, ASCE.* 114(2), 445–461.

Raynor, D., D. Lehman, and J. Stanton (2002). Bond-Slip Response of Reinforcing Bars Grouted in Ducts. *ACI Structural Journal.* 99(5), 568–576.

Rodriguez, M., J. Betero, and J. Villa (1999). Cyclic Stress-Strain Behavior of Reinforcing Steel Including Effects of Buckling. *Journal of Structural Engineering, ASCE.* 125(6), 605–612.

Suda, K., Y. Murayama, T. Ichinomiya, and H. Shimbo (1996). Buckling Behavior of Longitudinal Reinforcing Bars in Concrete Column Subjected to Reverse Lateral Loading. In *Proc., Eleventh World Conference on Earthquake Engineering.*

.

APPENDIX A: Material Test Data

Table A.1 Concrete and grout measured strengths.

Specimen	Area (in^2)	Load 1 (lb)	Load 2 (lb)	Load 3 (lb)	Avg. Stress (psi)
CT 5–6					
Footing 7 day	28.27	148,900	146,970		5232
Footing 28 day	28.27	190,890	204,310		6989
Column 7 day	28.27	119,900	119,100		4226
Column 28 day	28.27	153,650	152,030		5406
CT 5					
Grout 7 day	4.00	29,100	29,100		7275
Grout 28 day	4.00	25,200	25,000		6275
Footing test day	28.27	242,000	241,550		8551
Column test day	28.27	171,000	177,800	173,100	6153
Grout test day	4.00	39,100	39,300		9800
CT 6					
Footing test day	28.27	241,670	254,210		8769
Column test day	28.27	195,570	193,990	183,930	6761
CT 7–8					
Footing 7 day	28.27	128,340	132,850		4619
Footing 28 day	28.27	184,520	189,380	176,950	6494
Column 7 day	28.27	140,020	146,690		5070
Column 28 day	28.27	200,340	193,930	199,590	7001
Grout 7 day	4.00	30,900	30,900		7725
Grout 28 day	4.00	36,600	40,500		9638
CT 7					
Footing test day	28.27	209,850	209,180	187,530	7151
Column test day	28.27	200,340	193,930	199,590	7001
Grout test day	4.00	36,600	40,500		9638
CT 8					
Footing test day	28.27	208,430	229,770	195,650	7473
Column test day	28.27	213,170	223,150	212,640	7651
Grout test day	4.00	40,400	43,000	42,500	10492

APPENDIX B: Construction Drawings

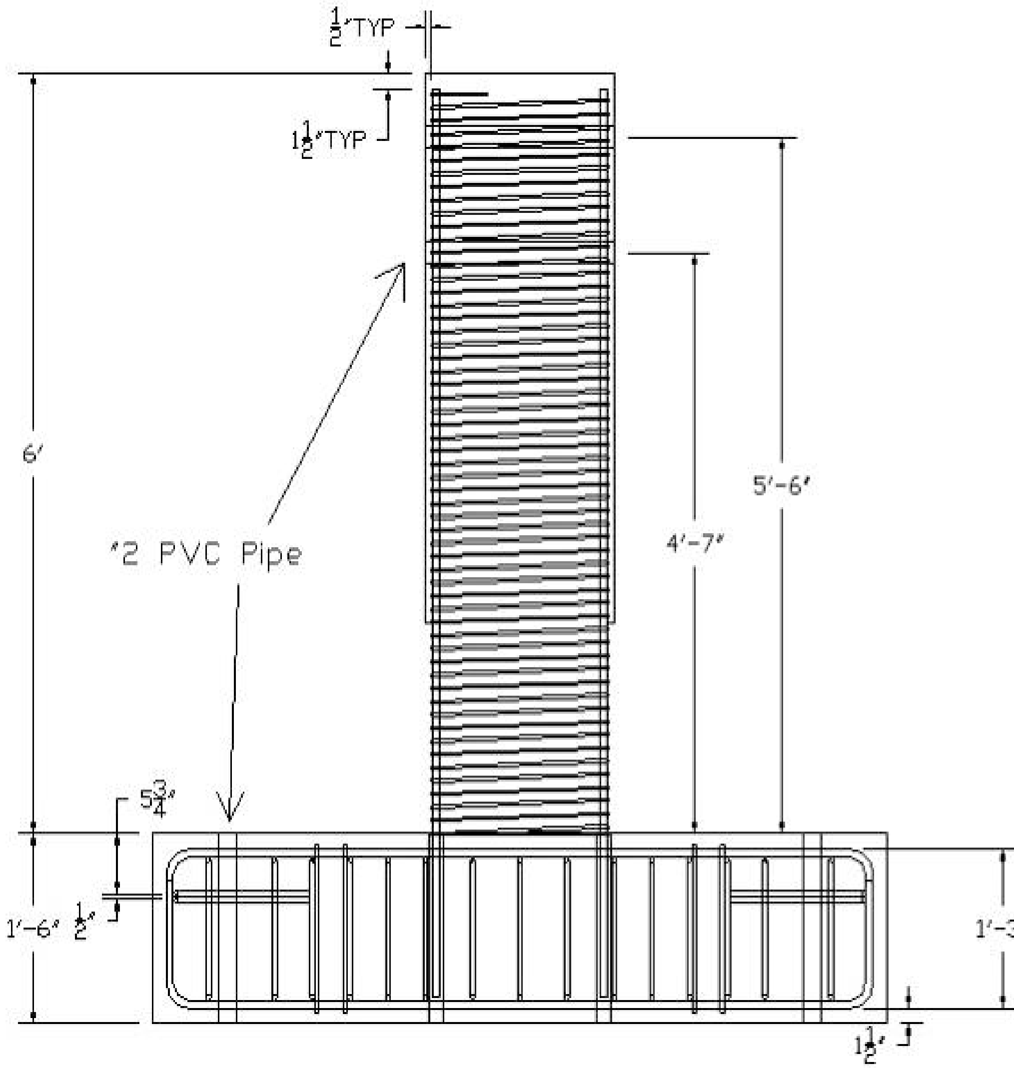

Fig. B.1 Side view of column.

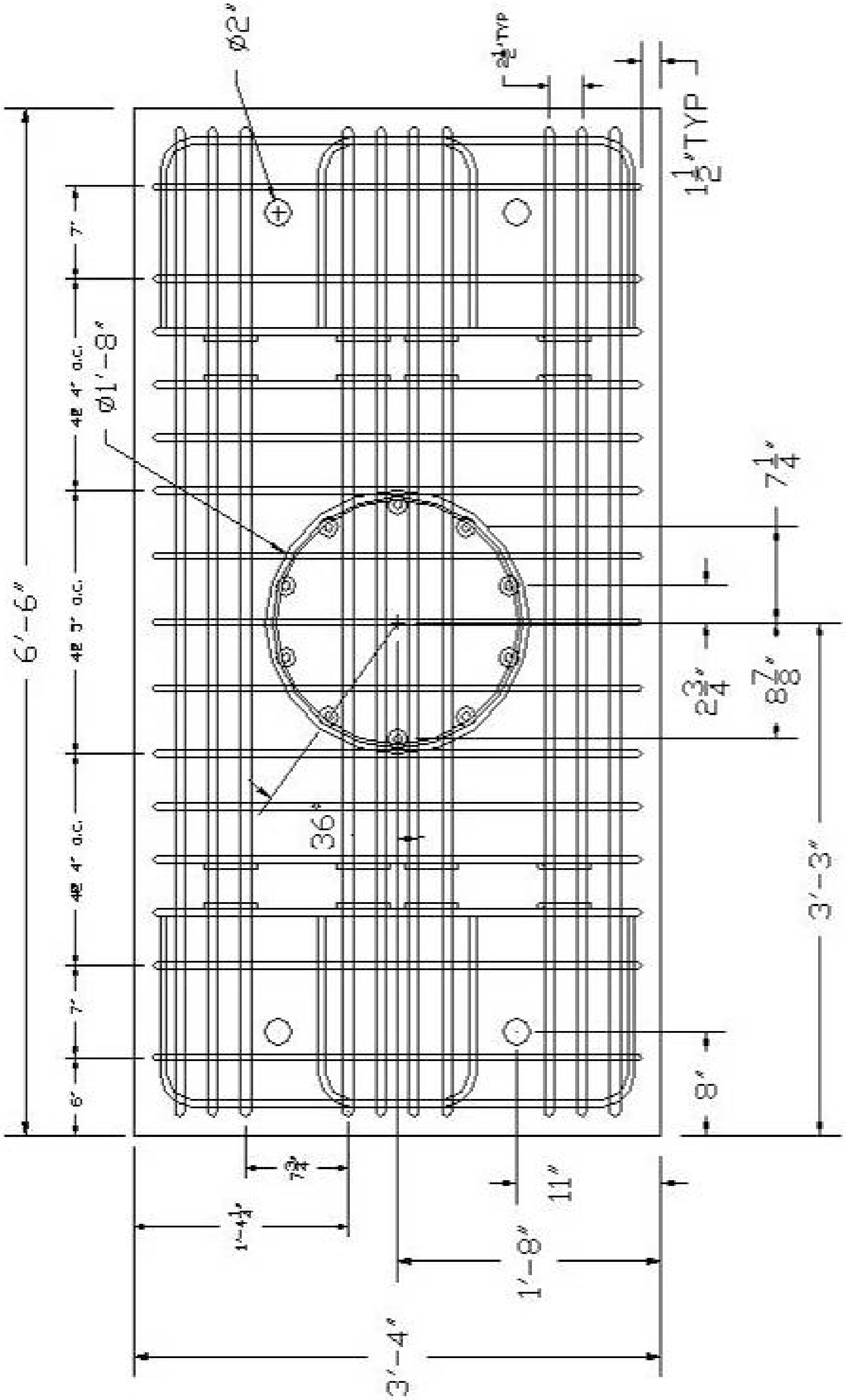

Fig. B.2 Top view of footing.

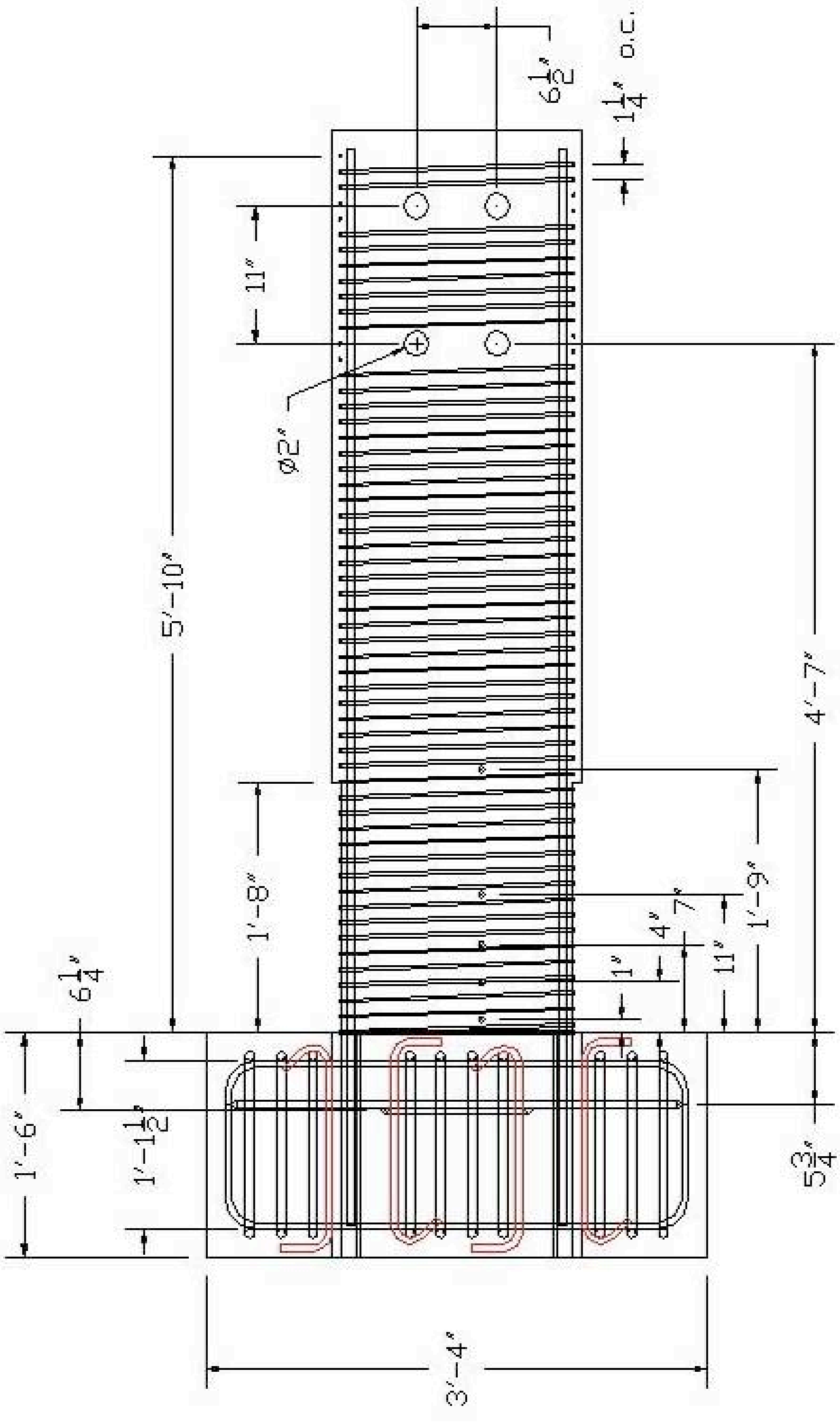

Fig. B.3 End view of column.

PEER REPORTS

PEER reports are available from the National Information Service for Earthquake Engineering (NISEE). To order PEER reports, please contact the Pacific Earthquake Engineering Research Center, 1301 South 46th Street, Richmond, California 94804-4698. Tel.: (510) 665-3405; Fax: (510) 665-3420.

PEER 2007/11 *Bar Buckling in Reinforced Concrete Bridge Columns.* Wayne A. Brown, Dawn E. Lehman, and John F. Stanton. February 2008.

PEER 2007/08 *Assessing Seismic Collapse Safety of Modern Reinforced Concrete Moment-Frame Buildings.* Curt B. Haselton and Gregory G. Deierlein. February 2008.

PEER 2007/06 *Development of Improved Procedures for Seismic Design of Buried and Partially Buried Structures.* Linda Al Atik and Nicholas Sitar. June 2007.

PEER 2007/05 *Uncertainty and Correlation in Seismic Risk Assessment of Transportation Systems.* Renee G. Lee and Anne S. Kiremidjian. July 2007.

PEER 2007/02 *Campbell-Bozorgnia NGA Ground Motion Relations for the Geometric Mean Horizontal Component of Peak and Spectral Ground Motion Parameters.* Kenneth W. Campbell and Yousef Bozorgnia. May 2007.

PEER 2007/01 *Boore-Atkinson NGA Ground Motion Relations for the Geometric Mean Horizontal Component of Peak and Spectral Ground Motion Parameters.* David M. Boore and Gail M. Atkinson. May. May 2007.

PEER 2006/12 *Societal Implications of Performance-Based Earthquake Engineering.* Peter J. May. May 2007.

PEER 2006/11 *Probabilistic Seismic Demand Analysis Using Advanced Ground Motion Intensity Measures, Attenuation Relationships, and Near-Fault Effects.* Polsak Tothong and C. Allin Cornell. March 2007.

PEER 2006/10 *Application of the PEER PBEE Methodology to the I-880 Viaduct.* Sashi Kunnath. February 2007.

PEER 2006/09 *Quantifying Economic Losses from Travel Forgone Following a Large Metropolitan Earthquake.* James Moore, Sungbin Cho, Yue Yue Fan, and Stuart Werner. November 2006.

PEER 2006/08 *Vector-Valued Ground Motion Intensity Measures for Probabilistic Seismic Demand Analysis*. Jack W. Baker and C. Allin Cornell. October 2006.

PEER 2006/07 *Analytical Modeling of Reinforced Concrete Walls for Predicting Flexural and Coupled–Shear-Flexural Responses.* Kutay Orakcal, Loenardo M. Massone, and John W. Wallace. October 2006.

PEER 2006/06 *Nonlinear Analysis of a Soil-Drilled Pier System under Static and Dynamic Axial Loading.* Gang Wang and Nicholas Sitar. November 2006.

PEER 2006/05 *Advanced Seismic Assessment Guidelines.* Paolo Bazzurro, C. Allin Cornell, Charles Menun, Maziar Motahari, and Nicolas Luco. September 2006.

PEER 2006/04 *Probabilistic Seismic Evaluation of Reinforced Concrete Structural Components and Systems.* Tae Hyung Lee and Khalid M. Mosalam. August 2006.

PEER 2006/03 *Performance of Lifelines Subjected to Lateral Spreading.* Scott A. Ashford and Teerawut Juirnarongrit. July 2006.

PEER 2006/02 *Pacific Earthquake Engineering Research Center Highway Demonstration Project.* Anne Kiremidjian, James Moore, Yue Yue Fan, Nesrin Basoz, Ozgur Yazali, and Meredith Williams. April 2006.

PEER 2006/01 *Bracing Berkeley. A Guide to Seismic Safety on the UC Berkeley Campus.* Mary C. Comerio, Stephen Tobriner, and Ariane Fehrenkamp. January 2006.

PEER 2005/16 *Seismic Response and Reliability of Electrical Substation Equipment and Systems.* Junho Song, Armen Der Kiureghian, and Jerome L. Sackman. April 2006.

PEER 2005/15 *CPT-Based Probabilistic Assessment of Seismic Soil Liquefaction Initiation.* R. E. S. Moss, R. B. Seed, R. E. Kayen, J. P. Stewart, and A. Der Kiureghian. April 2006.

PEER 2005/14 *Workshop on Modeling of Nonlinear Cyclic Load-Deformation Behavior of Shallow Foundations.* Bruce L. Kutter, Geoffrey Martin, Tara Hutchinson, Chad Harden, Sivapalan Gajan, and Justin Phalen. March 2006.

PEER 2005/13 *Stochastic Characterization and Decision Bases under Time-Dependent Aftershock Risk in Performance-Based Earthquake Engineering.* Gee Liek Yeo and C. Allin Cornell. July 2005.

PEER 2005/12 *PEER Testbed Study on a Laboratory Building: Exercising Seismic Performance Assessment.* Mary C. Comerio, editor. November 2005.

PEER 2005/11 *Van Nuys Hotel Building Testbed Report: Exercising Seismic Performance Assessment.* Helmut Krawinkler, editor. October 2005.

PEER 2005/10 *First NEES/E-Defense Workshop on Collapse Simulation of Reinforced Concrete Building Structures.* September 2005.

PEER 2005/09 *Test Applications of Advanced Seismic Assessment Guidelines.* Joe Maffei, Karl Telleen, Danya Mohr, William Holmes, and Yuki Nakayama. August 2006.

PEER 2005/08 *Damage Accumulation in Lightly Confined Reinforced Concrete Bridge Columns.* R. Tyler Ranf, Jared M. Nelson, Zach Price, Marc O. Eberhard, and John F. Stanton. April 2006.

PEER 2005/07 *Experimental and Analytical Studies on the Seismic Response of Freestanding and Anchored Laboratory Equipment.* Dimitrios Konstantinidis and Nicos Makris. January 2005.

PEER 2005/06 *Global Collapse of Frame Structures under Seismic Excitations*. Luis F. Ibarra and Helmut Krawinkler. September 2005.

PEER 2005//05 *Performance Characterization of Bench- and Shelf-Mounted Equipment.* Samit Ray Chaudhuri and Tara C. Hutchinson. May 2006.

PEER 2005/04 *Numerical Modeling of the Nonlinear Cyclic Response of Shallow Foundations.* Chad Harden, Tara Hutchinson, Geoffrey R. Martin, and Bruce L. Kutter. August 2005.

PEER 2005/03 *A Taxonomy of Building Components for Performance-Based Earthquake Engineering.* Keith A. Porter. September 2005.

PEER 2005/02 *Fragility Basis for California Highway Overpass Bridge Seismic Decision Making*. Kevin R. Mackie and Bozidar Stojadinovic. June 2005.

PEER 2005/01 *Empirical Characterization of Site Conditions on Strong Ground Motion.* Jonathan P. Stewart, Yoojoong Choi, and Robert W. Graves. June 2005.

PEER 2004/09 *Electrical Substation Equipment Interaction: Experimental Rigid Conductor Studies.* Christopher Stearns and André Filiatrault. February 2005.

PEER 2004/08 *Seismic Qualification and Fragility Testing of Line Break 550-kV Disconnect Switches.* Shakhzod M. Takhirov, Gregory L. Fenves, and Eric Fujisaki. January 2005.

PEER 2004/07 *Ground Motions for Earthquake Simulator Qualification of Electrical Substation Equipment.* Shakhzod M. Takhirov, Gregory L. Fenves, Eric Fujisaki, and Don Clyde. January 2005.

PEER 2004/06 *Performance-Based Regulation and Regulatory Regimes.* Peter J. May and Chris Koski. September 2004.

PEER 2004/05 *Performance-Based Seismic Design Concepts and Implementation: Proceedings of an International Workshop.* Peter Fajfar and Helmut Krawinkler, editors. September 2004.

PEER 2004/04 *Seismic Performance of an Instrumented Tilt-up Wall Building.* James C. Anderson and Vitelmo V. Bertero. July 2004.

PEER 2004/03 *Evaluation and Application of Concrete Tilt-up Assessment Methodologies.* Timothy Graf and James O. Malley. October 2004.

PEER 2004/02 *Analytical Investigations of New Methods for Reducing Residual Displacements of Reinforced Concrete Bridge Columns.* Junichi Sakai and Stephen A. Mahin. August 2004.

PEER 2004/01 *Seismic Performance of Masonry Buildings and Design Implications.* Kerri Anne Taeko Tokoro, James C. Anderson, and Vitelmo V. Bertero. February 2004.

PEER 2003/18 *Performance Models for Flexural Damage in Reinforced Concrete Columns.* Michael Berry and Marc Eberhard. August 2003.

PEER 2003/17 *Predicting Earthquake Damage in Older Reinforced Concrete Beam-Column Joints.* Catherine Pagni and Laura Lowes. October 2004.

PEER 2003/16 *Seismic Demands for Performance-Based Design of Bridges.* Kevin Mackie and Božidar Stojadinovic. August 2003.

PEER 2003/15 *Seismic Demands for Nondeteriorating Frame Structures and Their Dependence on Ground Motions.* Ricardo Antonio Medina and Helmut Krawinkler. May 2004.

PEER 2003/14 *Finite Element Reliability and Sensitivity Methods for Performance-Based Earthquake Engineering.* Terje Haukaas and Armen Der Kiureghian. April 2004.

PEER 2003/13 *Effects of Connection Hysteretic Degradation on the Seismic Behavior of Steel Moment-Resisting Frames.* Janise E. Rodgers and Stephen A. Mahin. March 2004.

PEER 2003/12 *Implementation Manual for the Seismic Protection of Laboratory Contents: Format and Case Studies.* William T. Holmes and Mary C. Comerio. October 2003.

PEER 2003/11 *Fifth U.S.-Japan Workshop on Performance-Based Earthquake Engineering Methodology for Reinforced Concrete Building Structures.* February 2004.

PEER 2003/10 *A Beam-Column Joint Model for Simulating the Earthquake Response of Reinforced Concrete Frames.* Laura N. Lowes, Nilanjan Mitra, and Arash Altoontash. February 2004.

PEER 2003/09 *Sequencing Repairs after an Earthquake: An Economic Approach.* Marco Casari and Simon J. Wilkie. April 2004.

PEER 2003/08 *A Technical Framework for Probability-Based Demand and Capacity Factor Design (DCFD) Seismic Formats*. Fatemeh Jalayer and C. Allin Cornell. November 2003.

PEER 2003/07 *Uncertainty Specification and Propagation for Loss Estimation Using FOSM Methods.* Jack W. Baker and C. Allin Cornell. September 2003.

PEER 2003/06 *Performance of Circular Reinforced Concrete Bridge Columns under Bidirectional Earthquake Loading.* Mahmoud M. Hachem, Stephen A. Mahin, and Jack P. Moehle. February 2003.

PEER 2003/05 *Response Assessment for Building-Specific Loss Estimation.* Eduardo Miranda and Shahram Taghavi. September 2003.

PEER 2003/04 *Experimental Assessment of Columns with Short Lap Splices Subjected to Cyclic Loads*. Murat Melek, John W. Wallace, and Joel Conte. April 2003.

PEER 2003/03 *Probabilistic Response Assessment for Building-Specific Loss Estimation.* Eduardo Miranda and Hesameddin Aslani. September 2003.

PEER 2003/02 *Software Framework for Collaborative Development of Nonlinear Dynamic Analysis Program.* Jun Peng and Kincho H. Law. September 2003.

PEER 2003/01 *Shake Table Tests and Analytical Studies on the Gravity Load Collapse of Reinforced Concrete Frames.* Kenneth John Elwood and Jack P. Moehle. November 2003.

PEER 2002/24 *Performance of Beam to Column Bridge Joints Subjected to a Large Velocity Pulse.* Natalie Gibson, André Filiatrault, and Scott A. Ashford. April 2002.

PEER 2002/23 *Effects of Large Velocity Pulses on Reinforced Concrete Bridge Columns.* Greg L. Orozco and Scott A. Ashford. April 2002.

PEER 2002/22 *Characterization of Large Velocity Pulses for Laboratory Testing.* Kenneth E. Cox and Scott A. Ashford. April 2002.

PEER 2002/21 *Fourth U.S.-Japan Workshop on Performance-Based Earthquake Engineering Methodology for Reinforced Concrete Building Structures*. December 2002.

PEER 2002/20 *Barriers to Adoption and Implementation of PBEE Innovations.* Peter J. May. August 2002.

PEER 2002/19 *Economic-Engineered Integrated Models for Earthquakes: Socioeconomic Impacts.* Peter Gordon, James E. Moore II, and Harry W. Richardson. July 2002.

PEER 2002/18 *Assessment of Reinforced Concrete Building Exterior Joints with Substandard Details.* Chris P. Pantelides, Jon Hansen, Justin Nadauld, and Lawrence D. Reaveley. May 2002.

PEER 2002/17 *Structural Characterization and Seismic Response Analysis of a Highway Overcrossing Equipped with Elastomeric Bearings and Fluid Dampers: A Case Study.* Nicos Makris and Jian Zhang. November 2002.

PEER 2002/16 *Estimation of Uncertainty in Geotechnical Properties for Performance-Based Earthquake Engineering.* Allen L. Jones, Steven L. Kramer, and Pedro Arduino. December 2002.

PEER 2002/15 *Seismic Behavior of Bridge Columns Subjected to Various Loading Patterns.* Asadollah Esmaeily-Gh. and Yan Xiao. December 2002.

PEER 2002/14 *Inelastic Seismic Response of Extended Pile Shaft Supported Bridge Structures.* T.C. Hutchinson, R.W. Boulanger, Y.H. Chai, and I.M. Idriss. December 2002.

PEER 2002/13 *Probabilistic Models and Fragility Estimates for Bridge Components and Systems.* Paolo Gardoni, Armen Der Kiureghian, and Khalid M. Mosalam. June 2002.

PEER 2002/12 *Effects of Fault Dip and Slip Rake on Near-Source Ground Motions: Why Chi-Chi Was a Relatively Mild M7.6 Earthquake.* Brad T. Aagaard, John F. Hall, and Thomas H. Heaton. December 2002.

PEER 2002/11 *Analytical and Experimental Study of Fiber-Reinforced Strip Isolators*. James M. Kelly and Shakhzod M. Takhirov. September 2002.

PEER 2002/10 *Centrifuge Modeling of Settlement and Lateral Spreading with Comparisons to Numerical Analyses***.** Sivapalan Gajan and Bruce L. Kutter. January 2003.

PEER 2002/09 *Documentation and Analysis of Field Case Histories of Seismic Compression during the 1994 Northridge, California, Earthquake.* Jonathan P. Stewart, Patrick M. Smith, Daniel H. Whang, and Jonathan D. Bray. October 2002.

PEER 2002/08 *Component Testing, Stability Analysis and Characterization of Buckling-Restrained Unbonded Braces™.* Cameron Black, Nicos Makris, and Ian Aiken. September 2002.

PEER 2002/07 *Seismic Performance of Pile-Wharf Connections.* Charles W. Roeder, Robert Graff, Jennifer Soderstrom, and Jun Han Yoo. December 2001.

PEER 2002/06 *The Use of Benefit-Cost Analysis for Evaluation of Performance-Based Earthquake Engineering Decisions.* Richard O. Zerbe and Anthony Falit-Baiamonte. September 2001.

PEER 2002/05 *Guidelines, Specifications, and Seismic Performance Characterization of Nonstructural Building Components and Equipment*. André Filiatrault, Constantin Christopoulos, and Christopher Stearns. September 2001.

PEER 2002/04 *Consortium of Organizations for Strong-Motion Observation Systems and the Pacific Earthquake Engineering Research Center Lifelines Program: Invited Workshop on Archiving and Web Dissemination of Geotechnical Data, 4–5 October 2001*. September 2002.

PEER 2002/03 *Investigation of Sensitivity of Building Loss Estimates to Major Uncertain Variables for the Van Nuys Testbed.* Keith A. Porter, James L. Beck, and Rustem V. Shaikhutdinov. August 2002.

PEER 2002/02 *The Third U.S.-Japan Workshop on Performance-Based Earthquake Engineering Methodology for Reinforced Concrete Building Structures*. July 2002.

PEER 2002/01 *Nonstructural Loss Estimation: The UC Berkeley Case Study.* Mary C. Comerio and John C. Stallmeyer. December 2001.

PEER 2001/16 *Statistics of SDF-System Estimate of Roof Displacement for Pushover Analysis of Buildings.* Anil K. Chopra, Rakesh K. Goel, and Chatpan Chintanapakdee. December 2001.

PEER 2001/15 *Damage to Bridges during the 2001 Nisqually Earthquake.* R. Tyler Ranf, Marc O. Eberhard, and Michael P. Berry. November 2001.

PEER 2001/14 *Rocking Response of Equipment Anchored to a Base Foundation.* Nicos Makris and Cameron J. Black. September 2001.

PEER 2001/13 *Modeling Soil Liquefaction Hazards for Performance-Based Earthquake Engineering.* Steven L. Kramer and Ahmed-W. Elgamal. February 2001.

PEER 2001/12 *Development of Geotechnical Capabilities in OpenSees.* Boris Jeremi . September 2001.

PEER 2001/11 *Analytical and Experimental Study of Fiber-Reinforced Elastomeric Isolators*. James M. Kelly and Shakhzod M. Takhirov. September 2001.

PEER 2001/10 *Amplification Factors for Spectral Acceleration in Active Regions.* Jonathan P. Stewart, Andrew H. Liu, Yoojoong Choi, and Mehmet B. Baturay. December 2001.

PEER 2001/09 *Ground Motion Evaluation Procedures for Performance-Based Design.* Jonathan P. Stewart, Shyh-Jeng Chiou, Jonathan D. Bray, Robert W. Graves, Paul G. Somerville, and Norman A. Abrahamson. September 2001.

PEER 2001/08 *Experimental and Computational Evaluation of Reinforced Concrete Bridge Beam-Column Connections for Seismic Performance*. Clay J. Naito, Jack P. Moehle, and Khalid M. Mosalam. November 2001.

PEER 2001/07 *The Rocking Spectrum and the Shortcomings of Design Guidelines.* Nicos Makris and Dimitrios Konstantinidis. August 2001.

PEER 2001/06 *Development of an Electrical Substation Equipment Performance Database for Evaluation of Equipment Fragilities*. Thalia Agnanos. April 1999.

PEER 2001/05 *Stiffness Analysis of Fiber-Reinforced Elastomeric Isolators.* Hsiang-Chuan Tsai and James M. Kelly. May 2001.

PEER 2001/04 *Organizational and Societal Considerations for Performance-Based Earthquake Engineering.* Peter J. May. April 2001.

PEER 2001/03 *A Modal Pushover Analysis Procedure to Estimate Seismic Demands for Buildings: Theory and Preliminary Evaluation.* Anil K. Chopra and Rakesh K. Goel. January 2001.

PEER 2001/02 *Seismic Response Analysis of Highway Overcrossings Including Soil-Structure Interaction.* Jian Zhang and Nicos Makris. March 2001.

PEER 2001/01 *Experimental Study of Large Seismic Steel Beam-to-Column Connections.* Egor P. Popov and Shakhzod M. Takhirov. November 2000.

PEER 2000/10 *The Second U.S.-Japan Workshop on Performance-Based Earthquake Engineering Methodology for Reinforced Concrete Building Structures.* March 2000.

PEER 2000/09 *Structural Engineering Reconnaissance of the August 17, 1999 Earthquake: Kocaeli (Izmit), Turkey.* Halil Sezen, Kenneth J. Elwood, Andrew S. Whittaker, Khalid Mosalam, John J. Wallace, and John F. Stanton. December 2000.

PEER 2000/08 *Behavior of Reinforced Concrete Bridge Columns Having Varying Aspect Ratios and Varying Lengths of Confinement.* Anthony J. Calderone, Dawn E. Lehman, and Jack P. Moehle. January 2001.

PEER 2000/07 *Cover-Plate and Flange-Plate Reinforced Steel Moment-Resisting Connections.* Taejin Kim, Andrew S. Whittaker, Amir S. Gilani, Vitelmo V. Bertero, and Shakhzod M. Takhirov. September 2000.

PEER 2000/06 *Seismic Evaluation and Analysis of 230-kV Disconnect Switches.* Amir S. J. Gilani, Andrew S. Whittaker, Gregory L. Fenves, Chun-Hao Chen, Henry Ho, and Eric Fujisaki. July 2000.

PEER 2000/05 *Performance-Based Evaluation of Exterior Reinforced Concrete Building Joints for Seismic Excitation.* Chandra Clyde, Chris P. Pantelides, and Lawrence D. Reaveley. July 2000.

PEER 2000/04 *An Evaluation of Seismic Energy Demand: An Attenuation Approach.* Chung-Che Chou and Chia-Ming Uang. July 1999.

PEER 2000/03 *Framing Earthquake Retrofitting Decisions: The Case of Hillside Homes in Los Angeles.* Detlof von Winterfeldt, Nels Roselund, and Alicia Kitsuse. March 2000.

PEER 2000/02 *U.S.-Japan Workshop on the Effects of Near-Field Earthquake Shaking.* Andrew Whittaker, ed. July 2000.

PEER 2000/01 *Further Studies on Seismic Interaction in Interconnected Electrical Substation Equipment.* Armen Der Kiureghian, Kee-Jeung Hong, and Jerome L. Sackman. November 1999.

PEER 1999/14 *Seismic Evaluation and Retrofit of 230-kV Porcelain Transformer Bushings*. Amir S. Gilani, Andrew S. Whittaker, Gregory L. Fenves, and Eric Fujisaki. December 1999.

PEER 1999/13 *Building Vulnerability Studies: Modeling and Evaluation of Tilt-up and Steel Reinforced Concrete Buildings.* John W. Wallace, Jonathan P. Stewart, and Andrew S. Whittaker, editors. December 1999.

PEER 1999/12 *Rehabilitation of Nonductile RC Frame Building Using Encasement Plates and Energy-Dissipating Devices.* Mehrdad Sasani, Vitelmo V. Bertero, James C. Anderson. December 1999.

PEER 1999/11 *Performance Evaluation Database for Concrete Bridge Components and Systems under Simulated Seismic Loads.* Yael D. Hose and Frieder Seible. November 1999.

PEER 1999/10 *U.S.-Japan Workshop on Performance-Based Earthquake Engineering Methodology for Reinforced Concrete Building Structures.* December 1999.

PEER 1999/09 *Performance Improvement of Long Period Building Structures Subjected to Severe Pulse-Type Ground Motions*. James C. Anderson, Vitelmo V. Bertero, and Raul Bertero. October 1999.

PEER 1999/08 *Envelopes for Seismic Response Vectors.* Charles Menun and Armen Der Kiureghian. July 1999.

PEER 1999/07 *Documentation of Strengths and Weaknesses of Current Computer Analysis Methods for Seismic Performance of Reinforced Concrete Members.* William F. Cofer. November 1999.

PEER 1999/06 *Rocking Response and Overturning of Anchored Equipment under Seismic Excitations.* Nicos Makris and Jian Zhang. November 1999.

PEER 1999/05 *Seismic Evaluation of 550 kV Porcelain Transformer Bushings.* Amir S. Gilani, Andrew S. Whittaker, Gregory L. Fenves, and Eric Fujisaki. October 1999.

PEER 1999/04 *Adoption and Enforcement of Earthquake Risk-Reduction Measures.* Peter J. May, Raymond J. Burby, T. Jens Feeley, and Robert Wood.

PEER 1999/03 *Task 3 Characterization of Site Response General Site Categories*. Adrian Rodriguez-Marek, Jonathan D. Bray, and Norman Abrahamson. February 1999.

PEER 1999/02 *Capacity-Demand-Diagram Methods for Estimating Seismic Deformation of Inelastic Structures: SDF Systems*. Anil K. Chopra and Rakesh Goel. April 1999.

PEER 1999/01 *Interaction in Interconnected Electrical Substation Equipment Subjected to Earthquake Ground Motions.* Armen Der Kiureghian, Jerome L. Sackman, and Kee-Jeung Hong. February 1999.

PEER 1998/08 *Behavior and Failure Analysis of a Multiple-Frame Highway Bridge in the 1994 Northridge Earthquake.* Gregory L. Fenves and Michael Ellery. December 1998.

PEER 1998/07 *Empirical Evaluation of Inertial Soil-Structure Interaction Effects.* Jonathan P. Stewart, Raymond B. Seed, and Gregory L. Fenves. November 1998.

PEER 1998/06 *Effect of Damping Mechanisms on the Response of Seismic Isolated Structures.* Nicos Makris and Shih-Po Chang. November 1998.

PEER 1998/05 *Rocking Response and Overturning of Equipment under Horizontal Pulse-Type Motions.* Nicos Makris and Yiannis Roussos. October 1998.

PEER 1998/04 *Pacific Earthquake Engineering Research Invitational Workshop Proceedings, May 14–15, 1998: Defining the Links between Planning, Policy Analysis, Economics and Earthquake Engineering.* Mary Comerio and Peter Gordon. September 1998.

PEER 1998/03 *Repair/Upgrade Procedures for Welded Beam to Column Connections*. James C. Anderson and Xiaojing Duan. May 1998.

PEER 1998/02 *Seismic Evaluation of 196 kV Porcelain Transformer Bushings.* Amir S. Gilani, Juan W. Chavez, Gregory L. Fenves, and Andrew S. Whittaker. May 1998.

PEER 1998/01 *Seismic Performance of Well-Confined Concrete Bridge Columns.* Dawn E. Lehman and Jack P. Moehle. December 2000.

ONLINE REPORTS

The following PEER reports are available by Internet only at http://peer.berkeley.edu/publications/peer_reports.html

PEER 2007/101 *Generalized Hybrid Simulation Framework for Structural Systems Subjected to Seismic Loading.* Tarek Elkhoraibi and Khalid M. Mosalam. July 2007.

PEER 2007/100 *Seismic Evaluation of Reinforced Concrete Buildings Including Effects of Masonry Infill Walls.* Alidad Hashemi and Khalid M. Mosalam. July 2007.